Computational investigations into the biophysical mechanisms of antibiotic resistance in bacterial biofilms

Lakshmi Machineni

A dissertation submitted to Indian Institute of Technology Hyderabad in partial fulfilment of the requirements for the degree of Doctor of Philosophy

भारतीय प्रौद्योगिकी संस्थान हैदराबाद
Indian Institute of Technology Hyderabad

Department of Chemical Engineering

December, 2017

Declaration

I declare that this written submission represents my ideas in my own words, and where others' ideas or words have been included, I have adequately cited and referenced the original sources. I also declare that I have adhered to all principles of academic honesty and integrity and have not misrepresented or fabricated or falsified any idea/data/fact/source in my submission. I understand that any violation of the above will be a cause for disciplinary action by the Institute and can also evoke penal action from the sources that have thus not been properly cited, or from whom proper permission has not been taken when needed.

16/5/2018

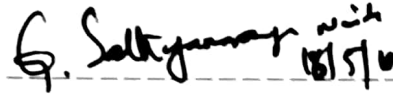(Signature)

Lakshmi Machineni

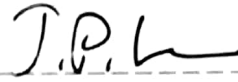(– Student Name –)

Ch09p004

(Roll No)

Approval Sheet

This thesis entitled "Computational investigations into the biophysical mechanisms of antibiotic resistance in bacterial biofilms" by Lakshmi Machineni is approved for the degree of Doctor of Philosophy from IIT Hyderabad.
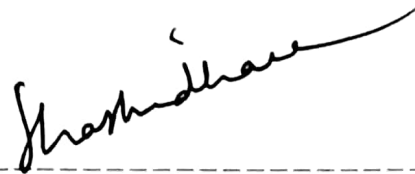
Prof. Satyanarayana N Gummadi, IIT Madras

External Examiner

Dr. Phanindra Varma Jampana, IIT Hyderabad

Internal Examiner

Dr. Parag D. Pawar, IIT Hyderabad

Adviser

Dr. Shashidhar, IIT Hyderabad

Chairman

Acknowledgments

I gratefully acknowledge Dr. Parag D. Pawar for his constant support and able guidance as my research advisor and for introducing me to the field of modelling biofilm development process and physiological resistance in biofilms. His positive outlook and confidence in my research inspired me and gave me confidence. His careful editing and penchant for clarifying the most convoluted of concepts in uncomplicated manner contributed enormously to the production of this thesis. Most importantly, I would like to thank him for his moral support and expert guidance during the tougher phase of this work.

I would like to express my sincere thanks to all my thesis committee: Dr. Kirti Chandra Sahu, Dr. Saptarshi Majumdar, and Dr. Renu John for their insightful comments throughout.

I acknowledge, with gratitude, Mr. Anil for the stimulating discussions, and for providing me valuable support during various stages of this project. I have to thank my fellow doctoral students Nikita, Vandana, Tejesh, Srinadh, and Goutham for their feedback, cooperation and of course friendship.

During my research work at IITH, I was fortunate to have the blessings and support of some kind people. I take this opportunity to express my appreciation for them: Mr. Kamaraju, and Varalakshmi. In addition I would like to express my gratitude to the staff of Information Service and Automation Cell, High Performance Computing, and Administrative section at IITH for the last minute favours.

Most importantly, I also would like to express my gratitude to former colleague Dr. Teja for always being there for me and camaraderie that he has provided me over the years.

Last but not the least, I am extremely thankful to the most important people in my life - my parents, my brother Mr. Ramu, my husband Mr. Praveen, and for always believing in me and for being very patient. I am also thankful to my 2-years old nephew Ruthvik Machineni for giving me happiness with his naughty and innocent acts during my thesis preparation.

Besides this, I would like to thank all the people who have knowingly and unknowingly helped me in the successful completion of this thesis.

Lakshmi Machineni

To my family

Abstract

When antibiotics were discovered for clinical use more than 85 years ago, many believed that this was the final solution for acute infectious diseases caused by planktonic bacteria. Unfortunately, within a few years bacteria controlled by antibiotics had developed marked resistance to these drugs. Today, bacterial infections have become a serious health problem worldwide, killing ~17 million people each year. We have reached a crisis where the supply of new antibiotics is drying up. Studies have shown that antibiotic resistance is more predominant in the biofilm mode of growth than antibiotic resistance of planktonic bacteria. A systematic investigation of the population growth dynamics, and antibiotic resistance mechanisms associated with biofilm-related infections may pave the way for novel therapeutic strategies to prevent or treat biofilms in health-care and industrial settings.

Biofilm development is crucial in the lifecycle of bacteria and is tightly regulated with both spatial and temporal control. Bacteria growing in biofilms occupy a spectrum of growth states from rapidly-growing and active to slow-growing and dormant, due in part to their adaptation to local environmental conditions. Consequently, distinct microcolonies with clusters of bacterial cells may develop within the biofilm where cellular physiology is different from surroundings in terms of metabolic activity, secretion of EPS, and concentrations of nutrients, autoinducer, and antimicrobial agents. This intrinsic physiological heterogeneity of biofilms may contribute to the protection of cells. Previous experimental investigations have revealed that it is only subpopulations of bacterial cells that exhibit increased resistance, and may protect the biofilm from eradication for later resuscitation when nutrients or space become available. An increased understanding of the structural properties of these micro-environments within the biofilm, and their heterogeneous response to antibiotic treatment may shed light on the biophysical mechanisms of antibiotic resistance in bacterial biofilms.

Because of the challenging experimental measurements, and the dynamic nature of biofilms, computational modelling of biofilms is an important tool to investigate biofilm growth dynamics, and its response to external stresses like treatment with antibiotics. In this work,

an individual-based 3D computational cellular automata model is developed to investigate the biophysical mechanisms of antibiotic resistance in bacterial biofilms. The model is used to simulate biofilm growth dynamics, and quantify spatial heterogeneity in the cell population as a function of growth phase, space, and time in response to antimicrobial agents in the presence and absence of quorum sensing.

Biofilm growth is simulated within the confines of a rectangular box. The bottom surface (square with side 120 µm) represents the substratum upon which the biofilm develops. A continuously replenished nutrient reservoir is placed at the top at a constant distance from the substratum. The interface between the nutrient reservoir and the biofilm domain is termed the diffusion boundary layer (DBL). The space between the DBL and the substratum is discretized into cubical elements of volume 27 µm³ each. During the simulation, each element may be occupied by one or more of the following entities: (i) bacterial cell, (ii) EPS, (iii) nutrient, (iv) autoinducer, and (v) antibiotic. The simulation represents a time march in which the occupancy status of each element is updated at every time step. At time $t = 0$, six cells, termed colonizers, are placed into random elements atop the substratum. Simultaneously, nutrient diffuses across the DBL. Cells consume nutrient, and subsequently grow and divide, resulting in the formation of a contiguous multicellular population. At the end of each time step, the nutrient reservoir is shifted vertically upwards such that a pre-determined distance from the topmost cell in the biofilm is always maintained. To simulate behavioural variability, parameter values for individual bacterial cells were obtained by random draws from a uniform distribution with $\pm 10\%$ variation. The resulting aggregate behaviour of the biofilm is therefore emergent from the local interactions between the individual bacteria, and their surroundings, rather than being a model input -- thereby allowing us to simulate the self-organized process of biofilm formation.

Biofilm development was simulated under varying bulk nutrient concentrations (1-8 gm³), in the presence and absence of quorum sensing. These results from causal modelling suggest that biofilms are comprised of at least three structurally distinct strata with respect to metabolic activity, growth phase, nutrient availability, and porosity: a high-biomass, low-heterogeneity section in the middle of the biofilm, sandwiched between two highly

heterogeneous low-biomass regions on the top and the bottom. Cell death occurred preferentially in layers in close proximity to the substratum, resulting in increased heterogeneity in this section of the biofilm; the thickness and heterogeneity of this lowermost layer increased with time, ultimately leading to sloughing. The model predicted the formation of metabolically dormant cellular microniches embedded within faster growing cell clusters. Biofilms utilizing quorum sensing were more heterogeneous compared to their non-quorum sensing counterparts, and resisted sloughing, featuring a cell-devoid layer of EPS atop the substratum upon which the remainder of the biofilm developed.

Since the model simulates spatiotemporal variability of biofilm constituents (such as biomass, EPS, nutrient, and signalling molecules), it may be instructive to correlate antibiotic-resistant of bacterial biofilms with the emergence of metabolically inactive cell clusters. In select runs, the biofilm was subjected to a continuous antimicrobial treatment for duration of 24 h, initiated after 64 h of growth. The minimum antibiotic concentration required to eradicate biofilms is first estimated, followed by estimation of largest antibiotic concentration that the biofilm is able to survive. These conditions are used to further investigate mechanisms of antibiotic resistance in biofilms. Small differences in the bulk antibiotic concentrations were amplified into much larger differences in local antibiotic concentrations to which cells are exposed.

These results indicate that small differences in the bulk concentrations of the antibiotic were amplified into much larger differences in local concentrations to which cells are exposed. This, in turn, triggers a transformation of certain cellular subpopulations from the dormant state to the metabolically active state, and that this transformation is a key mechanism of resistance, in the absence of quorum sensing. Biofilms associated with quorum sensing were more resilient to antibiotic treatment compared to non-quorum sensing strains, in part, due to the protective influence of exopolysaccharides matrix. Interestingly, under all conditions studied, a threshold antibiotic concentration was observed below which the biofilm lifetime was found to increase compared to the untreated biofilm. A clear understanding of heterogeneities at the local scale may be vital to solving the riddle of the persistence of biofilms to external stresses such as antibiotics. Overall, insights into these biophysical

mechanisms associated with the biofilm mode of growth may pave the way for novel therapeutic strategies to combat the antibiotic resistance of biofilms.

Advisor: Dr. Parag D. Pawar

Contents

List of figures

List of tables

List of Publications

[1] Lakshmi Machineni, Parag D. Pawar,

Bio Tech, March 13-15, 2015, IITKanpur; DOI 10.5176/2251-2489_BioTech15.37.

[2] Lakshmi Machineni, Parag D. Pawar

"A 3D Computational model to investigate the influence of spatial heterogeneity on the antibiotic tolerance of bacterial biofilms", Biomath, June 19-23, 2016, Blagoevgrad, Bulgaria. http://www.biomathforum.org/biomath/index.php/conference/article/view/694

[3] Lakshmi Machineni, Anil Rajapantul, Vandana Nandamuri, Parag D. Pawar, "Influence of nutrient availability and quorum sensing on the formation of metabolically inactive microcolonies within structurally heterogeneous bacterial biofilms: An individual-based 3D cellular automata model", Bull Math Biol. 2017 Mar; 79(3):594-618.

[4] Lakshmi Machineni, Vandana Nandamuri, Ch. Tejesh Reddy, Parag D. Pawar.

"An individual based model to investigate the influence of spatial heterogeneity on the antibiotic tolerance of bacterial biofilms", Mathematical Methods in the Applied Sciences, 2018 Mar; DOI - 10.1002/mma.4900.

Chapter 1. Introduction

1.1 Motivation

Before the 1950s, it was believed that microorganisms inhabited the planet predominantly in a suspended and free-floating planktonic form. It is now widely accepted that most bacteria found in natural, clinical, and industrial settings reside primarily in biofilms. A biofilm is a structured community of microbial cells that is irreversibly attached to a surface and enmeshed in a self-produced protective matrix comprised of extracellular polymeric substances (EPS). Biofilms can form on a wide variety of surfaces, including living tissues, indwelling medical devices, industrial or potable water system piping, or natural aquatic systems. Biofilm formation is known to be one of the microbial survival strategies because it provides bacteria with important advantages, including, (i) sequestration to a nutrient-rich area (colonization); (ii) protection against toxins and antibiotics; (iii) utilization of cooperative benefits (community), and (iv) shelter from predation and deleterious conditions. During the last few decades, biofilm formation by bacterial pathogens has attracted much attention, mainly in the medical and food processing fields, due to its potential risks, including extreme resistance to antibiotics, persistence, and virulence factor production [1-5].

In nature, ~ 99% or more of all bacteria are thought to exist as biofilms [6]. Biofilm formation is widely found in natural environments with water, and also in human diseases, especially in the patients with indwelling devices for the purpose of medical treatments [7]. With the progress of medical sciences, more and more medical devices and artificial organs are applied in the treatment of human diseases. However, as a consequence, infections associated with bacterial biofilms have become more prevalent. Biofilm-associated infectious diseases are now the second leading cause of death worldwide, causing ~17 million deaths every year [8]. In India, the infectious disease mortality rate is 416.75 per 100,000 persons and is twice the rate prevailing in the United States [9].

The important hallmarks of chronic biofilm-based infections are extreme resistance to antibiotics and an extreme capacity for evading the host defences [10]. For instance, Pseudomonas aeruginosa (P. aeruginosa) biofilms growing on a catheter irrigated with sterile artificial urine could withstand 1,000 µg/ml of tobramycin for 12 h, whereas planktonic populations were driven to eradication with 50 µg/ml within 6 hr of treatment [11]. Recent evidence suggests that the minimum biofilm eradication concentration (MBEC) of antibiotic required for biofilm-associated bacteria is ~100-150 fold higher compared to their planktonic counterparts [2, 12-14]. It has become increasingly difficult to discover new and effective antibiotics when those more prevalent in nature have already been discovered. As a result, today – many decades after the first patients were treated with antibiotics – bacterial infections have re-emerged as a key public health threat. Such infections often result in an increased number of hospitalizations, more treatment failures and the persistence of drug-resistant pathogens. Thus, a comprehensive understanding of biofilm development and survival mechanisms of clinically relevant microorganisms is highly desirable to reduce the risk of biofilm-related infections.

Over the last decade, much progress has been achieved in studying the growth-stage-specific physiology which may be important in detecting and controlling biofilms. Depending on local nutrient availability, within hours to days after the initial irreversible adhesion, the cell clusters progressively become stratified. Colonies then go on to form elaborate, heterogeneous structures with voids, and water channels [15]. A key factor in the efficiency and robustness of biofilms is their spatial organization [16]. A range of factors have been suggested to influence biofilm structure, including cell death [17], hydrodynamic shear [18, 19], quorum-sensing [20], and detachment [19].

Biofilms are known to employ a complex communication system – termed as quorum sensing (QS) – used to coordinate collective group behaviors based on population density. Bacterial cells constantly produce signaling molecules called autoinducers. At sufficiently high population densities, these signalling molecules reach threshold concentrations, leading to the upregulation or activation of genes involved in the production of EPS, and of toxins [21-23]. Each cell is in one of two states – up-regulated or down-regulated – between which it can

2

instantaneously switch, depending on the local autoinducer concentration [24]. Cells exhibiting enhanced EPS production in the presence of autoinducer molecules are said to be up-regulated. The EPS matrix provides several functional purposes for the biofilm, such as protecting bacteria from environmental threats, providing mechanical stability, and degrading macromolecules to be used by the cells [25, 26].

Microorganisms growing within biofilms display features distinct from their planktonic counterparts [1]. The more evident features common to all observed biofilms include genetic features and biophysical and cellular features [27]. Bacteria growing in biofilms are known to express genes different from those of planktonic cells. Expression of specific genes may allow biofilm bacteria to actively adapt to, and survive, external stresses such as, antimicrobial exposure [28-30]. These genetic features attribute resistance of the biofilm to antibiotic tolerance at the single-cell level [31].

Besides the genetic responses of biofilm microbes to external stresses, bacterial population displays multiple phenotypes with different functions during biofilm formation, due in part to their adaptation to local environmental conditions. They occupy a spectrum of growth states from rapidly growing and active to slow-growing and dormant [32]. Consequently, distinct microcolonies with microorganisms aggregated in clusters may develop within the biofilm where bacterial physiology is different from surroundings in terms of cell metabolic activity, EPS synthesis, concentrations of nutrient, and stress response. This intrinsic physiological heterogeneity inherent in the biofilm structure may contribute to the protection of cells. Experimental evidence suggests that it is only certain subpopulations within biofilms that show greatly increased phenotypic resistance totreatment, whereas the remaining cells exhibit sensitivity [29, 33]. The biophysical mechanisms underlying spatially non-uniform response of biofilms to antimicrobial treatment remain incompletely understood. A systematic investigation of the structural properties of these microcolonies within the biofilm, and their response to antibiotic treatment may shed light on the biophysical mechanisms of antibiotic resistance.

Because of the challenging experimental measurements and dynamic nature of natural biofilms, computational modelling of biofilms is an important tool to investigate the biophysical mechanisms of antibiotic resistance in bacterial biofilms. A computational model translates the conceptual understanding of the biofilm system into mathematical terms, usually by combining the important processes involved, and provides a qualitative as well as quantitative information about biofilm properties that are of interest, such as cell counts, cell viability, biofilm morphology and EPS structure, nutrient distribution, signalling molecules distribution as well as spatio-temporal variations in cellular metabolism during biofilm growth. In addition, in an experimental setting, it is difficult and sometimes challenging to separate the effects of different potential causes, e.g. to distinguish between shear induced and quorum sensing induced dispersal. In a mathematical modelling setup, it is easier to isolate particular aspects of a system. In this work, an individual-based 3D computational cellular automata model has been developed to simulate biofilm growth, and quantify heterogeneity as a function of growth phase, space, and time in response to antimicrobial agents, in the presence and absence of quorum sensing.

1.2 Scope of the work

Several models have successfully described the autonomous formation of tertiary macrostructures in bacterial biofilms [34-36], including the effects of EPS on biofilm structure [37]. These can be broadly classified into two categories: continuum models [34, 38, 39], and individual based models [40, 41]. In continuum models, the biofilm is considered to be a continuous medium, with porosity, surface shape, and density as input parameters. In contrast, individual based models treat bacterial cells as individual units with their own states, thereby allowing for variability between individual behaviours with respect to their growth rates, nutrient uptake rates, local nutrient concentration, signalling molecule production, up-regulation and down-regulation states, and EPS production. Consequently, chemical and structural heterogeneities within the biofilm emerge as a result of the actions and interactions of the cells with each other, and with the surrounding environment, rather than being a model input [40].

4

In earlier models, the cell density is assumed to be constant, thereby neglecting biofilm expansion that results from the production of new cells, and shrinkage caused by cell death and detachment. Recently, attempts have been made to use deterministic continuum models of quorum sensing in biofilms [42, 43]. Such models neglect the stochastic nature of the up- and down-regulation processes, and are unable to account for local heterogeneities in microbial subpopulations. However, to date, a single, comprehensive mathematical model that captures the interplay of all the above mentioned factors has not been developed. Equally importantly, a systematic analysis of the local structural and chemical heterogeneities in the biofilm interior has not been performed. An analysis of the spatial heterogeneity in bacterial growth rates could shed light on mechanisms of the emergence of dormant microcolonies containing cells that are potentially antibiotic-insensitive.

The goal of this study was to investigate the influence of the biophysical mechanisms of the biofilm mode of growth on antibiotic resistance, when each individual cell itself is not necessarily tolerant to antibiotics. I also wished to correlate the inherent spatial heterogeneity of biofilms at the cellular level to their heterogeneous response to treatment. Consequently, in this model, each bacterium is modelled as an independent entity, allowing us to monitor structural and chemical heterogeneities in the biofilm and in its response to treatment as a function of time and space.

To simulate behavioural variability, parameter values for individual bacterial cells were obtained by random draws from a uniform distribution with $\pm 10\%$ variation. The resulting aggregate behaviour of the biofilm is therefore emergent from the local interactions between the individual bacteria, and their surroundings, thereby allowing us to simulate the self-organized process of biofilm formation. Biofilm development was simulated under varying bulk nutrient concentrations (1-8 gm^3), in the presence and absence of QS. The simulations show that nutrient limitation, in the absence of genetic triggers, can account for the formation of microenvironments containing dormant, low-activity cells surrounded by high-activity ones.

5

Since the model simulates spatiotemporal variability of biofilm constituents (such as biomass, EPS, nutrient, and signalling molecules), it may be instructive to correlate antibiotic-resistant of bacterial biofilms with the emergence of metabolically inactive cell clusters. In select runs, the biofilm was subjected to a continuous antimicrobial treatment ($C_{ab,bulk}$ ranging from 15 to 60 gm^3) for duration of 24 h, initiated after 64 h of growth (cell number ~10,000). The minimum antibiotic concentration required to eradicate biofilms is first estimated, followed by estimation of largest antibiotic concentration that the biofilm is able to survive. These conditions are used to further investigate mechanisms of antibiotic resistance in biofilms. Small differences in the bulk antibiotic concentrations were amplified into much larger differences in local antibiotic concentrations to which cells are exposed.

During the initial stages of treatment, the proportion of the fast-growing, metabolically active subpopulation decreases due to exposure to the antibiotic. This results in an increase in the nutrient availability to the dormant cells in the inner regions of the biofilm. I propose that this triggers a transformation from the dormant state to the metabolically active state, and that this transformation is a key mechanism of resistance.

Biofilms associated with QS-positive strains were more resilient to antibiotic treatment compared to non-QS strains, due to the protective influence of EPS. Interestingly, under all conditions studied, a threshold antibiotic concentration was observed below which the biofilm lifetime was found to increase compared to the untreated biofilm. Overall, insights into these biophysical mechanisms associated with the biofilm mode of growth may pave the way for novel therapeutic strategies to combat the antibiotic resistance of biofilms.

1.3 Thesis objectives

The goal is to answer the following specific questions:

(i)   Can physical processes like nutrient starvation and localized cell death account for the formation of metabolically inactive microcolonies in biofilms, in the absence of genetic triggers?

(ii)   How does quorum sensing – and the associated EPS production – influence the structural heterogeneity of the biofilm?

6

(iii)   Do local physiological and chemical heterogeneities in the biofilm influence the spatially heterogeneous antibiotic resistance in the absence of genetic triggers?

(iv)   What role does EPS play in the heterogeneous response of the biofilm to antibiotic treatment?

(v)   What roles do biophysical and cellular processes play in enhanced biofilm formation in response to treatment with sub-lethal doses of antibiotics?

1.4 Thesis overview

In chapter 2, physics related to biofilm formation process, and growth dynamics are introduced. In addition, a comprehensive literature on experimental investigations on the heterogeneous response of biofilms to antibiotic is presented. Factors such as, influence of nutrient conditions, quorum sensing, EPS production, spatial heterogeneity, and subminimal biofilm eradication concentration (sub-MBEC) of antibiotic have been considered. Further, an overview of the computational models (individual-based and continuum models) used to predict biofilm behaviour and antibiotic resistance mechanisms are included.

In chapter 3, a detailed description of the geometry and sub-domains of the model biofilm system, and the biological processes implemented is provided. In chapter 4, findings pertinent to the effects of nutrient concentration and cell-cell signalling on the formation and development of biofilm are presented. Chapter 5 deals with the biofilm antibiotic resistance mechanisms; in particular the influence of sub- inhibitory concentration of antibiotic and spatial heterogeneity on reduced susceptibility is described. Suggestions for future work are presented in chapter 6.

Chapter 2. Literature Review

2.1 Biofilm formation and growth dynamics

The process of biofilm formation in response to external stresses occurs through a series of events leading to adaptation of bacteria to distinct environmental conditions. Biofilm formation is a dynamic self-assembly process in which free-floating bacterial cells undergo specific changes after anchoring to a stationary substratum, thereby mediating the spatial and temporal reorganization of the bacterial cells (Figure. 2.1) [30, 44].

Bacteria growing in biofilms differ from their planktonic counterparts in-terms of generation of EPS matrix, cell migration, subpopulation differentiation and interactions, and the up- and down- regulation of specific genes [3]. Biofilm processes which are physical, chemical, and biological in nature, occur over a broad range of time scales. While the characteristic time for the transport of nutrients is on the order of milliseconds, some other crucial developments, such as bacterial cell growth, division, death and detachment, take place over the course of hours to days [30].
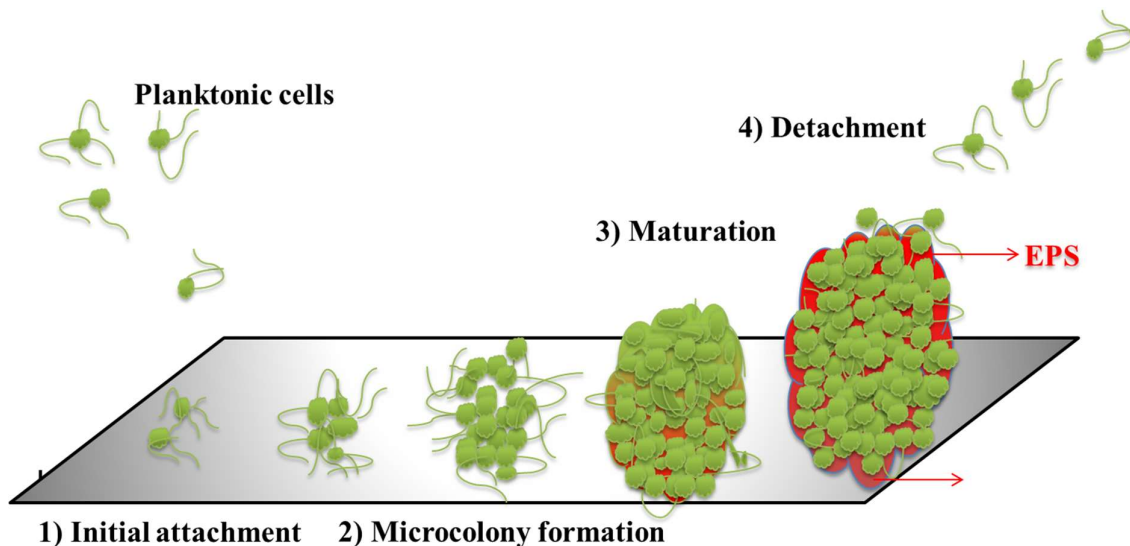
Figure 2.1. Stages of biofilm formation: (1) initial attachment, (2) irreversible attachment, (3) maturation, and (4) dispersal.

The process of biofilm formation involves the following stages:(1) attachment of free floating cells to a substratum(2) colony formation, (3) 3D structure formation and maturation, and (4) detachment [30].

2.1.1 Attachment

During initial attachment, free-floating bacteria attach to 1) physical surfaces, or 2) biological tissue, or 3) surface attached microbes via the locomotor structures present on cell surfaces such as flagella, pili, fimbriae, or proteins. This initial attachment is reversible, since some viable cells detach during this stage or attach only briefly [45]

2.1.2 Colony formation

Next, adhering bacteria become irreversibly attached through strong dipole–dipole forces, covalent ionic bonding, and hydrophobic interactions. Bacteria adsorbed on the substratum consume locally available nutrients and form into small colonies which are tens or hundreds of microns in diameter [46]. Formation of these small colonies leads to chemical communication between cells, termed QS. This further stimulates EPS synthesis [47]. QS is a system of stimuli to co-ordinate gene expression with other cells, and responses related to the density of their local population. EPS encapsulates the bacterial cells, forming a physical barrier, and shelters the microbial community from harsh external conditions, like antibiotic therapy [48].

2.1.3 3D structure formation and maturation

In the next stage of biofilm development, expression of biofilm-specific genes occurs. In time, by continual cell division and EPS production, a contiguous multicellular population evolves into complex and heterogeneous 3D structures. These structures typically exhibit mushroom-shaped architecture, filaments, and finger-forms with voids and water channels. Researchers have proposed that these water channels are like circulatory systems, distributing different nutrients to the cells in the micro-colonies of the biofilm [49].

2.1.4 Detachment

Lastly, dispersal of single cells or sloughing of cell clusters is believed to be crucial for the spreading of bacteria to new infection sites in the human body. Detachment events can lead

to the acute exacerbations observed in persistent, chronic infections. For instance, the dispersal of biofilm population provides to P. aeruginosa an opportunity to colonize new zones or niches and, thus, perpetuate infection, particularly ventilator associated pneumonia [47, 50].

Biofilm accumulation is determined by the balance of attachment, growth, and detachment processes. Some cells actively detach from the biofilm matrix as free-floating bacteria and they may adsorb on new surfaces and form biofilms in new environmental niches. While occurring continually at low levels, dispersion of biofilm population is thought to be induced as a response to environmental changes including nutrient limitation, low oxygen levels, and alterations in pH. The developmental life cycle comes full circle when dispersed biofilm cells revert to the planktonic mode of growth [15].

2.2 Bacterial growth dynamics and antibiotic resistance mechanisms

2.2.1 Nutrient concentration

Several experimental investigations have shown that growth of microorganisms in a nutritionally limiting environment is known to promote the transition from a planktonic to a surface-attached multi-cellular community, while nutritionally-rich environment tend to produce biofilms that are thicker and denser [51, 52]. Paul Stoodley's group visualized growth of discrete cell clusters in mature P. aeruginosa biofilms by using digital time-lapse microscopy. They have demonstrated that a biofilm could change its morphology from flat ripples and streamers to densely packed mound-like structures when the nutrient concentration was increased tenfold. These more densely packed P. aeruginosa and Pseudomonas putida biofilms formed at high nutrient concentrations had a greater tendency to slough off the substratum than did the ripples and streamers formed at lower concentration [53, 54]. It is possible that as more nutrients accumulate, more biofilm cells are produced and the conditions become unfavourable for interior cells due to concentration gradients within the biofilm, eventually resulting in detachment of the biofilms at high nutrient levels. At the other extreme, Stoodley also showed that the rate of detachment of cells from Aeromonas hydrophila biofilm was also increased by nutrient limitation [55]. So

10

perhaps either too much or too little nutrient predisposes to detachment. Nevertheless, there is ample experimental evidence supporting that, at least in vitro, nutrient conditions and detachment are associated [52, 55, 56].

Detachment stage is characterized by the observation of bacterial clusters that move away from the biofilm core leaving hollow structures or voids [52]. Formation of cavities or voids that determine the sloughing process exists due to insufficient nutrient concentration at the bottom interface to maintain bacteria alive. Thereby active cells atop may lose contact with the substratum and slough off. Several recent studies have reported that nutrient starvation induced cell death inside biofilm plays a key role in the differentiation and dispersal of surviving biofilm cells [57, 58].

Experimental evidence using Acinetobacter baumnnii as a model strain shows that the nutrient concentration influences adherence ability and morphology of the microorganism. Initially, reduced nutrient concentration promoted the development of small cocci, which formed the biofilm. Subsequent increases in nutrient levels resulted in division and the production of rod forms, which spread over the surface [59]. All these studies imply that, modification of nutrient levels is important to prevent biofilm formation of clinically important pathogens.

Furthermore, the role of nutrient availability in determining the local spatial heterogeneity in metabolic activity of microorganisms in biofilms was also presented. For instance, stratified patterns of growth were shown in P. aeruginosa biofilms. Active and fast growing cells in mature P. aeruginosa biofilm were restricted to a narrow band in the part of the biofilm adjacent to source of nutrient, while inactive and not growing cells due to nutrient starvation were restricted in the biofilm interior [60]. Even in the very early stages of biofilm growth, heterogeneity in growth rates which emerge from (and influence) spatial gradients in nutrient concentration have been shown [61]. Interestingly, such physiological heterogeneity has implications for microbial ecology and for understanding the reduced susceptibilities of biofilms to antimicrobial agents. Several recent papers have reported the relationship between physiological heterogeneity of growth and reduced susceptibility [60, 62]. For

example, while studying the properties of antibacterial resistance in detached large cell cluster or in stationary-state biofilms starvation induced dormancy is the common underlying mechanism for protection against biocides [63]. In thickP. aeruginosa biofilms, cells are physiologically distinct spatially, with cells deep in the biofilm in a viable but antibiotic-tolerant slow-growth state [64].

Collectively, these experimental investigations have shown the direct influence of nutrient accessibility on growth dynamics and physiological heterogeneity of growth within a biofilm. A more clear analysis of impact of nutrient concentration on the formation of inactive microcolonies that show significant resistance to treatment is crucial to discover new approaches to control biofilm formation in both medical and industrial settings.

2.2.2 Quorum sensing

Bacterial cells growing in biofilms "talk" with each other by releasing, sensing and responding to small diffusible signal molecules called autoinducers (AIs) to regulate their cooperative activities and physiological processes through a mechanism called QS. AIs accumulate in the environment as the bacterial population increases, and cells monitor this information to track changes in their number and collectively alter gene expression. QS controls genes that direct activities that are beneficial when performed by group of bacteria acting in synchrony [65]. Activates controlled by QS include biofilm formation in several opportunistic pathogens, EPS synthesis in P. aeruginosa [66, 67], induction of virulence factors inS. aureus [68], sporulation in Bacillus subtilus, competence development in Sterptococcus mutants, and bioluminescence in Vibrio cholera biofilms [23, 69, 70].

Cells in states of high and low AIs production described as being up-, and down-regulated, respectively. Each cell is in one of two states – up-regulated or down-regulated – between which it can instantaneously switch. In an up-regulated state they typically produce the signalling molecule at increased rate compared with down-regulated state. Up-regulated sub-population can spontaneously down-regulate, and it results in low levels of gene expression. The switch-over from up-regulated state to down-regulated state and/orvice versa occurs in response to local autoinducer concentrations [22]. For instance, the net result

of quorum sensing regulatory cascade in mature biofilm of S. aureus is up-regulation of secreted virulence factors such as α-toxin, and down-regulation of surface virulence factors, such as protein A [71].

The positive correlation between quorum sensing and EPS, and EPS interactions with the physio-chemical environment of clinically-relevant bacteria has brought together a large group of biologists interested in bacterial group dynamics. For instance, in a Pantoeastewartii biofilm, approximately ten-fold increase in EPS production per up-regulated cells than down-regulated cells upon quorum sensing induction was discovered by the experiments in [72]. The EPS matrix is responsible for the integrity of the three-dimensional structure of biofilms, cementing cells together and onto substratum [73]. Biofilms produced by quorum sensing and quorum sensing mutant of P. aeruginosa strain, have been used to determine the role of polysaccharides in biofilm development. Fluorescent micrographs of two biofilms revealed that the quorum sensing controlled biofilms were much thicker than those of the quorum sensing mutant [74]. Staining with alcian blue used to bind polysaccharides, quorum sensing P. aeruginosa cells appeared to be embedded in an EPS matrix; where most bacterial cells were at the top layers, whereas the bottom layers occupied predominantly with polysaccharides. The quorum-sensing-deficient mutant biofilms were closely packed with cells only [47].

Furthermore, the EPS matrix also provides protection for the biofilm cells from deleterious environmental conditions like antibiotic therapy. Recent findings from [25] suggested that EPS harvested form Acinetobacter baumannii biofilms act as a "universal protector" by inhibiting tobramycin activity against bacterial cells regardless of species. By using fluorescent labelling of antibiotics, alginate was shown to shield biofilm population from effective killing by hindering the diffusion of tobramycin at the periphery. Studies of EPS-producing (mucoid) and non-EPS producing (non-mucoid) S. aureus biofilms found that the mucoid strain exhibited profound resistance to aminoglycosides [75]. The mucoid phenotype P. aeruginosa isolated from the lungs of CF patients found to overproduce alginate. The contribution of QS regulated EPS production to biofilm architecture and resistance have been shown to vary depending on specific growth stages during biofilm formation [76]. However,

the exact mechanism of the EPS-antibiotic interaction is still unclear; with some investigations supporting non-charge-based interactions [77] while others supporting an ionic interaction [78]. The inhibition of quorum sensing by using quorum sensing inhibitors (QSI) to potentiate the effect of existing antimicrobial agents is an encouraging alternative to the development of new antibiotic formulations. QSI Hamamelitannin increases the antibiotic susceptibility of S. aureus biofilm towards vancomycin by affecting EPS synthesis [79].

Collectively, these experimental investigations highlight the role of quorum sensing signalling in EPS production in biofilm formation, and involvement of EPS in reduced susceptibility of biofilms. However, bacteria growing within biofilms are physiologically heterogeneous, in part because of their adaptation to existing chemical concentration gradients. Heterogeneity in growth rates within biofilms emerge from nutrient concentration gradients can result in spatial gradients in quorum sensing signalling and EPS synthesis. Importantly, spatial gradients in signalling molecule production parallel this heterogeneity in EPS, may play a role in heterogeneous response of the biofilm to antibiotic treatment. Therefore, investigations about the impact of quorum sensing, and the associated EPS production on structural heterogeneity of the growing biofilm under different nutrient conditions, and conversely role of EPS in the heterogeneous response of the biofilm to antibiotic treatment is required.

2.2.3 Spatial heterogeneity

A major challenge in biofilm research is the intrinsic heterogeneity in the biofilm structure, such as non-uniform distribution of the biomass, nutrients, and intercellular signalling, which leads to temporal and spatial variation in microbial metabolism and gene expression. Interestingly, previous investigations have shown that phenotypic variation of bacterial community could contribute to increased antibiotic resistance of biofilms [62, 80, 81]. On the other hand, important features associated with biofilm growth mode including, expression of genes involved in the general stress response [82], induction of biocide efflux pumps [83], and adaptive stress response [84] could also confer resistance to antibiotics [31]. However, since combinations of these features are at work, it is still difficult to fully understand the mechanisms of biofilm resistance to antibiotics.

Expression of specific genes may allow biofilm bacteria to actively adapt to, and survive, external stresses such as, antimicrobial exposure. For instance, the ndvB and tssC1 locus has been identified as P. aeruginosa biofilm-specific antibiotic resistant genes [85]. In response to antibiotic therapy, induction of biocide- efflux pumps contribute to the transition of biofilm cells to a relatively protected and distinct phenotype. For example, it has been demonstrated that expression of MexAB-OprM pump differs among P. aeruginosa biofilm populations, being maximum in cells located near the substratum, exhibit increased resistance to aztreonam, gentamycin, tetracycline, and tobramycin [86]. These genetic adaptations contribute to resistance of individual-bacteria growing in biofilms.

Besides the genetic responses of biofilm microbes to external stresses, physiological heterogeneity in biofilm subpopulation considered as one of the important adaptive mechanism of P. aeruginosa species within airways of lungs in patients with cystic fibrosis [50]. During recent years, the experimental investigations that are used to visualize microscale heterogeneity within biofilms have advanced greatly. For instance, selective green fluorescent protein (GFP) labelling P. aeruginosa biofilm cells shown that - cells at the top of the biofilm were rapidly-growing had high mRNA content, while mRNA levels for slowly-growing cells were low due to long-term anoxia [62]. Similarly, authors in [87] found that energy status of living cells -- based on adenylate concentration-- continuously changed all over the biofilm, indicating that metabolic functioning of cells within the spatially structured community exhibit heterogeneity. Spatial and temporal stratification in bacterial respiration and protein synthesis can also occur as a response to chemical gradients. For example, chemical concentration gradients of the nutrients in Klesbsiella pneumoniae and P. aeruginosa biofilms have been experimentally demonstrated by microelectrode technology. Nutrient concentration decrease at the bulk-liquid -biofilm interface, and get further depleted in the biofilm interior or near substratum [88].

Using tools such as the scanning electron microscope and, more recently, the confocal laser scanning microscope, biofilm researchers now confirmed the presence of spatially scattered antibiotic sensitive subpopulations within biofilms. For instance, antibiotic tobramycin specifically killed cells at the outer portion of the P. aeruginosa biofilms, while other biocides

including, colistin, sodium dodecyl sulfate, and gallium were effective on cells in the interior portion. Antibiotics that are known to effective against metabolically active cells actually interfere with fundamental physiological processes of bacterial cells, such as replication or translation. In stark contrast, biocides effective against metabolically inactive cells actually interfere with bacterial membrane structure and function, while active cells at the outer layer of the biofilm survive the treatment due to their ability to induce adaptive stress response associated with molecular system [89]. By using selective GFP labelling and cell sorting techniques, authors in [90], shown that cells at the bottom of the thick P. aeruginosa biofilm are in a slow-growth state and had reduced sensitivity to the antibiotic ciprofloxacin. Along the similar lines, a study of a dose-response killing of P. aeruginosa biofilms by the quinolones, ofloxacin and ciprofloxacin showed that the most of the cells were effectively killed by low concentrations of antibiotics, which is not much different from what was observed with planktonic cells. However, after an initial 3-to 4-log drop of bacterial cells in biofilm, a further increase in antibiotic concentration had zero effect on killing [91].

Taken as a whole, these experimental investigations reveal that it is only subpopulation of the cells that have increased resistance and protect biofilm from killing for later resuscitation when nutrients or space become available. While spatial heterogeneity in the biofilms is clearly important to selection of therapy for biofilm-related infections, little information is available on the way in which local environmental conditions influence the spatially heterogeneous antibiotic resistance? Because biofilms constitute a privileged way of life for bacteria, a clearer understanding of the processes involved in their marked resistance to disinfectants is of crucial importance for their control. Specifically, it is important to determine the role of limiting nutrients in the establishment of physiological gradients in the absence of genetic triggers to understand mechanisms of recalcitrance.

2.2.4 Subminimal biofilm eradication concentration (sub-MBEC)

Consider the empirically derived minimal biofilm eradication concentration (MBEC): according to National Committee for Clinical Laboratory Standards (NCCLS) guidelines, MBEC is the lowest concentration of an antimicrobial agent that results in the lowering of the number of live cells by $\leq 99.99\%$ after an overnight incubation under growth conditions [92]. Though sub-MBEC of antibiotics can inhibit biofilm formation, it is known that they

are not able to kill bacteria. On the other hand, numerous studies have found that, when present at concentrations below the MBEC, antibiotics can significantly induce biofilm formation in a variety of bacterial speciesin vitro [93-95]. This process may have clinical relevance because bacteria are exposed to low concentrations of antibiotics at the beginning and end of the dosing treatment or in case of continuously low doses therapy.

Subminimal biofilm eradication concentration of antibiotics namely, tobramycin, tetracycline, and norfloxacin caused significant increase in the expression of genes -- up to 7% of 555 genes in genomic array -- relevant for colonization and further stress response ofP. aeruginosa biofilms [96]. Biofilms became stronger instead of weaker when resistance is challenged with sub-MBEC. For instance, the cell wall-active antibiotics cephalothin and cephalexin [97, 98], and the protein synthesis inhibitor linezolid [99] at sub-lethal concentrations, usually$\leq$ $1/2\times$MBEC, enhanced S. aureus biofilm formation as much as 4-times on medical devices and tissues. Moreover, it is possible that enhanced biofilm formation by cells in response to sub-lethal concentrations of antibiotic may foster genetic exchange between cells and contribute to the spread of genes encoding resistance to antibiotics. The study in [100] showed $1/4$ MBEC of β-lactams induced alg gene that results in 10-fold increase in EPS synthesis, which in turn results in biofilm persistence, and extremely difficult to eradicate, even with very aggressive antibiotic therapy.

The outcome of above summarized studies suggests that sub-MBEC of biocides use leads to the adaptation and development of resistant bacterial population resulting in treatment failure, extended periods of hospital care, increased costs of medication, and increased morbidity. Therefore, stress the importance of maintaining effective bactericidal concentrations of antibiotics to fight biofilm-related infections is necessary. In addition, physiological heterogeneity may play a key role in induced biofilm formation and resistance in response to treatment with sub-MBEC. Importantly, earlier studies also highlight the need to investigate the reasons for survival of biofilms in response to sub-MBEC treatment of antibiotics may help delineate biophysical mechanisms of antibiotic resistance.

2.3 Mathematical models of bacterial biofilms

Parallel to experimental investigations, increasingly complex mathematical models and simulations continue to be developed to explain the formation, development, structures, and interactions of biofilms. The ability to perform in situ visualization of individual micro-colonies within a biofilm has fuelled the creation of biofilm models that reproduce biofilm growth dynamics and interactions. Due to the challenging experimental measurements and dynamic nature of natural biofilms, mathematical modellers are trying to explain the physical and biological mechanism to determine how biofilm grow and how they contribute to increased antibiotic resistance by numerical simulations. Moreover, the flexibility offered by modelling and because of the potential to integrate a multitude of processes into a single computational unit, mathematical modelling is becoming a more important tool in biofilm research. Mathematical framework that describes bacterial biofilms formation over the past years have greatly contributed to our understanding of physio-chemical and biological principles of biofilm spreading dynamics, which are take place across a broad range of time and length scales [41, 58, 101].

Modelling studies come in many forms which range from simple 1-D correlations to sophisticated 3-D algorithms that describe how a biofilm develops. Starting in the 1970s, couple of mathematical models were implemented to understand the growth source utilization for biomass growth and mass transport, namely diffusion. The important idea of these earlier models was to explain processes that generate chemical gradients emerge within the microcolony of single growth-limiting substance. Although these investigations presumed the simple geometry and homogenous biomass distribution, they revealed the key phenomenon that local nutrient availability in the biofilm interior decrease over time. The models have taken averaged nutrient gradients are in 1-D, perpendicular to the solid support on which the biofilm is allowed to grow [102, 103]. In the 1980s, models expanded to include heterogeneous distribution of different species biomass inside the biofilm, but these models continued with 1-D geometry [104]. A key idea behind these models was to elucidate the overall flux of nutrient and metabolic products through liquid- biofilm interface.

The visualization of 3D features of biofilms in recent years using advanced fluorescence laser scanning microscopy has elicited the development of sophisticated and computationally-intensive models in which the 3D complex structures of the bacterial clusters are simulated. Starting in the 1990s, mathematical models are being developed to investigate the influence of physical, chemical, and biological factors that drive the formation of 2D and 3D biofilm structures. Thus, all features can be quantified in multi-dimensional space, as well as time and generate realistic complex physical and ecological structures [36, 58, 105, 106].

The heterogeneity of biofilm structure and the interdependence of physical, chemical and biological processes occurring at different time and space scales make mathematical modelling of biofilm growth and structure a special challenge for researchers. Although there are many different ways of relating mathematical models to natural systems, biofilm models are mainly divided into two main categories: Continuum models and Individual based models. Individual-based and continuum models differ in the approach used to handle biomass.

2.3.1 Continuum models

Despite the fact that continuum models generate results in agreement with experimental observations, continuum approach present the biomass distribution globally rather than the micro-structure [38, 39, 107, 108]. In this approach, local changes in biomass are averaged into a continuum body, thus behaviours of all individuals are evaluated according to same rules based on methods like volume averaging are used instead of the individual cell representation. Since, continuum models do not take directly into account the behaviour of individual microorganisms as they treat biomass as a unicuum, based on population-averaged behaviour of different properties. Therefore it is difficult to maintain and measure physiological heterogeneity of the bacterial cells growing within biofilm.

Because of the dependence of biofilm structure features on biomass growth, division, and detachment, a robust computational model requires the ability to predict population behaviours at single cell resolution.

2.3.2 Individual based models

In contrast to continuum modelling approach, the individual based approach seems to be very appealing to microbiologists because it allows individual variability and, by treating bacterial cells as the fundamental units with their own state and behaviour [40, 109]. Consequently, structural and chemical heterogeneities within the biofilm emerge as a result of the actions and interactions of the cells with each other and with the surrounding environment, rather than being a model input Thereby, it allow variability between individual cell behaviours with respect to their growth rates, nutrient uptake rates, local nutrient concentration, signalling molecule production, up-regulation and down-regulation states, EPS production, and antibiotic concentration fields etc. [106]. In order to determine the increasing resistance of bacterial biofilms towards antibiotic agents, it is important to understand this physiological heterogeneity.

The benefit of using individual based approach can account for individual cells behaviour to their environmental conditions, so the evolution of the whole system arises from the dynamics that govern each cell rather than imposed precondition. In addition using individual based approach, more local rules are easily added to understand more processes, such as sloughing and cell death, biomass heterogeneous nature, and local chemical concentration gradients across the biofilm. Such local rules motivated from biological principles, instead of analysis from a mathematical and physical framework. Therefore, during the last decade, the IbM approach has been widely used to predict several structural features of microbial biofilms and the results match experimental observations [41, 110, 111].

2.4 Modelling of biofilm structures

Several biofilm growth models have been introduced to predict the effects of various processes such as, cell death, detachment, and chemical gradients on biofilm development. It has been shown that actively growing biofilms develop steep nutrient gradients within the interior resulting in cell death and sloughing of large sections of the biofilm. These nutrient gradients cause the formation of two distinct regions of cell growth activity within the developing biofilms: metabolically active and inactive cells. This metabolic heterogeneity in growth rates arise due to nutrient consumption by cells located on the periphery of biofilm colony and

decreased diffusion of nutrients through the biofilm starve cells located in the interior [58, 106, 111]. While, this spatial physiological heterogeneity of growth within biofilms is known to decrease susceptibility of bacteria to antibiotics, but as yet biofilm models have not advanced any further to incorporate such new information. In addition, those two models, have focused on 2D model of the biofilm, data obtained from which may not be physiologically relevant. Because a 2D geometry probably misses out the following morphological features of biofilm: areal porosity, horizontal diffusion gradients. Also the biomass contact rules in 2D system overestimate the rate at which detachment events will occur. In the context of generating biofilm structures that better reflects a more realistic distribution of bacteria, the 3D geometry appears to be better choice for accurate quantification of biofilm morphological features, like biomass, thickness, and diffusion coefficients etc.

The individual based approach introduced by Kreft et al. [109] has been used later to test several evolutionary and ecological hypotheses. Recently, 3D individual based models have been developed to investigate the influence of localized cell death [58], biomass detachment mechanisms [111], and concentration profiles [110] on biofilm growth dynamics and morphology. However, these models focus much more on specific aspect of physical processes than intercellular processes (cell-cell communication/QS, EPS production).Representing EPS as individual particulate entity allow simulating different types of matrix components, such as DNA or proteins that are possibly produced by bacteria.

In 2006, Anguige, King, and Ward developed a 1D deterministic continuum biofilm growth model which included EPS production as a function of quorum sensing signalling molecules during initial stages of biofilm growth under slow flow regimes [112]. Thereafter, a 2Ddeterministic continuum models investigated the influence of quorum sensing on architecture of the biofilm in hydrostatic environment, where EPSis not clearly included but implicitly subsumed in the variables that describe bacterial biomass [108] The QS biofilms rapidly change from a state of cell growth to a state of EPS production; in other words, quorum sensing is used as a signal for the biofilms to switch from a colonization mode to a protection mode [107].

QS process is first included in an IBM by Nadell [22] - this deterministic model suggested that repressing EPS secretion facilitate QS biofilm dispersal. Recently, a 2D deterministic individual based model is used to reproduce all the stages of Bacillus subtilis biofilm formation observed in laboratory experiments, but the model assumed that, transition from the non-matrix producer to the matrix-producer phenotype is irreversible [41]. Since biofilm population density modifies the nature of QS process which cannot be captured by the simplicity of a deterministic models, new theoretical approaches with stochastic nature in cell switch between up and down regulation is necessary.

However, to date, a comprehensive 3D model that describes the effect of physiological heterogeneity and QS on biofilm growth dynamics with the aim of elucidating reduced susceptibility of biofilms growing in various nutrient conditions has not been investigated yet.

2.5 Modelling antibiotic resistance

Many 1D and 2D mathematical models have been developed to simulate and elucidate the increased antimicrobial resistance of microbes in biofilms [35, 113-118]. It has been suggested that nutrient limitation in biofilm results in diminished bacterial growth rate and this physiological change account for the reduced susceptibility to antibiotic agents. Using a deterministic mathematical model, Szomolay and colleagues have shown that reaction-diffusion-limited penetration of antibiotic allow transition of bacteria in deeper portions of thick biofilm to adapted physiological state, which is highly resistant state to the antibiotic [114]. However, these models assumed that biofilm neither grows nor detaches, and biofilm geometry is a flat slab with constant total cell density. This simplification is insufficient in the cases of sub-MBEC antimicrobial agents or abundant availability of nutrients or other growth promoters e.g. oxygen for aerobic biofilms.

During last two decades, numerous computational models have been implemented and concluded that antibiotic resistance is modulated by multiple factors, including, persisters, nutrient starvation, antibiotic concentration, and neutralization of antibiotic. Persisters are a small fraction of quiescent bacterial cells that survive lethal antibiotics or stresses but can regrow under appropriate conditions. Mark E. Robertset al.'s developed a 1D model to

22

investigate the biofilm survival upon antibiotic challenge due to 'persisters'. Fraction of persister cells are increased in nutrient-limited region and associated with reduced susceptibility [117]. The rate of killing by the antibiotic is assumed to be proportional to the local metabolic activity of cells. Zones of no growth or zero metabolic activity are found within the biofilm due to nutrient limitation and subsequently scattered and assorted spatial patterns of killing occurred. The model is later included a hypothetical damaged cell state, which is nonviable but still consume nutrient [118]. Cogan, Cortez, and Fauci predicted the influence of antimicrobial agent concentration and different dosing strategies on biofilm resistance using 2D model. This model showed that exposing the bacterial clusters to low antibiotic concentration for longer time is profoundly effective than short time dosing with high concentration [115].

A variety of multidimensional mathematical models developed in recent years help to improve our understanding of biofilm antibiotic resistance mechanisms. For instance, a 3D solute diffusion model coupled with the cellular automaton principles by Hunt group shown that gradients in nutrient concentration cause corresponding gradients in the microbial growth rate and activity. This physiological heterogeneity contributes to the protection of biofilms [35]. But, this model assumed that dead bacteria physical presence imposes a resistance to the transport of chemical substances –substrate and antibiotic-- into the depths of the biofilm. In other words, dead cells shield their more deeply embedded living neighbours and retard the advance of the killing effects of the antibiotic as the deeply embedded cells in a state of nutrient deprivation. These investigations showed that dead cells are localized preferentially in the surface layers of the biofilm, where substrate concentrations is highest; while the slow growing and non-respiring bacteria are protected from antibiotic therapy because of their inactivity due to inadequate nutrient supply. However, one would expect that as the growing bacteria in a biofilm are killed, nutrients should penetrate the biofilm, which would influence growth of more deeply embedded cells and render them susceptible to antibiotic treatment. This is a reason to be skeptical of a biofilm defense based on nutrient limitation and slow growth.

In addition, previous models assumed that, the rate of persister cell formation was simply taken to be directly proportional to the live cell concentration. This simplification is unreasonable particularly in the stage of increased local nutrient availability during treatment period, and also do not account gradients in microbial growth rate [62, 119]. Moreover, presence of dead cells also reduces antibiotic penetration into the biofilm, which would results a greater chance of surviving the treatment than actual survival due to penetration limitation.

Several 3D individual based models help for better understanding of biofilm formation[34] and no systematic research has been carried out to elucidate the antibiotic susceptibility of biofilms in the presence and absence of quorum sensing-regulated EPS matrix. Since, EPS distribution prevent the effectiveness of lethal dose from entering cells, it seems reasonable to investigate how quorum sensing associated EPS secretion modulates bacterial susceptibility to antibiotics. In contrast to the abundant experimental literature on function of polysaccharides in biofilm-associated antibiotic resistance, reports on mathematical modelling of EPS as an important factor which contribute to the survival of biofilms are scarce.

Despite the clinical relevance of biofilms, there is still limited knowledge on the key factors behind their heterogeneous response towards antibiotic agents. In this regard, development of a comprehensive model to clarify biofilm growth dynamics, and particularly to evaluate the key features -- including, physiological heterogeneity and quorum sensing related EPS – that contribute to the survival of subpopulation of cells in biofilms growing in different environmental conditions. Understanding the protective role of spatial-temporal heterogeneity would be beneficial to treating biofilm-related infections or diseases by offering clues to strategies that might be used to counteract or bypass biofilm protection.

24

Chapter 3. Computational Methods

3.1 Biofilm compartments and entities relevant to modelling

1. Compartments—are the different domains of the biofilm system; for example nutrient reservoir, biomass domain, diffusion boundary layer, and substratum.

2. Within each compartment or element, solid and liquidentities or components such as biomass, nutrient, EPS, and autoinducer molecules would exist.

3. These entities can undergo transformation, transport, and transfer processes. For instance, as nutrient is consumed by cells, which results in the bacterial cells growth and division.

4. All processes influence each entity in each compartment are combined together mathematically- into a mass balance equations that include rate terms and parameters for respective biological and physio-chemical process.
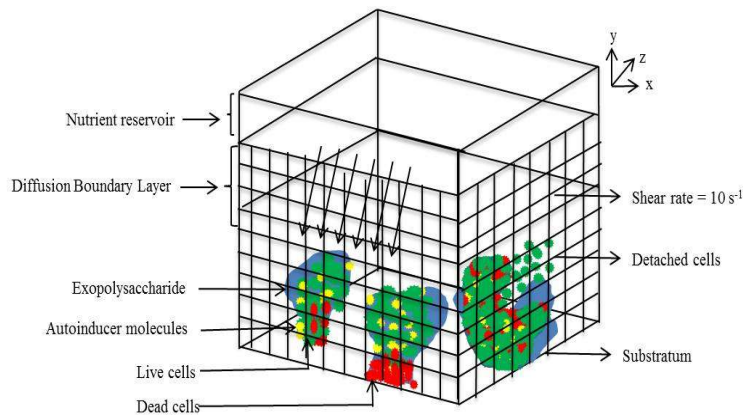
Figure 3.1. The simplified schematic of biofilm model showing geometry and domains of the model, and the biological processes implemented. Bacterial cells, EPS, nutrient, and autoinducer molecules coexist with each other in the same cubical element. Arrows indicates the direction of nutrient diffusion.

3.1.1 The substratum

The living or non-living surface on which the biofilm develops is called the substratum[120]. In this model, an inert and impermeable planar surface is chosen as substratum, and initially, at time t = 0 h, six bacterial cells are randomly colonized on the substratum. The substratum at the bottom forms the system boundary.

3.1.2 The biofilm compartment

The biofilm compartment domain contains both solid and liquid entities. The solid entities include live cells, dead and detached cells, and EPS; whereas liquid entities include nutrient, autoinducer molecules, and antibiotic. This 3D- individual based model track each of the solid and liquid entities individually instead of treating everything within the biofilm domain as only one solid-like entity broadly termed as "biomass" as in continuum models.

3.1.3 The bulk-liquid compartment

A bulk-liquid domain located above the biofilm compartment. Bulk-liquid domain can be very large as compared to the biofilm domain, such as for a biofilm developing on the sediment of a lake, or it can be a thin layer of water, as in a trickling filter. The simplest way to incorporate the bulk-liquid compartment is integrating it as boundary conditions for the biofilm domain. One very simple way to do this is to specify the concentrations of solutes in the bulk-liquid compartment [120].

3.1.4 The mass transfer boundary layer

Experimental observations have shown the presence of concentration gradients within and around the biofilm when dissolved entities are consumed (nutrient, antibiotic) or produced (autoinducer) by the bacterial cells in the biofilm. Consequently, the local chemical concentrations within the biomass domain are not the same as those in the bulk-fluid. Thus, the earlier simple boundary condition -- where solute concentration at the periphery of the biofilm is equal to bulk-liquid concentration -- is incorrect. Therefore, a new and more appropriate boundary condition is required, and it is achieved by creating another domain, known as diffusion boundary later (DBL) or mass-transport boundary layer (MTBL).

3.2 Model description

A 3D individual-based model has been developed to simulate the growth dynamics of a bacterial biofilm in response to treatment with antibiotics. Biofilm growth is simulated within the confines of a rectangular box. The bottom surface (square with side 120 μm) represents the inert substratum upon which the biofilm develops. Periodic boundary conditions are applied in the horizontal directions, thereby eliminating edge effects, and ensuring continuity of biomass [36, 121]. A continuously replenished nutrient reservoir is placed at the top at a distance of 18 μm from the substratum. The interface between the nutrient reservoir and the biofilm domain is termed the diffusion boundary layer (DBL). It is assumed that the DBL has a constant thickness of 18 μm, and remains parallel to the substratum in the low-flow regime considered in this work. For the flow regime considered in this work, the nutrient concentration at a vertical distance of 18 μm from the highest cell in the biofilm was greater than 95% of the bulk nutrient concentration, even at time points corresponding to the highest cell numbers. It is worth noting that at high velocities, the diffusion boundary could follow the surface of the biofilm, and may not be necessarily stratified as is assumed here [122].

The space between the DBL and the substratum is discretized into cubical elements of volume 27 μm^3 each. During the simulation, each element may be occupied by one or more of the following entities: (i) bacterial cell, (ii) EPS, (iii) nutrient, and (iv) autoinducer. These entities are assumed to be capable of coexisting with each other in the same cubical element. The simulation represents a time march in which the occupancy status of each element is updated at every time step. At time $t = 0$, six cells, termed colonizers, are placed into random elements atop the substratum. Simultaneously, nutrient diffuses across the DBL. Cells consume nutrient, and subsequently grow and divide, resulting in the formation of a contiguous multicellular population. At the end of each time step, the nutrient reservoir is shifted vertically upwards such that a pre-determined distance from the topmost cell in the biofilm is always maintained. It is assumed here that the biofilm does not pose an obstacle to flow, and that it is subjected to a constant linear velocity gradient of 10^{-1}s with zero velocity at the substratum, and maximum velocity at the highest point. This latter is updated every time the height of the biofilm changes, so as to maintain a shear rate of 10^{-1}s.

Using this domain geometry I was able to simulate biofilms containing up to 23368 ± 218 bacterial cells; recent individual-based models of biofilm formation and growth have shown that simulations involving up to 10,000 bacteria are sufficient to demonstrate that all steps of biofilm formation observed in experiments can be reproduced [41].

Each bacterial cell in the grid is modelled and tracked as an independent unit, with its own set of parameters (Table 3.2) and behaviours. To simulate behavioural variability, parameter values for individual bacterial cells were obtained by random draws from a uniform distribution around the values listed in Table 3.2 while discarding all negative values, and those outside $\pm 10\%$ of the mean; these precautions are necessary with distributions ranging from $-\infty$ to $+\infty$[109]. This feature is particularly useful for studying complex systems where individual heterogeneity is important, like in the case of biofilms. The parameter values used in the model are summarized in Table 3.2.

The resulting aggregate behaviour of the biofilm is therefore emergent from the local interactions between the individual bacteria, and their surroundings, thereby allowing us to simulate the self-organized process of biofilm formation. The simulation represents 400 h duration of biofilm growth in which every solid and liquid entity is tracked individually, allowing for the quantification of spatiotemporal variations of heterogeneities of the biomass, EPS, nutrients, signalling molecules, and antibiotics. The time duration of 400 h was chosen to simulate 4 distinct biofilm growth phases of biofilm lifecycle [58].

3.3 Key assumptions

The following are the key assumptions made:

(1) The biofilm does not pose an obstacle to flow, and is subjected to a constant linear velocity gradient of 10 s^1 with zero velocity at the substratum, and maximum velocity at the highest point. It has been shown that giving up the conservation principles for fluid flow in the biofilm domain leads to increased deviations with respect to concentration fields and fluxes [123]. The magnitude of deviation is in some cases small ($< 2\%$, at slow bulk flow velocities of ~0.0001 ms^1), and considerable in other ($> 20\%$, at fast bulk flow velocities of 0.01 ms^1). The results presented in this work correspond to the low bulk

flow regime (maximum velocity of ~0.0006 ms^{-1}). Consequently, deviations in concentration fields and fluxes have been neglected. Such low fluid shear rates (10-50 s^{-1}), experienced within the intestine, and veins, have been shown to be effective in simulating S. aureus biofilm colonization and development [124, 125].

(2) The DBL remains parallel to the substratum throughout the simulation, and moves upwards as the biofilm thickness increases with time. It is worth noting that at high fluid velocities, the diffusion boundary could follow the surface of the biofilm, and may not be necessarily stratified as is assumed here [122].

(3) The DBL has a constant thickness of 18 μm. For the low-flow regime considered in this work, the nutrient concentration at a vertical distance of 18 μm from the highest cell in the biofilm was greater than 95% of the bulk nutrient concentration, even at time points corresponding to the highest cell numbers. Traditionally, this value is taken to be 99%. But to reduce the computational cost, lower value of ~94.5% is used in these simulations. Thus, it is assumed that the DBL has a constant thickness of 18 μm, and remains parallel to the substratum in the low-flow regime considered in this work.

(4) EPS is capable of coexisting with a bacterial cell within a cubical element. This is consistent with previous experimental work showing the accumulation of extracellular polysaccharides such as β-glucan found intercalating between micro colonies of Streptococcus mutans [126]. Consequently, it has been assumed that new bacterial cells embed themselves into existing EPS, instead of pushing it aside.

(5) The spatial locations of cell death events are recorded at each time step for further analysis. Subsequently, dead cells are discarded from the simulation domain, and are no longer tracked. Experimental work involving biofilms grown in flow cells has shown that hollow cell clusters are formed, and that lysed cells are apparent in the internal strata [57]. Furthermore, it has been suggested that approximately 50 cells must die in order to support one cell division [127]. Extensive modelling work in the past where lysed cells contributed nutrients to the neighbouring cells found no significant difference in the results [58]. Therefore, the contribution of nutrients from lysed cells has been omitted here.

A full mathematical description of the various components and processes incorporated in the model is presented below.

29

3.4 Convergence study for biofilm geometry choice

The domain volume used in the model was arrived at after performing a convergence study using a variable domain sizes (number of grid cells in the horizontal directions = 30, 35, 40, 48, and 60 with a variable domain size such as 90 μm x 90 μm, 105 μm x 105 μm, 120 μm x 120 μm, 144 μm x 144 μm, and 180 μm x 180 μm respectively in the horizontal plane). The total biomass and average nutrient concentration were compared across these runs (Table 3.1). 120 μm x 120 μm horizontal volume was used for further simulations since further increase in domain size resulted in a less than 15% change in accuracy of the tested quantities. The results are tabulated below:

Table 3.1. QS biofilm growth dynamics using a variable domain size

Number of Grid Elements in the Horizontal Directions (x and z)	Total Biomass (μg)	Estimated Relative Spatial Discretization Error (%)	Average Nutrient Concentration (dimensionless)	Estimated Relative Spatial Discretization Error (%)
30	0.00458		0.1865	
35	0.00562	18.50	0.2419	22.90
40	0.00632	11.07	0.2713	10.83
48	0.00665	4.951	0.2954	8.03
60	0.00697	10.25	0.3042	12.1

The above mentioned numerals are quantified for QS biofilm growth dynamics.

3.5 Nutrient reaction and transport

The spatial distribution of nutrient concentration within the biofilm influences biomass growth rate. In turn, bacterial behaviour (growth, division, spreading, death, and detachment) affects nutrient concentration fields. The temporal and spatial distribution of nutrient concentration $C_N(\bar{x}, t)$ is, therefore, intimately dependent on the local biomass concentration $(C_B(\bar{x}, t))$. $C_N(\bar{x}, t) = C_N(x, y, z, t)$ represents the nutrient concentration value at each element (x, y, z) of the spatial domain at time t. The nutrient uptake rate is described by the Herbert-Pirt model (Eq. 3.1) [128, 129].

$$r_N(\bar{x}, t) = \left(\frac{\mu_{max}}{Y_{NB}} + m \right) C_B \left(\frac{C_N(\bar{x},t)}{C_N(\bar{x},t)+K_N} \right) \tag{3.1}$$

where μ_{max}, Y_{NB}, and m represent the maximum specific growth rate, yield coefficient, and maintenance coefficient of the bacteria, respectively, and K_N is the half-saturation coefficient. Schulze and Lipe defined "maintenance supply," later termed "maintenance coefficient" by Pirt, as the minimum nutrient consumption to maintain the cells. In other words, maintenance has been defined as "the energy consumed for functions other than the production of new cell material". Maintenance estimates should explicitly describe each non-growth component. The nongrowth components thus included, shifts in metabolic pathways, defense mechanisms, cell motility, and storage of polymers, or extracellular losses. The most popular equation used to describe microbial growth, is the Monod equation. However, when measurements of maintenance showed deviations from a constant maintenance, additional growth-rate-dependent maintenance parameter is introduced [130].

The nutrient concentration within each element of the domain changes because of consumption, diffusion, and convection, and is given by

$$\frac{\partial C_N(\bar{x},t)}{\partial t} = -r_N\big(C_N(\bar{x},t), C_B(\bar{x},t)\big) + D_N \sum_{i=1}^{3} \frac{\partial^2 C_N(\bar{x},t)}{\partial x_i^2} - \nabla \cdot (v C_N) \tag{3.2}$$

Here, D_N is the nutrient diffusivity, and v is the local fluid velocity. $C_N(\bar{x}, t)$ is set to $C_{N,bulk}$ at the top surface, and to 0 at the substratum. Diffusion coefficients within bulk flow (region with no biomass) and the biofilm domain (region with biomass) are assumed to be identical, i.e. solutes diffuse through liquid-filled and biomass-filled regions at the same rates. The 3D reaction–diffusion-convection equation is solved numerically with the following boundary conditions:

a) A Dirichlet boundary condition is imposed at the DBL, i.e., the nutrient concentration remains constant at the interface between boundary layer and bulk liquid.

b) Neumann boundary condition is imposed at the substratum, where the nutrient flux is zero.

c) Periodic boundary conditions are applied at the lateral boundaries.

3.6 Biomass growth

A portion of the consumed nutrient is utilized by the bacterium towards endogenous metabolism. The leftover nutrient is assumed to be converted to biomass with an efficiency called the yield coefficient, Y_{NB} [58]. The net accumulation of biomass is, therefore, given by:

$$\frac{\partial C_B(\bar{x},t)}{\partial t} = Y_{NB}\left[r_N\big(C_N(\bar{x},t), C_B(\bar{x},t)\big) - mC_B(\bar{x},t)\right]$$
(3.3)

Real biomass growth is governed by the specific growth rate, μ_{max} and decay of biomass is included by incorporating the maintenance coefficient, m, and yield coefficient Y_{NB}. This allows for negative net biomass growth under low nutrient conditions.

3.7 Cell division
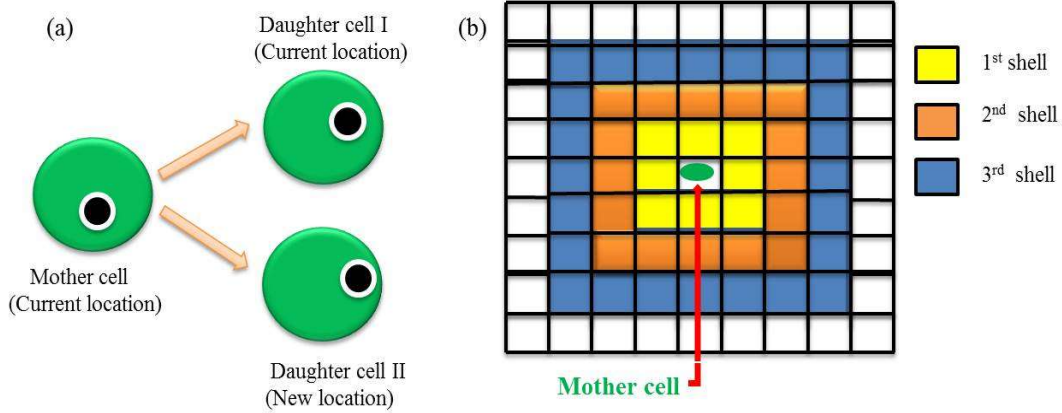
Figure 3.2. A mother cell divides into two daughter cells (a), Two-dimensional view of the neighbouring elements at increasing distances from mother cell (b).

When the biomass of a bacterium reaches twice its native value it divides into two daughter cells (Fig. 3.2a). Whereas one daughter cell continues to remain in the same element as the dividing mother cell, the other is pushed into a bacterium-free element in the immediate neighbourhood. The immediate neighbourhood -- termed the Moore neighbourhood --

32

comprises of 26 cubical elements surrounding the central element. If multiple bacterium-free elements are available for occupation in the Moore neighbourhood, one is chosen at random [129]. On the other hand, if all elements in the Moore neighbourhood are occupied by bacteria, an unoccupied element is identified at the nearest Chebyshev distance from the location of the mother cell. The occupancy statuses of elements is checked at successively larger Chebyshev distances (starting with a Chebyshev distance of 2, and moving outward, layer by layer), until an empty element is found. Each of the bacterial cells that lies between the mother cell and the closest bacterium-free element is then shifted by one grid element – away from the mother cell, and towards the empty element – creating a bacterium-free element in the Moore neighbourhood of the mother cell (Fig. 3.2b). This newly created bacterium-free element is then occupied by the daughter cell; thereby ensuring that the daughter cell is always placed immediately next to the dividing bacterium. The biological basis for this pushing mechanism is that dividing cells push each other outward to a larger extent, potentially towards a region where still unexploited nutrients can be accessed. This competition for space and for nutrient generates the biofilm structure. On the other hand, this structure influences further development of the biofilm by changing the nutrient transport.

3.8 Cell death

Cell death is assumed to occur via one of two mechanisms: (i) limited nutrient uptake [57], or (ii) starvation caused by prolonged stay in the stationary phase [131, 132]. Nutrient uptake is quantified by the ratio(R) of the rate of biomass formation$(Y_{NB}r_N(C_N, C_B))$ to that of endogenous metabolism $(Y_{NB}mC_B)$ (Eq. 3). Cell death by limited nutrient uptake is assumed to occur when R falls below a certain threshold (R_{min}) [58]. Along similar lines, if$R$ falls below 1, the cell exhibits zero or negative net growth, and is said to have entered the stationary phase. Cell death is assumed to occur if the cell remains in this growth-arrested phase for a preset number of hours (t_{SP}). This is consistent with observations where bacteria in the stationary phase gradually lose their ability to reproduce, and exhibit signs of senescence and eventually loss of viability by accumulating oxidatively damaged proteins [131, 132].

Moreover, if the biofilm is subjected to antibiotic treatment, then cells die based on probability of killing by antibiotic which is a function of the rate of consumption of antibiotic (Eq. 13).

3.9 Cell detachment

Cell detachment in bacterial biofilms is a complex process influenced by a host of external and internal factors such as fluid shear forces [133], internal stresses [134], chemical gradients [135], erosion [133], and nutrient starvation [57]. Here, a simplified geometrical model was implemented wherein cell detachment is governed by (i) localized cell death resulting from nutrient limitation, and (ii) EPS formed as a consequence of quorum sensing. Cell detachment is determined by evaluating the connectivity of cells to the substratum. Within the biofilm, bacteria connect to the substratum either directly, or indirectly through a group of live bacteria in which at least one bacterium is directly bound to the substratum [136]. In addition to live bacteria, in QS^+ biofilms, cells can also continue to remain connected to the substratum via EPS. At the end of each time step, detachment events are recorded, and detached cells are removed from the domain.

3.10 Quorum Sensing

In QS^+ biofilms, bacterial cells are modelled as being in either the up-regulated, or the down-regulated state. Cells switch between these states at rates dependent on the local autoinducer concentration $(C_A(\bar{x}, t))$. The transition rate from the down-regulated to up-regulated state is given by

$$TR^+ = \alpha \, \frac{C_A(\bar{x}, t)}{1 + \gamma C_A(\bar{x}, t)}$$

(3.4)

Along similar lines, the transition rate between the up-regulated to down-regulated states is given by [137]

$$TR^- = \beta \, \frac{1}{1 + \gamma C_A(\bar{x}, t)}$$

(3.5)

where α and β are the spontaneous up- and down-regulation rates, and γ is the transition constant. The probabilities of switching from one state to another within a time interval of Δt are then given by

$$P_u = (TR^+)\Delta t$$
$$P_d = (TR^-)\Delta t$$

(3.6)

where P_u is the probability of up-regulation, and P_d is the probability of down-regulation.

3.11 Autoinducer Production and Transport

Up-regulated and down-regulated cells are assumed to secrete autoinducer molecules at constant rates of $r_{A,u}$ and $r_{A,d}$, respectively.

$$r_A = \begin{cases} r_{A,u} \\ r_{A,d} \end{cases}$$

(3.7)

where $r_{A,u} > r_{A,d}$ (Table 3.2). The secreted autoinducer is treated as a dissolved entity that is transported via diffusion and convection. The time evolution of the autoinducer concentration within the biofilm is given by

$$\frac{\partial C_A(\bar{x},t)}{\partial t} = D_A \sum_{i=1}^{3} \frac{\partial^2 C_A(\bar{x},t)}{\partial x_i^2} + \frac{r_A}{\Delta V} - \nabla \cdot (v C_A)$$

(3.8)

Where D_A is the autoinducer diffusivity, and ΔV is the element volume. Eq. 3.8 is subject to the Dirichlet boundary condition at the DBL $(C_{A,DBL} = 0)$, and the no-flux condition at the substratum.

For each bacterium, at every time step, the simulation generates a random number (n_R) from a uniform distribution on the interval [0, 1]. If $P_u > n_R$, then the bacterium switches from the down-regulated state to an up-regulated state. On the other hand, if $P_d > n_R$, then the bacterium switches from the up-regulated to the down-regulated state.

3.12 EPS production

EPS is treated as a discrete entity and is tracked individually in a manner similar to that of a bacterial cell. Furthermore, quantities of EPS and bacterial biomass that can be

accommodated in a single element are assumed to be independent of each other [126]. Bacterial growth and EPS production are assumed to occur concurrently from nutrient that is leftover after maintenance has been accounted for. It is assumed that EPS is produced only by upregulated cells, at a rate given by

$$\frac{\partial C_E(\bar{x},t)}{\partial t} = Y_{NE}\left[r_N\big(C_N(\bar{x},t), C_B(\bar{x},t)\big) - mC_B(\bar{x},t)\right] \qquad (3.9)$$

where, Y_{NE} is the yield coefficient for EPS, i.e. the efficiency with which nutrient that has not been consumed for endogenous metabolism is converted to EPS. EPS do not grow, die or consume nutrient, but they occupy space and undergo division. EPS division is handled similar to cell division described above, wherein daughter "EPS cells" are placed into the nearest element that does not contain EPS.

In QS^+ biofilms, upregulated cells secrete EPS and autoinducer molecules at an enhanced rate, compared to their downregulated counterparts. In a feedback-like mechanism, enhanced production of autoinducer by upregulated cells results in the upregulation of an increasing number of cells in the neighbourhood.

The consumption of antibiotic by EPS is governed by Monod-like kinetics (Eq. 3.11). This is an attempt to account for the reaction-diffusion barrier to penetration by the antibiotic that EPS provides.

3.13 Antimicrobial drug administration

In select runs, the biofilm is subjected to a continuous antibiotic treatment for duration of 24 h. The antibiotic concentration in the bulk fluid is held constant throughout the treatment period. As the antibiotic diffuses through the DBL, live bacterial cells and EPS consume the antibiotic in a Monod-like reaction [35]. The consumption of antibiotic by non-quorum sensing bacteria is assumed to be a function of the local antibiotic concentration and biomass concentrations, is given by Eq. (3.10)

$$r_{ab}\left(C_{ab}(\bar{x},t), C_B(\bar{x},t)\right) = \left(\frac{C_{ab}(\bar{x},t)}{C_{ab}(\bar{x},t)+K_{ab}}\right) K_{B\text{Max}} C_B(\bar{x},t) \qquad (3.10)$$

where $K_{B\text{Max}}$ is the maximum specific reaction rate of antibiotic with respect to biomass, K_{ab} is the Monod half-saturation coefficient of antibiotic, and $C_{ab}(\bar{x},t) = C_{ab}(x,y,z,t)$ represents local antibiotic concentration in each grid element, at time point t. In QS biofilms, the consumption of antibiotic by bacteria and EPS is given by Eq. (3.11).

$$r_{ab}\left(C_{ab}(\bar{x},t), C_B(\bar{x},t)\right) = \left(\frac{C_{ab}(\bar{x},t)}{C_{ab}(\bar{x},t)+K_{ab}}\right) [K_{B\text{Max}} C_B(\bar{x},t) + K_{E\text{Max}} C_E(\bar{x},t)] \qquad (3.11)$$

where K_{Emax} represents the maximum specific reaction rate of antibiotic by EPS, and C_E represents the EPS biomass. The dynamics of the antibiotic concentration field $C_{ab}(\bar{x},t)$ is given by the following reaction-diffusion equation:

$$\frac{\partial C_{ab}(\bar{x},t)}{\partial t} = -r_{ab}\left(C_{ab}(\bar{x},t), C_B(\bar{x},t)\right) + D_{ab} \sum_{i=1}^{3} \frac{\partial^2 C_{ab}(\bar{x},t)}{\partial x_i^2} - \nabla \cdot (v C_{ab}) \qquad (3.12)$$

where D_{ab} is the antibiotic diffusivity, and v is the local fluid velocity.

The probability of cell death due to antibiotic consumption is given by:

$$P_{death} = \left(\frac{r_{ab}(\bar{x},t) - r_{Min}}{r_{Max} - r_{Min}}\right) \qquad (3.13)$$

r_{Min} and r_{Max} are the rates of consumption of the antibiotic at minimum and maximum inhibitory concentrations of one bacterium, respectively. At each time step during treatment, a random number (n_R) is generated for each cell. If $P_{death} > n_R$, then the bacterium dies, and is removed from the simulation domain.

3.14 Heterogeneity

Biofilm heterogeneity, h, was defined as the extent of non-uniform distribution of the (i) total accumulated biomass, (ii) nutrient, (iii) EPS, and (iv) autoinducer concentrations.. It was quantified as the coefficient of variation with respect to selected component.

$$h = \frac{\sigma}{\mu}$$

where, σ is the standard deviation, and μ is the mean of the quantity whose heterogeneity is being evaluated. Thus, h measures the extent of variability with respect to the mean of the population. Two separate calculations were performed for each component: (i) an overall heterogeneity to track the variability throughout the entire domain, and (ii) a grid-layer-wise evaluation to delineate the spatial variation of heterogeneity. For the former σ and μ were computed over the entire biofilm domain, whereas for the latter calculations were performed over individual grid layers.

3.15 Numerical Scheme

The state of the simulation domain is updated at discrete time steps Previous work analysing the kinetics of the switching process from the vegetative state to the competent (EPS producing) state of Bacillus subtilis has shown that the duration of the switching period was 1.4 ± 0.3 h [138]. In addition, analysis of Bacillus subtilis at the interface between the culture medium and air indicates that bacteria switch from the motile to the matrix-producing phenotype (downregulated to upregulated) between 10 min to 1h [41]. Consequently, here a multiscale integration approach has been used with two distinct time scales are used: (i) cellular processes (biomass growth (Eq. 3.3), switching between up- and down-regulated states (Eq. 3.6), EPS production (Eq. 3.9), and death by antibiotic (Eq. 3.13), cell division, and detachment) are monitored every 1 h, and (ii) within this "outer" time loop, concentrations of dissolved entities (nutrient (Eq. 3.2), autoinducer (Eq. 3.8), and antibiotic (Eq. 3.12)) are tracked by solving the diffusion-convection equations at a finer time resolution of $1\text{x}10^{-6}$ h. Forward-Time Central-Space scheme was used for the diffusion-convection equations whose von Newman stability analysis yields the following condition

$$\frac{v^2 \delta t}{2} \ll D$$

where, v is the fluid velocity, D is the diffusion coefficient, and δt is the time step. For the low shear regime tested in these simulations (shear rate = 10 s^{-1}), and for the time step $\delta t = 1\times10^{-6}$h, the above stability requirement is satisfied.

The diffusion-convection equation does not need to run for 1,000,000 time steps- as soon as substrate concentration equilibrium tolerance limit is reached (roughly take few 1000 times)- substrate model execution is stopped and so able to reduce computational cost efficiently. The same approach is used for other dissolved entities like autoinducer, and antibiotic (Eq.(3.8), and (3.11), respectively). At each time step, Eq.(3.3) and (3.9) are solved using the updated nutrient concentration field.

Due to stochastic nature of the model, running four simulations with the same parameters never really gave identical results but they are comparable. The key sources of variability in this model are at the cellular level: (i) each bacterial cell is treated as an individual entity with its own set of parameters (chosen randomly from a uniform distribution), (ii) stochasticity introduced in the modelling of cellular behaviours such as division (placement of daughter cells, cell death due to antibiotic), and (iii) the calculations for the probabilities of up- and down-regulation of individual cells. Since I have been analysed tens of thousands of cells during each simulation run, I posit that present results, averaged over a fairly large population of bacterial cells, provide meaningful observations. For instance, the peak cell numbers (averaged over 4 simulation runs) for quorum-sensing-negative (QS) biofilms are 23368 ± 218 for the bulk nutrient concentration $(C_{N,bulk})$ of 8 gm^{-3}, 15623 ± 165 for $C_{N,bulk} = 4$ gm^{-3}, and 4505 ± 156 for $C_{N,bulk} = 1$ gm^{-3}. Several individual-based CA models similar to this model have reported results based on 3-6 replicate simulations [16, 27, 32]. The simulations involving up to 10,000 bacteria are sufficient to demonstrate that all the steps of biofilm formation that are observed in the experiments can be reproduced [41].

Numerical solutions to the diffusion-convection equations are obtained using a second-order Forward-Time Central-Space scheme. Periodic boundary conditions are applied in the horizontal directions, and the Dirichlet boundary condition is imposed in the vertical

direction. The Java programming language is used since it provides a convenient object-oriented framework that is well-suited for the individual based model described here.

Finite difference scheme

The rectangular computational domain is discretized with a Cartesian grid. The indices for the grid points are i = 1, 2,. . N (N = 40); j = 1, 2,. . N; and k = 1, 2,. . N (N = 40); for x, y and z spatial dimension respectively with a grid point distance of h (3 μm). A finite difference scheme is presented on a rectangular grid based on a first order difference approximation for the time derivative and the usual second order spatial difference for diffusion and convection terms in system of second order partial differential equations (for Eq. (3.2), (3.8), and (3.11)). The standard finite difference scheme reads to evaluate the local chemical (nutrient (Eq. 2.2); autoinducer (Eq. 3.8); antibiotic (Eq. 3.11)) concertation reads as follows.

$$\text{Diffusion term} = D_N \sum_{i=1}^{3} \frac{\partial^2 C_N}{\partial x_i^2}$$

$$= D_N * [(C_{Nx(i+1)} - (2 * C_{Nx(i)}) + C_{Nx(i-1)}) +$$

$$(C_{Ny(i+1)} - (2 * C_{Ny(i)}) + C_{Ny(i-1)}) +$$

$$(C_{Nz(i+1)} - (2 * C_{Nz(i)}) + C_{Nz(i-1)})] / h^2$$

$$\text{Convection term} = \nabla \cdot (v C_N)$$

$$= [(C_{Nx(i+1)} - C_{Nx(i-1)}) / (2 * h)] * \text{fluidVelocity}$$

Where fluidVelocity $= \gamma * (\text{slicenumber} * \text{elementLength})$

Biologically, the system was conceptualized as a single species whose growth rate is determined by the concentration of a single nutrient, according to Herbert-Pirt kinetics. The bacteria are discrete immotile cells with kinetic and yield parameters, which may vary randomly around a given mean.

Reaction term: $\left(\frac{\mu_{max}}{Y_{NB}} + m\right) C_B \left(\frac{C_N}{C_N + K_N}\right)$

3.16 Simulation flowchart
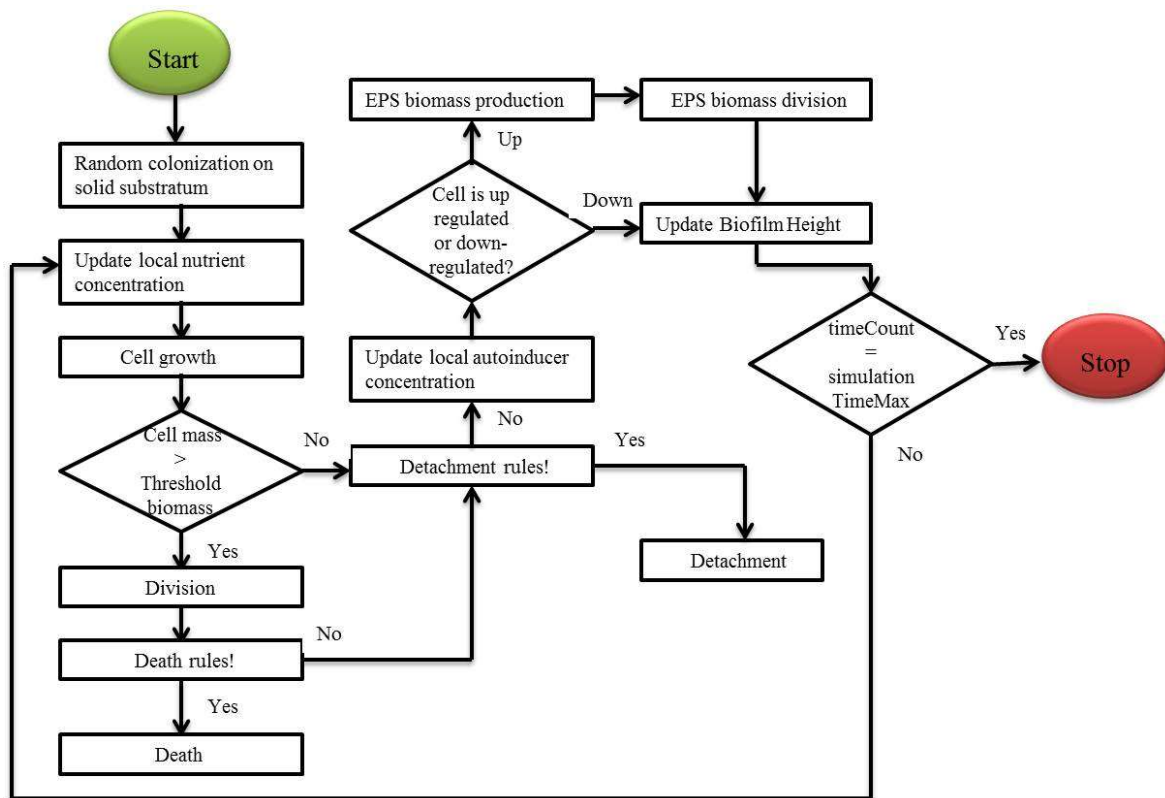
Figure 3.3. Flowchart representation of simulation steps

The parameter values used in the model are summarized in below table (Table 3.2).

Table 3.2. Model parameters

Parameter	Description	Value	Unit	Reference
Δx	Element length	3	μm	
	Thickness of the DBL	18	μm	[58]
N_j $(j = x,$ $z)$	Number of elements in the jth direction	40		
N_0	Initial number of bacterial cells	6		
m	Maintenance coefficient	0.036	h^{-1}	[58]
μ_{max}	Maximum specific growth rate of bacterial population	0.3125	h^{-1}	[58]
Y_{NB}	Yield coefficient for biomass	0.45		[58]
t_{SP}	Time in the stationary phase at which cell death occurs	24	h	[58]
R_{min}	Ratio of the rate of nutrient consumption to that of endogenous metabolism below which cell death occurs	0.15		[58]
	Threshold biomass at which cell division occurs	2 x 10-12	g	[139]
D_N	Diffusion coefficient of nutrient	0.84 x 10-6	$m^2 h^{-1}$	[58]
K_N	Monod saturation constant	2.55	$g\ m^{-3}$	[58]
$C_{N,bulk}$	Bulk nutrient concentration	1, 4, 8	$g\ m^{-3}$	
Y_{EN}	Yield coefficient for EPS	0.27		[34]
	Threshold concentration at which EPS division occurs	33000	$g\ m^{-3}$	[34]
D_A	Diffusion coefficient of autoinducer	1 x 10-6	$m^2\ h^{-1}$	

$r_{A,u}$	Autoinducer production rate by up-regulated cells	73800	$molecules\ h^{-1}$	[137]
$r_{A,d}$	Autoinducer production rate by down-regulated cells	498	$molecules\ h^{-1}$	[137]
α	Spontaneous up-regulation rate	7.89×10^{-17}	$m^3 molecule^{-1}h^{-1}$	[137, 140]
β	Spontaneous down-regulation rate	0.975	h^{-1}	[137, 140]
γ	Transition constant	7.96×10^{-17}	$m^3 molecule^{-1}$	[137, 140]
D_{ab}	Diffusion coefficient of antibiotic	0.36×10^{-6}	$m^2 h^{-1}$	[35]
K_{ab}	Antibiotic half-saturation coefficient	1	$g\ m^{-3}$	[35]
K_{BMax}	Maximum specific reaction rate of antibiotic with bacterial cell	2.5	h^{-1}	[35]
BIC	Biofilm inhibitory concentration	1- 64	$g\ m^{-3}$	[141]
K_{EMax}	Maximum specific reaction rate of antibiotic with EPS	0.25	h^{-1}	

Chapter 4. Influence of nutrient availability and quorum sensing on the formation of metabolically inactive microcolonies within structurally heterogeneous bacterial biofilms: An individual-based 3D cellular automata model

4.1 Introduction

Although microorganisms have been traditionally investigated as single-cell, planktonic entities, analyses of bacterial communities in diverse environments have led to the conclusion that planktonic growth rarely exists for microorganisms in nature [142]. Instead, bacteria preferentially form self-organized assemblages -- termed biofilms -- composed of surface-adherent cells embedded in a protective matrix comprised of extracellular polymeric substances (EPS) [142, 143]. Encased in this matrix of biopolymers, microbial communities develop physically diverse structures containing cell clusters, interstices, water channels [144], and large mushroom-shaped assemblies [145-150]. The transition from planktonic to biofilm mode of growth, and biofilm architecture are influenced by a range of local and macroscopic signals and stimuli, such as nutrient concentrations, intercellular communication, and environmental stresses [53, 151-153].

Bacterial biofilms forming on damaged tissues [154-156] or on biomimetic devices [157-160], are a leading cause of chronic infections, since the cells within the biofilm are extremely resistant to antibiotics, and are adept at evading host immune responses. Interestingly, whereas biofilm-associated bacteria are more tolerant to antibiotics than their planktonic counterparts, it is only subpopulations within the biofilms -- termed persister cells -- that

exhibit enhanced antibiotic tolerance [161-166]. This spatially nonuniform response to antibiotic treatment suggests that biofilms are comprised of structurally and functionally heterogeneous microcolonies that may differ from their surroundings with respect to metabolic activity, growth phase, and gene- expression patterns [71, 167]. For instance, in $P.$ aeruginosa biofilms, it has been shown that dormant cells were more tolerant to tobramycin and silver ions. In addition, active cells had bigger cell size and higher intracellular density compared to dormant cells. It is possible that cells in these metabolically inactive microniches exhibit reduced antibiotic uptake rates. In addition, drug tolerance in dormant cells has been attributed to lower cytoplasmic drug accumulation as a result of enhanced efflux activity [168]. Furthermore, these bacteria may be sheltered within a reaction-diffusion barrier presented by surrounding, faster-growing cells and EPS, thereby reducing local antibiotic penetration [169, 170].

Quorum sensing (QS) is a mechanism of intercellular communication used to collectively coordinate group behaviours based on population density [70, 171-173]. This process relies on the production, release, and group-wise detection of signal molecules called autoinducers (e.g. acyl-homoserine lactones in Gram-negative bacteria) which rapidly diffuse in the liquid phase and across cell populations, and accumulate in the biofilm over time. Experimental work suggests that there is a positive correlation between QS and EPS production [23, 66, 72, 174]. For instance, in Pantoea stewartii biofilms, approximately ten-fold increase in EPS production upon QS induction was observed [72]. Cells exhibiting enhanced EPS production in the presence of autoinducer molecules are said to be up-regulated. QS-induced EPS production allows a biofilm to switch rapidly from a colonization mode to a protection mode [107]. The EPS matrix confers structural integrity to the biofilm by providing mechanical strength, and reducing the extent of cell detachment [175, 176]. In addition, the effect of QS-regulated EPS production on biofilm architecture has been shown to be a function of the growth stages during biofilm formation [78, 177].

The mechanisms of emergence of protected microcolonies in growing biofilms remain poorly understood. One possible explanation is nutrient limitation. When suspended in a solution of nutrients, microorganisms disrupt the uniform distribution of dissolved nutrients by

locally depleting them and generating nutrient concentration gradients. The spatial distribution of accumulated biomass within the biofilm is, therefore, intimately interconnected with local nutrient concentration gradients. In addition, concentration gradients may also be set up for signalling molecules such as autoinducers resulting in spatially nonuniform production and distribution of EPS. Consequently, the biofilm may comprise of numerous microenvironments where local chemistries are distinctly different from the surroundings with respect to biomass density, nutritional availability, and concentrations of EPS and signalling molecules. Another possibility is that quorum-sensing signals allow the bacteria to trigger expression of protective genes, resulting in the formation of persister cells [178, 179].

A key challenge in modelling the structural development of a biofilm arises from the complex interaction between many processes. Current biofilm models can be broadly classified into two categories: continuum models [38, 39], and individual based models [40]. In continuum models, the biofilm is considered to be a continuous medium, with porosity, surface shape, and density as input parameters. In contrast, individual based models treat bacterial cells as individual units with their own states, thereby allowing for variability between individual behaviours with respect to their growth rates, nutrient uptake rates, local nutrient concentration, signalling molecule production, up-regulation and down-regulation states, and EPS production. The discrete, 3D nature of individual based models, combined with physical dynamics, allows for the calculation of concentration profiles of soluble entities, as well as the spatial distribution of biomass, and distribution in clusters. Consequently, chemical and structural heterogeneities within the biofilm emerge as a result of the actions and interactions of the cells with each other, and with the surrounding environment, rather than being a model input [40].

Several models have investigated quorum sensing in biofilms [108, 137, 180]. Most quorum sensing models focus on up-regulation, with only a few including the effect of quorum sensing on biofilm architecture, and growth dynamics [107, 181]. In many models, the cell density is assumed to be constant [42, 43], thereby neglecting biofilm expansion that results from the production of new cells, and shrinkage caused by cell death and detachment. Recently,

attempts have been made to use deterministic continuum models of quorum sensing in biofilms [108]. Such models neglect the stochastic nature of the up- and down-regulation processes, and are unable to account for local heterogeneities in microbial subpopulations. In the past, mechanistic computational models have successfully described the autonomous formation of tertiary macrostructures in bacterial biofilms [34-36], including the effects of EPS on biofilm structure [37]. However, a systematic analysis of the local structural and chemical heterogeneities in the biofilm interior has not been performed. An analysis of the spatial heterogeneity in bacterial growth rates could shed light on mechanisms of the emergence of dormant microcolonies containing cells that are potentially antibiotic-insensitive. Here, a prototype individual-based 3D computational cellular automata model is presented to simulate biofilm growth, and quantify heterogeneity as a function of growth phase, space, and time. The goal is to answer the following questions: (i) can physical processes like nutrient starvation and localized cell death account for the formation of metabolically inactive microcolonies in biofilms, in the absence of genetic triggers? (ii) How does quorum sensing – and the associated EPS production – influence the structural heterogeneity of the biofilm? Specifically, the roles of (i) carbon source concentration, (ii) localized cell division, death, and dispersal, (iii) QS, and (iv) EPS production on the structural and chemical heterogeneity of mono-microbial biofilms have been investigated. The model incorporates the following processes: nutrient diffusion, reaction, and convection; biomass growth kinetics, cell division, death, and dispersal; autoinducer production, and transport; and EPS production. The simulation represents a 400 h duration of biofilm growth, in which cells are tracked individually, allowing us to quantify spatiotemporal variations of heterogeneities of the biomass, EPS, nutrients, and signalling molecules.

Results from causal modelling suggest that biofilms are comprised of at least three structurally distinct strata with respect to metabolic activity, growth phase, nutrient availability, and porosity: a high-biomass, low-heterogeneity section in the middle of the biofilm, sandwiched between two highly heterogeneous low-biomass regions on the top and the bottom. In QS-positive (QS^+) biofilms, an additional layer comprising of EPS, and devoid of cells, exists in close proximity to the substratum. The simulations show that nutrient limitation, in the absence of genetic triggers, can account for the formation of microenvironments containing dormant, low-activity cells surrounded by high-activity ones.

Cell death occurs preferentially in the bottom section of the biofilm, leading to increase in heterogeneity in the biomass distribution in this region, and ultimately to sloughing. A clear understanding of heterogeneities at the local scale may be vital to solving the riddle of the resistance of biofilms to external stresses such as antibiotics.

4.2 Results and Discussion

4.2.1 Biofilm growth dynamics: Influence of nutrient concentration

As a first step, biofilm growth dynamics have been simulated for a QS-negative (QS$^-$) strain that does not produce autoinducer or EPS. At time $t = 0$, six colonizers were placed at random locations on the substratum. Nutrient diffuses into the domain across the DBL, and is subsequently consumed by bacterial cells, thereby causing their biomass to increase. This, in turn leads to cell growth, division, and expansion of the biofilm. Fig. 4.1 shows a representative time evolution of a QS$^-$ biofilm associated with a bulk nutrient concentration of 4 gm^{-3}, illustrating the formation of a distinct 3D macrostructure as the biofilm matures, and the various growth stages including: (i) colonization, (ii) early exponential phase, (iii) late exponential phase, (iv) maturation, (v) sloughing, and (vi) regrowth.
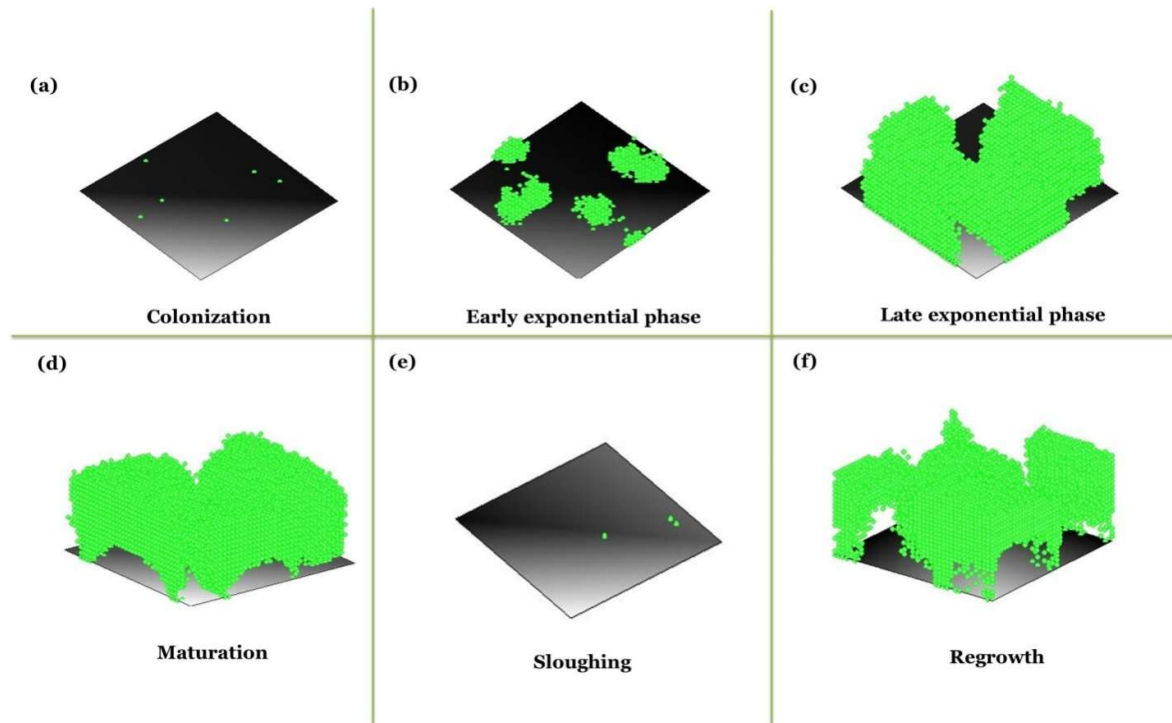
Figure 4.1. Representative 3D renderings of the time evolution of a QS- biofilm for $C_{N,bulk} = 4$ gm^{-3}, illustrating different phases of growth at 0 h (a), 30 h (b), 60 h (c), 110 h (d), 120 h (e), and 330 h (f).
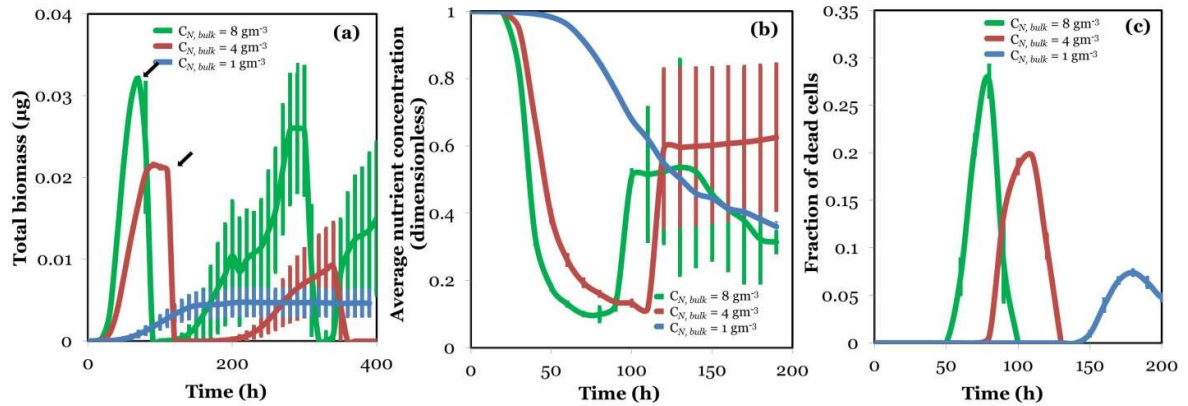
Figure 4.2. Growth dynamics for QS biofilms. Comparison of the development of total biomass (a), average nutrient concentration (b), and fraction of dead cells (c) for $C_{N,bulk}$= 8 gm^{-3}(green), 4 gm^{-3}(red), and 1 gm^{-3} (blue). The arrows in panel (a) mark the end of the stationary phase and the initiation of sloughing for $C_{N,bulk}$ = 8 gm^{-3} and $C_{N,bulk}$ = 4 gm^{-3}. Data represent mean ± standard error of mean (SEM) of four separate simulations.

To delineate the influence of nutrient availability on biofilm growth, the total accumulated biomass and average nutrient concentrations are tracked within the biofilm for varying bulk nutrient concentrations (1, 4, and 8 gm^{3}), in the absence of QS (Figs. 4.2a, 4.2b). In close agreement with experimental evidence [182, 183], the model was able to simulate four distinct growth phases: exponential growth, stationary phase, sloughing, and regrowth. Biofilm growth rates and peak cell numbers in the exponential phase increased with increasing bulk nutrient concentrations (Fig. 4.2a, Table 4.1). In close agreement with experimental observations [51], sloughing in the faster growing biofilms ($C_{N,bulk}$ = 8 gm^{-3}) occurred earlier (~80 h) compared to the slower growing ones ($C_{N,bulk}$ = 4 gm^{-3}; ~110 h). Regrowth of the biofilm occurred post-sloughing. There is considerable variability between results across simulation runs in this phase, due to the high sensitivity to the conditions post-sloughing – i.e., the number of cells that survive detachment (Fig. 4.2a). Whereas under moderate ($C_{N,bulk}$ = 4 gm^{-3}) and excess ($C_{N,bulk}$ = 8 gm^{-3}) nutrient supply conditions, the average nutrient concentration within the biofilm dropped rapidly in the exponential growth phase, there was a gradual decrease when the nutrient supply was low ($C_{N,bulk}$ = 1

gm^{-3}) (Fig. 4.2b). Post-sloughing, due to the marked decrease in the total accumulated biomass, the average nutrient concentration increased rapidly (Fig. 4.2b).

The marked decline observed in the total biomass content of the biofilm at the end of the stationary phase could be a consequence of either (i) annihilation of the bacterial population in its entirety, or (ii) live cells detaching from the substratum (sloughing). To investigate which of these two possibilities was predominantly responsible for the drop in biomass, fraction of dead cells with time is tracked. As shown in Fig. 4.2c, peak cell death occurred just prior to sloughing (for $C_{N,bulk}$ = 8 gm^{-3} ~30% of the cells die at ~80 h; for $C_{N,bulk}$ = 4 gm^{-3} ~20% of the cells die at ~110 h). Fraction of dead cells is calculated as the ratio between-- total number of dead cells at current time step and total number of live cells at the previous time step. Since the fraction of dead cells was much less than 1 under all conditions tested, we conclude that the drastic reduction in the biomass is a consequence of live cells losing contact with the substratum, because of cell death occurring in the lower layers of the biofilm.

The biofilm associated with the bulk nutrient concentration of 1 gm^3 exhibited a prolonged stationary phase in which both the total biomass (Fig. 4.2a) and the fraction of dead cells (Fig. 4.2c) remained virtually constant, indicating that a balance was established between the rates of biomass formation and depletion. Sloughing did not occur under these conditions. This could be the consequence of the fact that under these nutrient-depleted conditions cells die at a slow rate, which ensures the presence of enough number of cells at the bottom of the biofilm to keep it attached to the substratum at all times.

4.2.2 Biofilm growth dynamics: Influence of QS
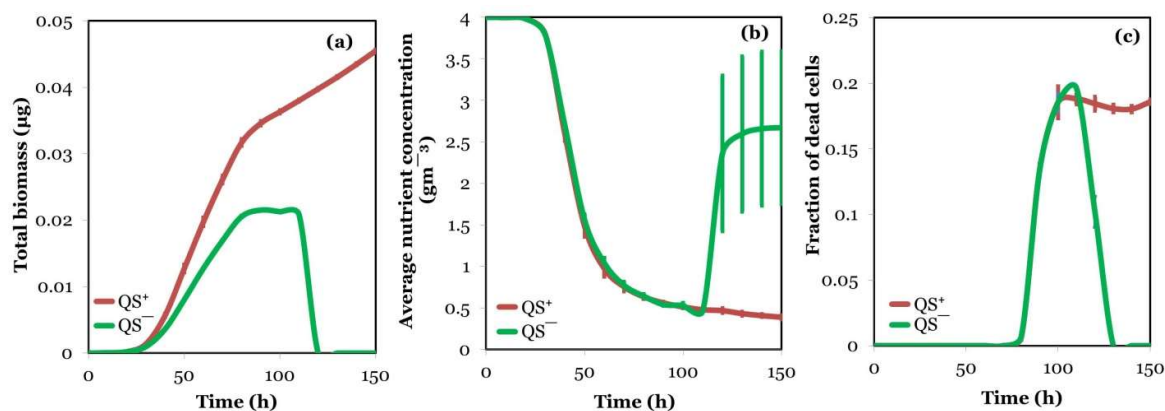
Figure 4.3. Influence of QS on biofilm growth dynamics. Comparison of total accumulated biomass (a), average nutrient concentration (b), and fraction of dead cells (c) for QS[+] (red) and QS[-] (green) biofilms for $C_{N,bulk}= 4$ gm^{-3}. The total biomass for the QS[+] biofilm includes mass of the EPS produced by upregulated cells. Data represent mean $\pm$ SEM of four separate simulations.

QS had minimal impact on the bacterial growth rates during the exponential growth phase (Table 4.1). The total biomass (bacteria + EPS) was higher than that for the EPS-devoid QS[-] biofilm in both the exponential and stationary growth phases. In stark contrast to the QS[-] biofilm, the QS[+] biofilm exhibited a prolonged stationary phase; no sloughing occurred even for the bulk nutrient concentrations of 4 gm^3 (Fig. 4.3a) and 8 gm^3 (data not shown), because of the presence of EPS which prevents live cells from detaching. QS did not alter the growth dynamics of the biofilm under low nutrient supply conditions ($C_{N,bulk} = 1$ gm^{-3}), even in the stationary phase (data not shown). Taken together with the observation that QS[-] biofilms were resistant to sloughing under these conditions (Fig. 3.2a), this result indicates that EPS plays a limited role in stabilizing the biofilm structure under low nutrient conditions. The average nutrient concentration decreased monotonically with time in the exponential growth phase, and then remained virtually constant (Fig. 4.3b). For $C_{N,bulk} = 4$ gm^{-3}, first instances of cell death were observed at ~80 h; peak cell death occurred at 100 h, and then remained virtually constant (Fig. 4.3c).

Table 4.1. Biomass growth and EPS production rates

$C_{N,bulk}$ (gm^{-3})	Growth rate of bacterial biomas (gm^{-3} h^{-1})*		Production rate of EPS (gm^{-3}h^{-1})*
	QS$^-$	QS$^+$	
1	48.5 ± 6.3	54.7 ± 19.1	29.1 ± 8.7
4	256.8 ± 29.5	295.7 ± 19.3	191.3 ± 21.9
8	492.1 ± 32.5	519.5 ± 15.1	329.6 ± 23.5

* Rates of bacterial biomass growth and EPS production were calculated as the net increase in bacterial biomass or EPS per unit time for the duration of the exponential growth phase (60 h for $C_{N,bulk}$ = 8 gm^{-3}, 80 h for $C_{N,bulk}$ = 4 gm^{-3}, and 170 h $C_{N,bulk}$ = 1 gm^{-3}).

4.3.3 QS-induced upregulation of cells and EPS Production
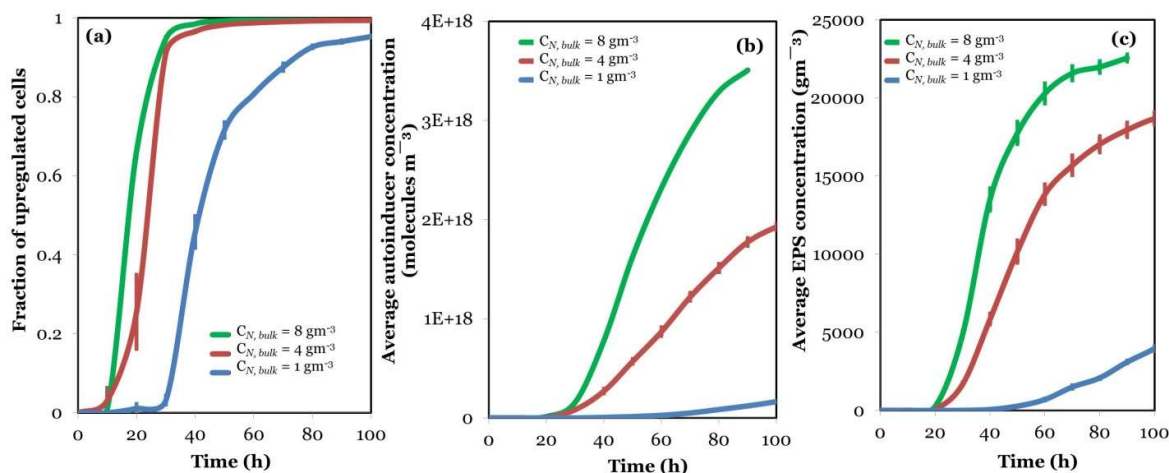
Figure 4.4. The fraction of upregulated cells (a), and average autoinducer (b) and EPS (c) concentrations for $C_{N,bulk}$ = 8 gm^{-3} (green), 4 gm^{-3} (red), and 1 gm^{-3} (blue). Data represent mean ± SEM of four separate simulations.

Cells in the QS$^+$ biofilm produced and locally released autoinducer molecules which spread throughout the biofilm via diffusion and convection. After the autoinducer concentration reached a threshold value, nearby bacterial cells upregulated resulting in the enhanced production of the autoinducer as well as that of EPS. The fraction of upregulated cells

increased during the exponential growth phase until virtually the entire biofilm rapidly switched from low to high QS activity (Fig. 4.4a). This switch was delayed under low nutrient supply conditions ($C_{N,bulk}$ = 1 gm^{-3}). The average autoinducer concentration increased monotonically with time for all three bulk nutrient concentrations (Fig. 4.4b). Analogous to the variation of total accumulated biomass, the average EPS concentration in the biofilm also increased rapidly with time in the exponential growth phase, before plateauing in the stationary phase (Fig. 4.4c). The rate of EPS production during the exponential growth phase was highest for the bulk nutrient concentration of 8 gm^3, and decreased for the lower bulk nutrient concentrations (Table 4.1).
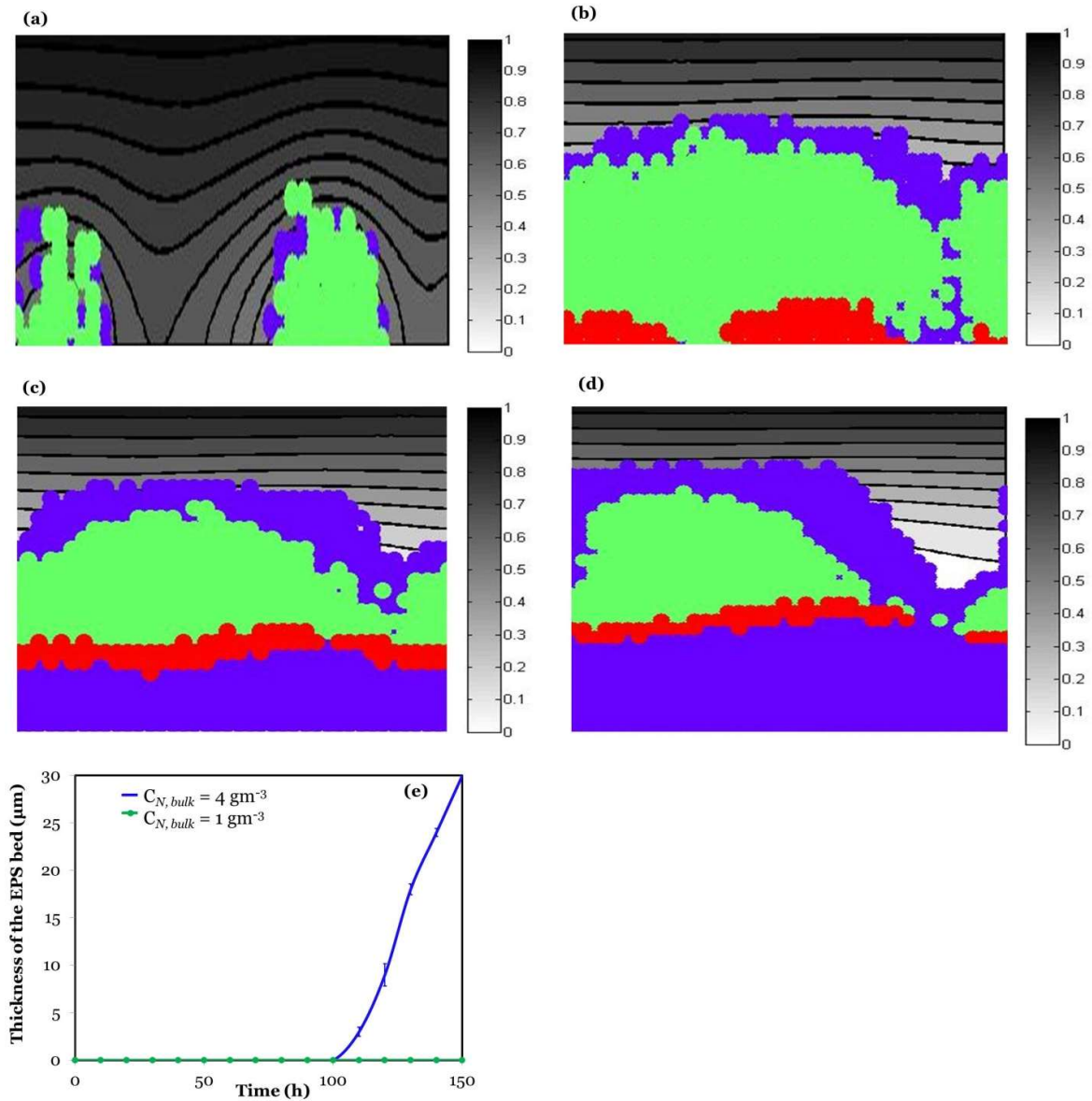
Figure 4.5. Distribution of EPS. Visualization of 2D cross-sections showing live cells (green), locations of cell death (red), and EPS without cells (purple) of the QS biofilm for $C_{N,bulk}$ = 4 gm^{-3} at 40 h (a), 90 h (b), 120 h (c), 150 h (d). It is to be noted that the green and red elements may also contain EPS. The isolines show the nutrient concentration distribution. The thickness of the cell-devoid EPS bed for $C_{N,bulk}$ = 4 gm^{-3} (blue) and $C_{N,bulk}$ = 1 gm^{-3} (green) is shown in panel (e).

For $C_{N,bulk}$ = 4 gm^{-3}, upon initiation of cell death (~80 h) on the bottom layers, a bed of EPS -- devoid of cells -- developed adjacent to the substratum upon which the rest of the biofilm grew (Figs. 4.5b, c, and d). The height of the EPS bed increased with time (Fig. 4.5e). These results clearly indicate that production of EPS by upregulated cells -- and its subsequent accumulation in the lower regions of the biofilm -- plays a key role in stabilizing the biofilm structure by reducing detachment events. Formation of the EPS bed was not observed for $C_{N,bulk}$ = 1 gm^{-3} (Fig. 4.5e), validating the idea that under depleted nutrient conditions, bacterial cells at the bottom hold the biofilm together, and that EPS plays a limited role.

4.2.4 Formation of metabolically dormant cellular micro-compartments
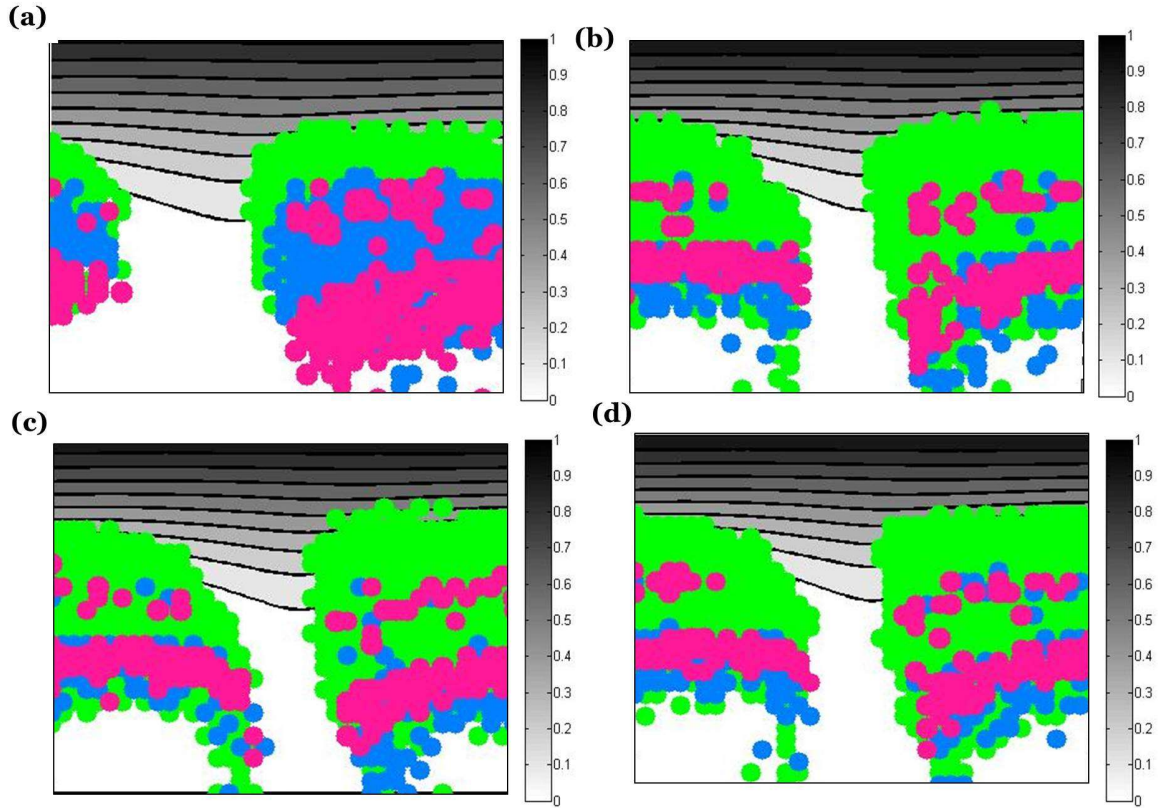
Figure 4.6. Illustrative cross-sections showing metabolically inactive cellular micro-compartments in QS biofilms for $C_{N,bulk} = 8$ gm^{-3} at 70 h; cells are categorized into three distinct subpopulations with high (green; greater than 3600 gm^{3}h^{-1}), intermediate (blue; 425-3600 gm^{3}h^{-1}), and low (pink; less than 425 gm^{3}h^{-1}) growth rates. The isolines show the nutrient concentration distribution.

Next, live bacterial cells are categorized into three groups based on their growth rates as follows: dormant cells (growth rate less than 425 gm^{3}h^{-1}), and those exhibiting high (greater than 3600 gm^{3}h^{-1}), and intermediate (425-3600 gm^{3}h^{-1}) growth rates. Fig. 4.6 shows representative cross-sections of the mature biofilm associated with the bulk nutrient concentration of 8 gm^3, illustrating the formation of microcolonies in the lower and intermediate layers of the biofilm structure. Low-activity cells (red) were encased within cell clusters of high activity (green). Similar micro-compartments were observed for QS biofilms (data not shown). In this model, the cellular growth rates are influenced by two

variables: C_N, and C_B (eq. 3.3). Based on these factors, I propose two possible explanations for the presence of dormant cellular microcolonies in the biofilm: (i) horizontal nutrient concentration gradients may be set up, resulting in increased nutrient concentrations in the lower layers, and hence higher cellular growth rates; and (ii) cells in the red regions may have lower biomass (possibly being newly divided) compared to cells in the green regions underneath, once again resulting in lower nutrient consumption rates, and hence lower growth rates.
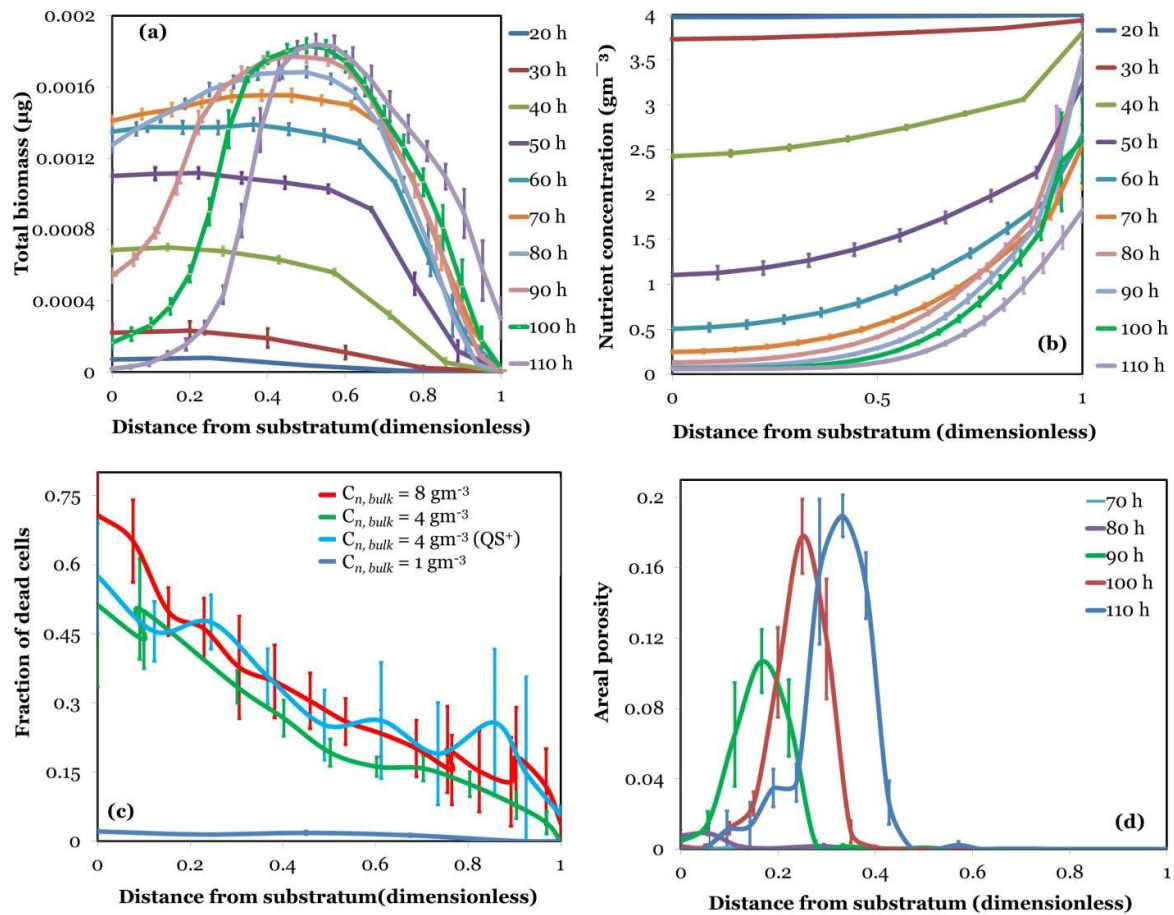
Figure 4.7. Distributions of biomass (a), nutrient concentration (b), fraction of dead cells (c), and areal porosity (d) at varying distances from the substratum for $C_{N,bulk}$ = 4 gm^{-3} for growth times of 20-110 h. The fractions of dead cells in (c) are reported at the time of sloughing for the respective bulk nutrient concentrations. Data represent mean ± SEM of four separate simulations.

To investigate the spatial variation of heterogeneity, the distribution of biomass and nutrient concentrations at varying distances from the substratum for the bulk nutrient concentration of 4 gm^{-3} were determined. In the early and late exponential growth phases (up to 70 h), the biofilm was homogeneous in the lower and intermediate layers with uniform biomass distribution. The distribution in the upper layers was non-uniform, with biomass decreasing rapidly with increasing distance from the substratum (Fig. 4.7a). The heterogeneity at the

top layers is a consequence of the fact that during cell division new daughter cells are randomly placed in the closest neighbouring locations.

The biomass distribution underwent a dramatic change in the late exponential phase (80-110 h) with a high proportion of the biomass concentrated in the intermediate layers (25-40 μm from the substratum) (Fig. 4.7a). In contrast, the nutrient concentration decreased monotonically with decreasing distance from the substratum (Fig. 4.7b), indicating that a large portion of the nutrient is consumed at the surface, and in the intermediate layers leading to nutrition-depleted niches in the depths. However, it should be noted that under these conditions nutrient concentration levels in the lower layers was high enough to not cause cell death (Fig. 4.7c).

The value of the maximal biomass and the height at which it occurred increased with time (Fig. 4.7a). For instance, at 60 h maximal biomass is observed at a height of 12 μm (0.0014 μg). On the other hand, at 110 h maximal biomass is observed at a height of 33 μm (0.0018 μg). Biomass in the layers in close proximity to the substratum declined rapidly due to cell death occurring in this region of the biofilm (Fig. 4.7c). This can be explained by the fact that in the stationary growth phase the nutrient concentrations reduced to very low levels ($<0.2 \pm 0.06$ gm^{-3}) within a distance of 24 μm from the substratum (Fig.4.7b). This, in turn, is a consequence of the fact that cells in the topmost and intermediate layers of the biofilm consume nutrient, allowing less of it to penetrate to the depths of the biofilm.

Immediately prior to sloughing, maximal cell death was observed in the lower layers of the biofilm for bulk nutrient concentrations of 4 and 8 gm^3 (Fig. 4.7c). Approximately three-fourths of the cells on the lowest layer died for $G_{N,bulk} = 8$ gm^{-3}, whereas a little over half the cells on the lowest layer died for $G_{N,bulk} = 4$ gm^{-3}. On the other hand, for the lowest bulk nutrient concentration of 1 gm^3, the distribution of dead cells remained virtually constant across all layers of the biofilm (Fig. 4.7c). Sloughing did not occur under these conditions (Fig. 4.7a).

Interestingly, for the highest bulk nutrient concentration (8 gm^3), cell death happened due

to starvation (low nutrient consumption-to-maintenance ratio) whereas for the intermediate and low bulk nutrient concentrations (1, 4 gm^3), cell death occurred due to cells being in the stationary phase for the prescribed limit (24 h). Along these lines, nutrient availability -- and hence the nutrient consumption rate -- in the lower layers was less for the higher bulk nutrient concentration of 8 gm^3 compared to that for $C_{N,bulk} = 4$ gm^{-3} and $C_{N,bulk} = 1$ gm^{-3}. For instance, the average nutrient concentrations at the dimensionless biofilm height of 0.5 increased with decreasing bulk nutrient concentrations (0.08 $\pm$ 0.007 gm^3, 0.26 $\pm$ 0.03 gm^{-3}, and 0.95 $\pm$ 0.01 gm^{-3} for bulk nutrient concentrations of 8 gm^3, 4 gm^{-3}, and 1 gm^{-3}, respectively). Consequently, amongst the three bulk nutrient concentrations studied, the nutrient consumption rates near the substratum were the lowest for $C_{N,bulk} = 8$ gm^{-3} compared to those for $C_{N,bulk} = 1, 4$ gm^{-3}. A similar behaviour was observed for QS^- biofilms (Fig. 4.7c).

Thus, there was a negative correlation between the bulk nutrient concentration and nutrient availability in the lower regions of the biofilm, with nutrient availability being the lowest for the highest bulk nutrient concentration of 8 gm^3, and the highest for the bulk nutrient concentration of 1 gm^3. This effect became more pronounced towards the end of the exponential growth phase, as the biofilm approached the stationary phase. This can be explained by the fact that because of the high growth rate, the number of cells/total biomass in the intermediate regions is highest for $C_{N,bulk} = 8$ gm^{-3} . This, in turn, causes the nutrient consumption rates to be high, consequently reducing the availability of nutrients in the lower regions.

The areal porosity was minimal in the exponential growth phase (up to 80 h) (Fig. 4.7d). Subsequently, in the stationary phase, areal porosity increased with time. This is a consequence of an upsurge in cell death events in the stationary phase, thereby creating cell-devoid pockets in the interior of the biofilm. Maximal areal porosity was observed in the intermediate layers, and decreased for layers closer to the substratum. This indicates that although the biomass density near the substratum is low, the biofilm is more compact in this region. Prior to sloughing, the biomass and nutrient distributions were found to be similar for the QS^+ biofilms (data not shown).

61
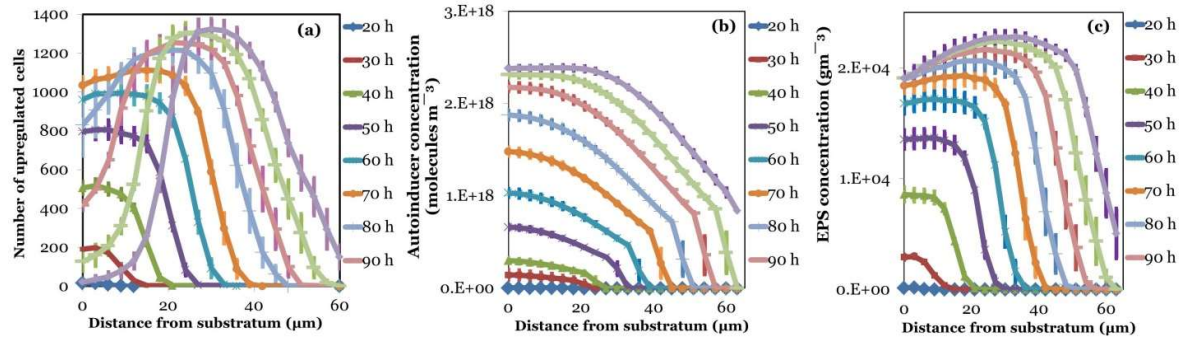
Figure 4.8. Distribution of upregulated bacterial cells (a), and concentration distributions for the autoinducer (b) and EPS (c) for $C_{N,bulk}$ = 4 gm^{-3} for QS+ biofilms. Data represent mean $\pm$ SEM for four separate simulations.

For biofilms utilizing QS, the number of upregulated cells increased with time (Fig. 4.8a), resulting in a corresponding increase in the average autoinducer (Fig. 4.8b) and EPS concentrations (Fig. 4.8c). Although the entire biofilm was primarily comprised of upregulated cells (Fig. 4.4a), maximal autoinducer and EPS concentrations occurred in the lower layers, and decreased farther away from the substratum (Figs. 4.8b, 4.8c). This could be explained as follows: nonuniform distribution of bacterial biomass results in spatially irregular rates of autoinducer production. Maximal autoinducer production occurs in the intermediate layers (with highest biomass concentrations), with production rates decreasing in the top and bottom layers. Thus, vertical autoinducer concentration gradients are set up, resulting in diffusion towards the DBL and the substratum. The no-flux boundary condition at the substratum results in the accumulation of the autoinducer in the lower region of the biofilm. On the other hand, the Dirichlet condition applied at the DBL causes the autoinducer in the top layers to be removed from the domain. In the stationary growth phase, although biomass density near the substratum was low, EPS concentrations were high and uniform. This is a consequence of the fact that EPS produced by cells prior to dying remains within the domain, causing EPS to accumulate in this part of the biofilm.
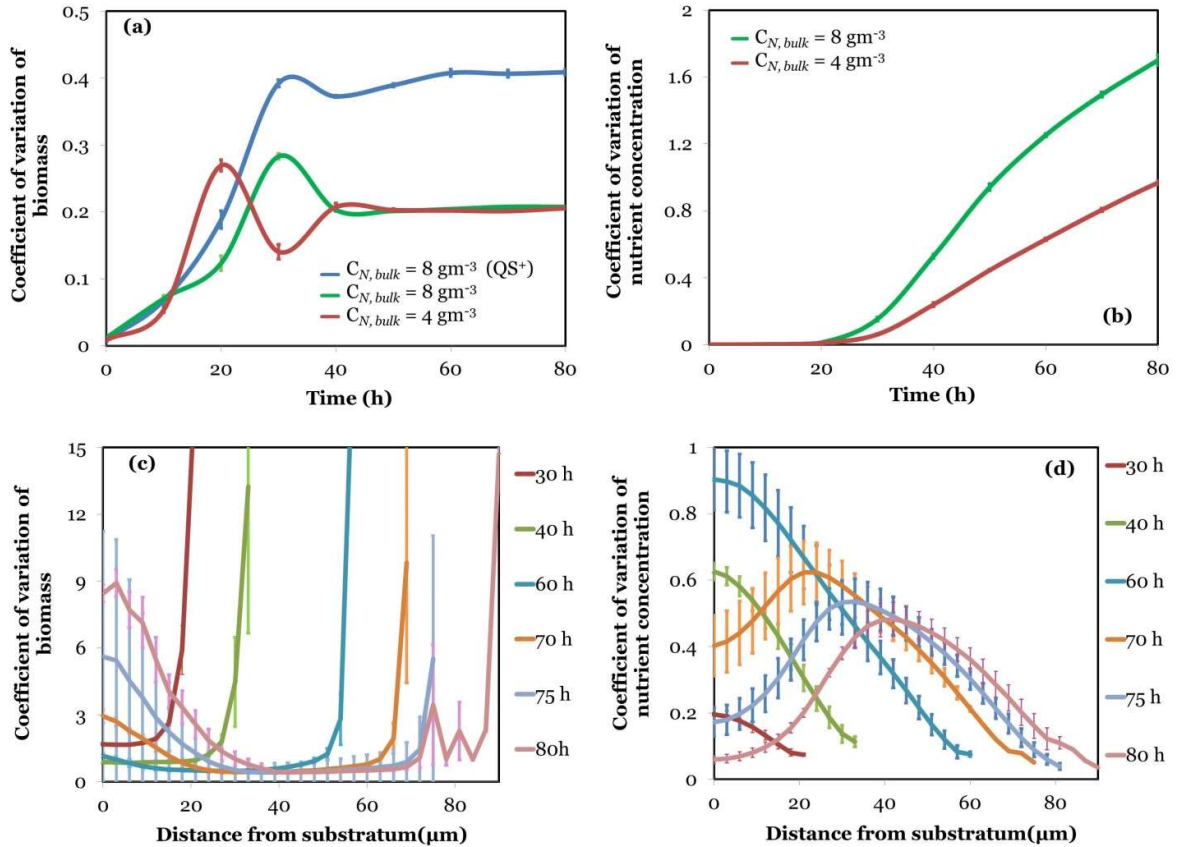
Figure 4.9. Biofilm heterogeneity, expressed as the coefficients of variation for the biomass (a) and nutrient concentration (b), tracked over time under two nutrient conditions ($C_{N,bulk}$ = 8, 4 gm^{-3}); variation of heterogeneity in biomass (c) and nutrient concentration (d) as a function of the distance from the substratum; comparison of biomass heterogeneity for QS$^-$ and QS$^-$ biofilms for $C_{N,bulk}$ = 8 gm^{-3} is shown in panel (a).Data represent mean $\pm$ standard error of mean (SEM) of four replicate simulations.

At the bulk nutrient concentration of 8 gm^3, the overall biomass heterogeneity increased rapidly in the early exponential phase, and reached a maximum of 0.28 $\pm$ 0.004 at 30 h. As the biofilm developed further -- resulting in an increase in the number of mature cells -- a corresponding lowering of the overall biomass heterogeneity was observed. Heterogeneity remained virtually constant after 40 h of biofilm growth. A similar trend was observed for biofilms associated with the bulk nutrient concentration of 4 gm^3 (Fig. 4.9a). The QS$^+$

biofilm was more heterogeneous compared to the QS biofilm at all times tested (Fig. 9a). This could be a direct consequence of the nonuniform distribution of EPS in the QS biofilm (Fig. 4.8c). In contrast, the coefficient of variation for the nutrient concentration increased monotonically with time in the exponential growth phase for both bulk nutrient concentrations studied (Fig. 4.9b). In the lag phase, nutrient concentration was homogeneous throughout the biofilm (Fig. 4.9b). In the early exponential growth phase nutrient heterogeneity was maximal in the lowermost layers (Fig. 4.9d). In the late exponential and stationary phases, maximal heterogeneity was observed in the intermediate layers (Fig. 4.9d). This correlates with the observation that in the late exponential phase the proportion of biomass in the intermediate layers is maximal (Fig. 4.7a).

Next, the spatial variation of biofilm heterogeneity for the bulk nutrient concentration of 8 gm^{-3} was investigated. At low time points (up to 60 h), biofilm heterogeneity was low throughout the bulk of the biofilm, and was virtually independent of the distance from the substratum. The heterogeneity showed a marked increase near the DBL because of the stochastic nature of the cell division process in the top layers. Beyond 60 h, biofilm heterogeneity showed a significant increase in the lower layers (Fig. 3.9c). This is a consequence of the initiation of cell death events at the 60 h time point. At 80 h, the heterogeneity at the lowest layer reached a maximum (8.4 $\pm$ 0.4), resulting in sloughing of the biomass. Taken together, this analysis suggests that sloughing of the biofilm is a direct consequence of the increased biomass heterogeneity in the lower regions of the biofilm. The enhancement of the local heterogeneity near the substratum can be explained by the increased rates of cell death in this portion of the biofilm.

4.3 Conclusions

While it is well-known that biofilm-associated microorganisms are more tolerant to antibiotics compared to their planktonic counterparts, it is only subpopulations of cells that exhibit increased antibiotic resistances. However, the underlying biophysical mechanisms for the emergence of these antibiotic-insensitive subpopulations remain obscure. A systematic investigation of the spatiotemporal variation of structural and chemical heterogeneity in biofilms could aid in delineating mechanisms of antibiotic resistance at the fine scale. In this

work, an individual-based cellular automata model is used to simulate biofilm growth under diverse nutrient conditions, in the presence and absence of quorum sensing. Each bacterium was modelled as an independent entity, allowing us to monitor structural and chemical heterogeneity of the biofilm as a function of time and space.

The key findings are summarized below:

1. Mature biofilms comprise of three structurally distinct layers: a highly porous homogeneous region sandwiched between two compact regions of high heterogeneity. This results in the formation of a mushroom-like structure with a low-density, high-volume "head," supported by a compact, low-volume "stalk" underneath.

2. Biofilms utilizing QS grow faster and are more heterogeneous compared to their QS counterparts. An additional layer of EPS -- devoid of cells -- forms atop the substratum, upon which the rest of the biofilm continues to develop. In agreement with experimental results, the model predicts that biofilms utilizing QS are structurally more stable, exhibiting a prolonged stationary growth phase, and a resistance to sloughing.

3. Whereas the biomass distribution is virtually uniform throughout the biofilm in the lag and early exponential growth phases, it undergoes a dramatic transformation in the late exponential and stationary phases with maximal biomass occurring in the middle layers of the biofilm. The heterogeneity and thickness of the lowermost layer increased with time, ultimately leading to sloughing. This is a direct consequence of preferential cell death occurring in close proximity to the substratum.

4. This model is able to illustrate the formation of microcolonies comprising of metabolically inactive cells surrounded by cells exhibiting high growth rates. We hypothesize that these dormant cellular micro-compartments represent sites of low antibiotic susceptibility. There are two possible reasons for this: (i) the surrounding high-activity cell clusters may present a reaction-diffusion barrier, thereby decreasing antibiotic penetration to the microniches, and (ii) low-activity cells may consume antibiotics at a diminished rate, thereby reducing efficacy of treatment. A systematic investigation of the structural properties of these sections of the biofilm, and their response to antibiotic treatment may shed light on the biophysical mechanisms of antibiotic resistance.

In the future, we plan to use the current model to investigate the response of bacterial

biofilms to antibiotic treatment. Since the model simulates spatiotemporal variability of biofilm constituents (such as biomass, EPS, nutrient, and signalling molecules), it may be instructive to correlate antibiotic-resistant of bacterial biofilms with the emergence of metabolically inactive cell clusters.

Chapter 5. A 3D individual-based model to investigate the spatially heterogeneous response of bacterial biofilms to antimicrobial agents

5.1 Introduction

Biofilms are surface-associated communities of microorganisms embedded in an extracellular matrix composed primarily of self-produced polysaccharides [3, 184]. Biofilms shelter bacteria from environmental stresses and from the host immune response, thereby increasing resistance to antibiotics and phagocytosis, as well as to other components of the innate and adaptive immune systems [185, 186]. Several mechanisms -- acting synergistically -- contribute to the reduced antimicrobial and biocide susceptibility that is characteristic of biofilm communities. Expression of specific genes may allow biofilm bacteria to actively adapt to, and survive, antimicrobial exposure [29, 187-190]. For instance, the ndvB locus has been identified as a P. aeruginosa biofilm-specific antibiotic resistant gene; ΔndvB biofilms were 16-fold more susceptible to tobramycin and 8-fold more susceptible to both gentamicin and ciprofloxacin than wild-type biofilms [82]. In response to antibiotic treatment, overexpression of toxins that inhibit essential functions such as translation may contribute to the transformation of biofilm bacteria to an antibiotic tolerant phenotype [191]. These genetic mechanisms attribute resistance of the biofilm to antibiotic tolerance at the single-cell level [192, 193].

Antibiotic resistance may also emerge as a consequence of physiological characteristics inherent to the biofilm mode of growth [3, 194]. Biofilms are characterized, among other things, by the presence of nutrient and antibiotic gradients, diffusion and penetration limitations, and a matrix of extracellular polymeric substances (EPS) [32, 195, 196]. Bacteria growing in biofilms are physiologically heterogeneous, due in part to their adaptation to local environmental conditions. They occupy a spectrum of growth states

from rapidly growing and active to slow-growing and dormant. Consequently, distinct microcolonies with clusters of bacterial cells may develop within the biofilm where cellular physiology is different from surroundings in terms of metabolic activity, secretion of EPS, and concentrations of nutrients and antimicrobial agents [31, 32, 197, 198]. This intrinsic physiological heterogeneity of biofilms may play a role in the adaptive stress response, and contribute to the protection of cells [62]. Experimental evidence suggests that it is only certain subpopulations within biofilms that show greatly increased phenotypic resistance to treatment, whereas the remaining cells exhibit sensitivity [33, 89, 199]. A particular antimicrobial agent may effectively target certain populations of cells, but leave the remaining cells viable, allowing them to repopulate the biofilms when the treatment is stopped. For instance, cells deep within P. aeruginosa biofilms are reported to be in a metabolically inactive, antibiotic-tolerant state, whereas cells at the periphery are faster growing, and susceptible to antimicrobial agents such as ciprofloxacin, tetracycline, and tobramycin [200, 201]. The biophysical mechanisms underlying this spatially non-uniform response of biofilms to antimicrobial treatment remain incompletely understood.

The lowest concentration of the antimicrobial agent required to eradicate the biofilm is termed the minimum biofilm eradication concentration (MBEC) [92]. Subjecting the biofilm to sub-lethal concentrations of the antibiotic (sub-MBEC) enhances biofilm formation in vitro [202-204]. For instance, subjecting P. aeruginosa biofilms to sub-MBEC treatment induces genetic triggers that result in the enhanced formation of colonic acid [205]. This, in turn, causes an increase in the synthesis of EPS which contributes to the protection of the bacterial population. Antibiotic-induced biofilm formation has clinical relevance because bacteria are exposed to low concentrations of antibiotics at the beginning and the end of treatment, or continuously during low-dose therapy [204]. Investigating the reasons for survival of biofilms in response to sub-MBEC treatment of antibiotics may help delineate biophysical mechanisms of antibiotic resistance.

Quorum sensing (QS) is a process by which bacteria coordinate their behaviour in a cell-density dependent manner by producing and detecting signalling molecules called autoinducers [65, 69, 70]. QS has been shown to control the amount of EPS synthesis in P.

aeruginosa biofilms [66, 67, 72, 78, 173]. Furthermore, experimental investigations support the role of QS-regulated EPS in the resistance of P. aeruginosa biofilms to antibiotic treatment [74]. The EPS matrix protects the biofilm by impeding penetration of tobramycin via ionic interactions at the periphery [25, 78]. In addition, antibiotic susceptibility of S. aureus biofilms towards vancomycin increases in the presence of QS-inhibitors by deactivating EPS biosynthesis [79]. Nutrient concentration gradients in QS biofilms may induce spatio-temporal heterogeneity in autoinducer secretion, which may, in turn, result in microscale variation in EPS production. How the spatial heterogeneity of EPS influences the heterogeneous response of biofilms to antibiotics is currently not known.

Previously a three-dimensional, individual-based computational model is formulated and analysed to simulate biofilm growth dynamics, and to quantify spatial heterogeneity in the bacterial population as a function of nutrient availability and quorum sensing [106]. The model treats bacterial cells as individual entities with their own states, thereby allowing for variability between individual behaviours with respect to their growth rates, antibiotic and nutrient uptake rates, autoinducer production, up-regulation and down-regulation states, and EPS secretion. The individual-based, discrete nature of the model combined with physical dynamics causes chemical and structural heterogeneities within the biofilm to emerge as a consequence of the actions and interactions of the cells with each other, and with the surrounding environment, rather than being a model input. In this work, response of QS and QS^+ biofilms to treatment with antibiotics, and the influence of heterogeneity on this response are investigated. The goal was to answer the following questions: (1) Do local physiological and chemical heterogeneities in the biofilm influence the spatially heterogeneous antibiotic resistance in the absence of genetic triggers? (2) What roles do biophysical and cellular processes play in enhanced biofilm formation in response to treatment with sub-lethal doses of antibiotics? (3) What role does EPS play in the heterogeneous response of the biofilm to antibiotic treatment? These results indicate that during the initial stages of treatment, the proportion of the fast-growing, metabolically active subpopulation decreases due to exposure to the antibiotic. This results in an increase in the nutrient availability to the dormant cells in the inner regions of the biofilm. I propose that this triggers a transformation from the dormant state to the metabolically active state, and that this transformation is a key mechanism of resistance. When subjected to sub-MBEC treatment,

antibiotic-induced cell death at the biofilm surface leads to increased nutrient availability in the inner regions, resulting in enhanced growth compared to the untreated biofilm. Due to the protective influence of EPS, QS^+ biofilms required a higher concentration of the antibiotic to eradicate compared to the QS^- biofilms.

5.2 Methods

5.2.1 Bacterial heterogeneity based on growth rates

Cells within the biofilm are classified into three groups based on their growth rates: cells exhibiting (i) high (HGR), (ii) intermediate, and (iii) low growth rates (LGR). The growth rate of each cell is evaluated as the change in biomass over a period of 4 h. Growth rates vary from ~10 to ~10,000 gm^3h^{-1}. After 64 h of growth (in the absence of antibiotic treatment), cells are sorted from highest to the lowest growth rates. The top 10% of the cell population is classified as HGR, and the bottom 10% as LGR. This percentage of HGR is in agreement with experimental observations that suggest that the proportion of active bacteria in biofilms is range from ~5-35% [206, 207]. Using this methodology, the threshold growth rate above which cells ae classified as HGR is set to 6000 gm^3h^{-1}, and that below which cells are classified as LGR is set to 425 gm^3h^{-1}.

5.3 Results

5.3.1 Biofilm growth dynamics in response to antibiotic treatment
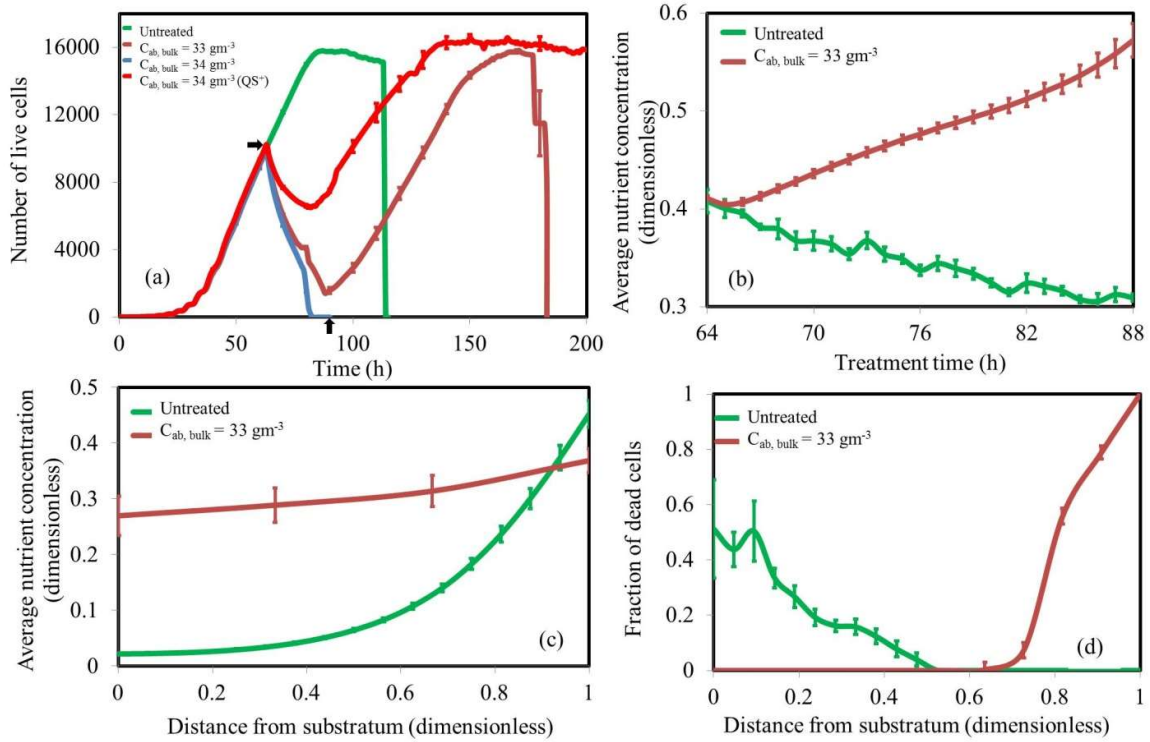
Figure 5.1. Growth dynamics of QS$^-$ and QS$^+$ biofilms in the absence and presence of antibiotic treatment. The number of live cells as a function of time for $C_{N,bulk} = 4\ gm^{-3}$ for the untreated QS$^-$ biofilm (green), and when subjected to a continuous 24h (64-88 h) treatment of sub-MBEC ($C_{ab,bulk} = 33\ gm^{-3}$, red), and MBEC ($C_{ab,bulk} = 34\ gm^{-3}$, blue); the QS$^+$ biofilm is subjected to $C_{ab,bulk} = 34\ gm^{-3}$ (orange) (a), comparisons of average nutrient concentration (b), spatial distribution of average nutrient concentration (c) and spatial distribution of fraction of dead cells (d) for the QS$^-$ biofilm subjected to sub-MBEC and the untreated biofilm. Data in panels (c) and (d) are reported at 88 h, the time point at which treatment stops. The arrows in panel (a) represent – initial (64 h) and end (84 h) time points of antibiotic treatment. Data represent mean ± standard error of mean (SEM) of four replicate simulations.

The growth dynamics of a bacterial biofilm over a period of 200 h was simulated, in the presence and absence of QS. In select runs, the biofilm was subjected to a continuous antimicrobial treatment ($C_{ab,bulk}$ ranging from 15 to 60 gm^{-3}) for duration of 24 h, initiated after 64 h of growth (cell number ~10,000). Whereas subjecting the biofilm to $C_{ab,bulk}$ of 34 gm^{-3} resulted in complete removal after 21 ± 0.5 h of treatment (Fig. 5.1a), a slightly lower antibiotic concentration (33 gm^{-3}) was insufficient to eradicate the biofilm. Interestingly, biofilms treated with sub-MBEC ($C_{ab,bulk}$ of 33 gm^{-3}) exhibited a prolonged lifetime compared to even the untreated biofilms, with the former sloughing off at 184 ± 2.7 h while the latter at 113 ± 0.5 h (Fig. 5.1a). This is in line with the experimental observation that sub-MBEC treatment enhances biofilm formation [208]. The average nutrient concentration within the sub-MBEC-treated biofilm increased monotonically with time, and was higher compared to the untreated one (Fig. 5.1b). This is a consequence of the fact that antibiotic-induced cell death in the sub-MBEC-treated biofilm causes the live cell number – and hence, the overall nutrient consumption – to decrease. In contrast, bacterial biomass in the untreated biofilm increases with time, resulting in increased nutrient consumption and reduced average nutrient concentration compared to the sub-MBEC-treated biofilm. The spatial distribution of nutrient concentration (measured as a function of the distance from the substratum) shows that nutrient penetration to the lower layers in the untreated biofilm was lower compared to the treated biofilm (Fig. 5.1c). This, in turn, causes cell death to occur near the bottom for the untreated biofilm, subsequently leading to sloughing (Fig. 5.1d). These findings are in agreement with experimental results showing that localized nutrient starvation is an environmental cue for the sloughing of biofilms [57]. In contrast, cell death was restricted to the top layers in the sub-MBEC-treated biofilm (Fig. 5.1d). In agreement with experimental observations, sub-MBEC-treatment does not fully eradicate bacteria during the treatment phase [101], and biofilm thickness was restored to pre-treatment levels within 24 h after exposure to the antibiotic.

MBEC for the QS$^+$ biofilm was 51 gm^{-3}, and was significantly higher than that for QS$^-$. Comparing responses of the QS$^-$ and QS$^+$ biofilms when subjected to a bulk antibiotic concentration of 34 gm^{-3} showed that whereas there was no significant difference in the viable cell counts for the first 8 hours of treatment, the live cell number for the QS$^-$ biofilm reduced at a lower rate for the rest of the treatment (Fig. 5.1a).

5.3.2 Comparison of responses to MBEC- and sub-MBEC-treatments
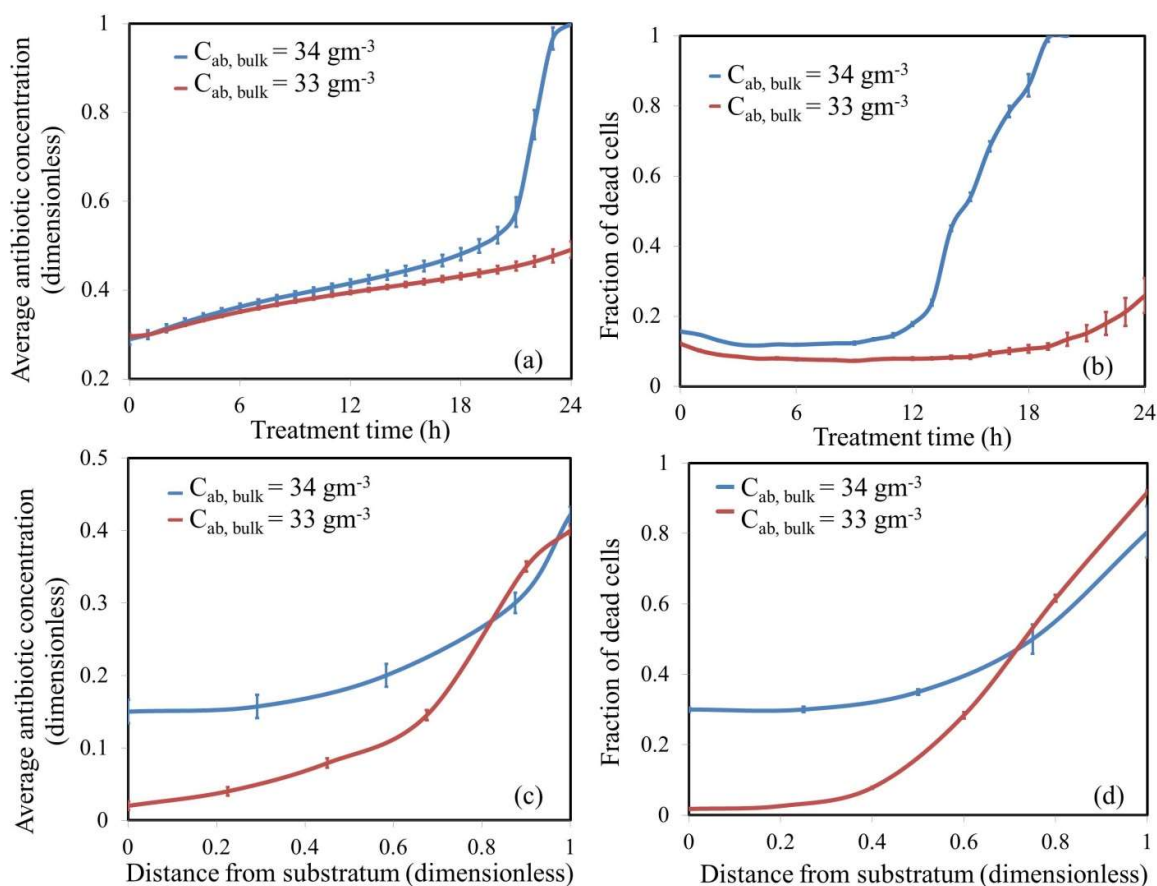
Figure 5.2. Response of the biofilm to MBEC and sub-MBEC treatments. The average antibiotic concentration (a) and fraction of dead cells (b) as a function of time, upon treatment with MBEC (blue) and sub-MBEC (red). Spatial profiles for antibiotic concentration (c), and fraction of dead cells (d) after 16 h of treatment for the MBEC-treated (blue) and sub-MBEC-treated (red) biofilms. Data represent mean ± standard error of mean (SEM) of four replicate simulations.

To investigate the dramatically different responses of the QS biofilms subjected to two slightly different antibiotic concentrations (MBEC and sub-MBEC), the temporal variation in the average antibiotic concentrations within the biofilms was tracked. A small difference in the bulk antibiotic concentrations (1 gm³) was amplified to a much larger difference in average antibiotic concentrations within the biofilms; this difference was more pronounced

at higher time points (after ~12 h of treatment) (Fig. 5.2a). This, in turn, led to higher cell death events in MBEC-treated biofilms compared to the ones treated with sub-MBEC (Fig. 5.2b). Under these conditions (after ~12 h of treatment), antibiotic penetration to the lower layers was more effective in the biofilm treated with MBEC compared to the one treated with sub-MBEC (Fig. 5.2c). For instance, after 16 h of treatment, the average antibiotic concentration at the substratum of the biofilm exposed to MBEC was ~7.5 times that of the biofilm treated with sub-MBEC (Fig. 5.2c). This marked difference in local antibiotic concentrations in the lower regions of the biofilm resulted in significantly higher death events for the MBEC-treated biofilm compared to the biofilm treated with sub-MBEC (Fig. 4.2d). Whereas ~30% of the cells in the lowest layer died when the biofilm was subjected to MBEC, negligible cell death (~2%) occurred near the substratum of the sub-MBEC-treated biofilm (Fig. 4.2d). This difference in the fraction of dead cells at the bottom layers of the biofilm was observed at all treatment time points, ultimately leading to the eradication of the MBEC-treated biofilm. Similar trends were observed for the QS biofilm upon MBEC- (51 gm^{-3}) and sub-MBEC (50 gm^{-3}) treatments (data not shown).

5.3.3 Correlation between cellular metabolism rates and antibiotic-induced death

Biofilms comprise of bacterial cells in a wide range of physiological states, resulting in a spatially heterogeneous system. To investigate the influence of this spatial heterogeneity on the response of the biofilm to MBEC- and sub-MBEC treatments, live cells were categorized into three groups based on their growth rates: (i) metabolically active cells, exhibiting high growth rates (HGR), (ii) intermediate, and (iii) dormant cells, exhibiting low growth rates (LGR). There was a strong correlation between dead cells and HGR-cells in the presence of antibiotic treatment. On an average, during treatment, 59.79 ± 6.1% of HGR died at any given time step. On the other hand, LGR-cells were less susceptible to killing by antibiotic (~ 0.001%). In stark contrast, in the absence of antibiotic treatment, there was a strong correlation between dead cells and LGR-cells, with 34.15 ± 2.8% of LGR dying on an average at any given time step. Under these conditions, cell death occurred predominantly due to nutrient starvation at later time points (80 h onwards). The number of dead HGR-cells was negligible in the untreated biofilm.

5.3.4 Spatial distribution of heterogeneous subpopulations in biofilms during treatment
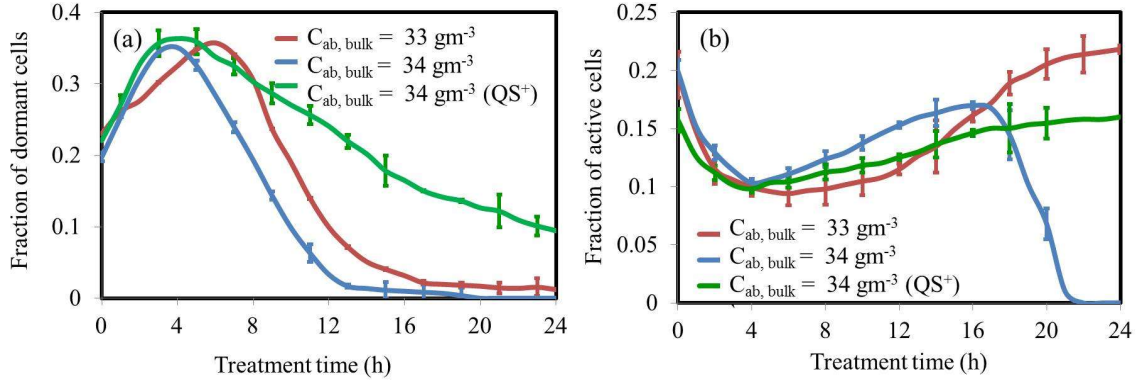
Figure 5.3. Growth dynamics of subpopulations in the presence of antibiotic. Comparison of fraction of dormant cells (a), fraction of metabolically active cells (b) as a function of time for $C_{N,bulk} = 4$ gm-3. QS- biofilms treated with MBEC (blue) and sub-MBEC (red), and QS+ biofilm subjected to $C_{ab,bulk}$ of 34 gm-3 (green). Data represent mean ± standard error of mean (SEM) of four replicate simulations.

Next, the dynamics of the distinct growth-rate-based cell subpopulations in QS and QS+ biofilms in response to antibiotic treatment were tracked. Based on the fraction of HGR- and LGR-cells, three distinct phases were observed during 24 h of continuous antibiotic treatment (Figs. 5.3a and 5.3b). In the first phase that lasted ~4h, the total biomass reduced dramatically (~40% reduction). In this phase, the fraction of dormant cells increased with time, reaching a peak after 4h of treatment (Fig. 5.3a). On the other hand, the subpopulation of active cells decreased with time (Fig. 5.3b). After 4 h, the antibiotic consumption rates by dormant cells in the MBEC-treated biofilms were ~17 times higher compared to those of active cells (50.5 ± 9.4 gm³ h^{-1} for dormant cells, versus 850.5 ± 65.4 gm^{-3} h^{-1} for active cells). This indicates that metabolically active cells at the distal edge of the biofilm act as a reaction-diffusion barrier, thereby reducing antibiotic penetration to the LGR-cells near the substratum. This results in lower antibiotic uptake rates by the LGR-cells, allowing them to survive antibiotic treatment. The second phase lasted for ~8h, and was characterized by a decrease in the number of dormant cells (Fig. 5.3a). For the biofilm treated with MBEC, phases I and II were qualitatively similar to those observed for sub-MBEC treated biofilm. However phase II is delayed and prolonged in the biofilms treated

75

with sub-MBEC (~5 h to 18 h) in comparison with MBEC-treated biofilms (4h to 12 h). The third phase was characterized by the complete eradication of the MBEC-treated biofilm. In contrast, the sub-MBEC-treated biofilm survived in phase III. More importantly, the fraction of active cells in the third phase of sub-MBEC treatment increased, resulting in the regrowth of the biofilm after the termination of antibiotic treatment.

The QS^+ biofilm survived treatment at $C_{ab,bulk}$ of 34 gm^{-3}. In contrast to the QS^- biofilm, the fraction of dormant cells increased monotonically in the third phase of QS^+ biofilms (Fig. 5.3a). This could be a direct consequence of the increased viable cell number during treatment (Fig. 5.1a), resulting in reduced nutrient availability in the lower regions of the biofilm. This starvation may lead to lower metabolic activity. Although both QS^- and QS^+ biofilm survived treatment with 33 gm^3, the mechanisms of survival appear to be different. Whereas the QS^- biofilm survives by rapidly transforming the metabolically inactive cells into active ones, the survival of the QS^+ biofilm is a consequence of reduced exposure of the dormant cells to antibiotic.

5.3.5 Spatial distribution of growth rates

Figure showing spatial distribution across three columns: $C_{ab,\,bulk} = 33$ gm^{-3} (QS$^-$), $C_{ab,\,bulk} = 34$ gm^{-3} (QS$^-$), and $C_{ab,\,bulk} = 34$ gm^{-3} (QS$^+$). Rows show Fraction of active cells (a, b, c), Fraction of dormant cells (d, e, f), Fraction of dead cells (g, h, i), Average nutrient concentration (dimensionless) (j, k, l), and Average antibiotic concentration (dimensionless) (m, n, o) plotted against Distance from substratum (dimensionless). Legend time points: 0 h, 4 h, 12 h, 20 h, 24 h.

Figure 5.4. Spatial heterogeneity in treated QS and QS$^+$ biofilm. Comparison of sub-MBEC (panels a, d, g, j, and m) and MBEC-treated QS biofilms (panels b, e, h, k, n) and MBEC- treated QS$^+$ biofilms (panels c, f, i, l, o) at different time points during 24 h treatment period. The spatial distribution of the fraction of dormant cells (panels a-c), active cells (panels d-f), and dead cells (panels g-i), local nutrient (panels j-l), and antibiotic concentrations (m-o). Data represent mean $\pm$ standard error of mean (SEM) of four replicate simulations.

To investigate the biophysical mechanisms for the formation of surviving cell pockets within the antibiotic-treated biofilm, the growth rates of individual cells, the distribution of dead cells, and local nutrient and antibiotic concentrations as a function of their position within the biofilm were tracked. Prior to exposure to antibiotics (64 h of growth), a majority of the metabolically active cells are located at the upper layers (Figs. 5.4a-c), and dormant cells are localized at the lower layers (Figs. 5.4d-f). Upon initiation of treatment, cells at the biofilm-bulk liquid interphase are exposed to the antibiotic, resulting in cell death; cell death in the lower regions during this time period is negligible (Figs. 5.4g-i). Because of the consumption of antibiotic by active cells in the top layers, antibiotic penetration to lower layers is reduced (Figs. 5.4m-o). Cells in the lower layers are, thus, able to survive the initial period of treatment. Consequently, the fraction of dormant cells increases near the substratum and active cells decreased at the top (Figs. 5.4d-f). At the end of phase I (4-6 h of treatment), nutrient penetration increased to the interior of the biofilm (Figs. 5.4j, 4.4k). Subsequently, dormant cells located in the lower layers of the biofilm had improved nutrient accessibility, resulting in increased growth rates. This, in turn, results in the transformation of inactive cells to the metabolically active state. This is validated by the observation that the fraction of dormant cells decreases and the fraction of active cells increases near the substratum over time (Figs. 5.4a, 5.4b, 5.4d, 5.4e).

Antibiotic penetration to the lower layers in the MBEC-treated biofilm was higher compared to that in the sub-MBEC-treated biofilm (Fig. 5.4m, 5.4n). In the surviving QS biofilm (exposed to $C_{ab,bulk}$ of 34 gm^{-3}), even the topmost bacterial cell was exposed to a local antibiotic concentration that was always less than 30% of the bulk value (Fig. 5.4o).

This is a direct consequence of the sequestration of the antibiotic by the cell-devoid layer of EPS that forms at the distal edge of the biofilm (Fig. 5.5a). In stark contrast, in the QS biofilm subjected to treatment with MBEC, the local antibiotic concentration even at the substratum increased with time, reaching a maximum value of 22.5% of the bulk antibiotic concentration (after 20 h of treatment). Under these conditions, the local antibiotic concentration to which the topmost cell in the biofilm was exposed was as high as 50%.

5.3.6 Influence of QS-regulated EPS production on antibiotic resistance in biofilms
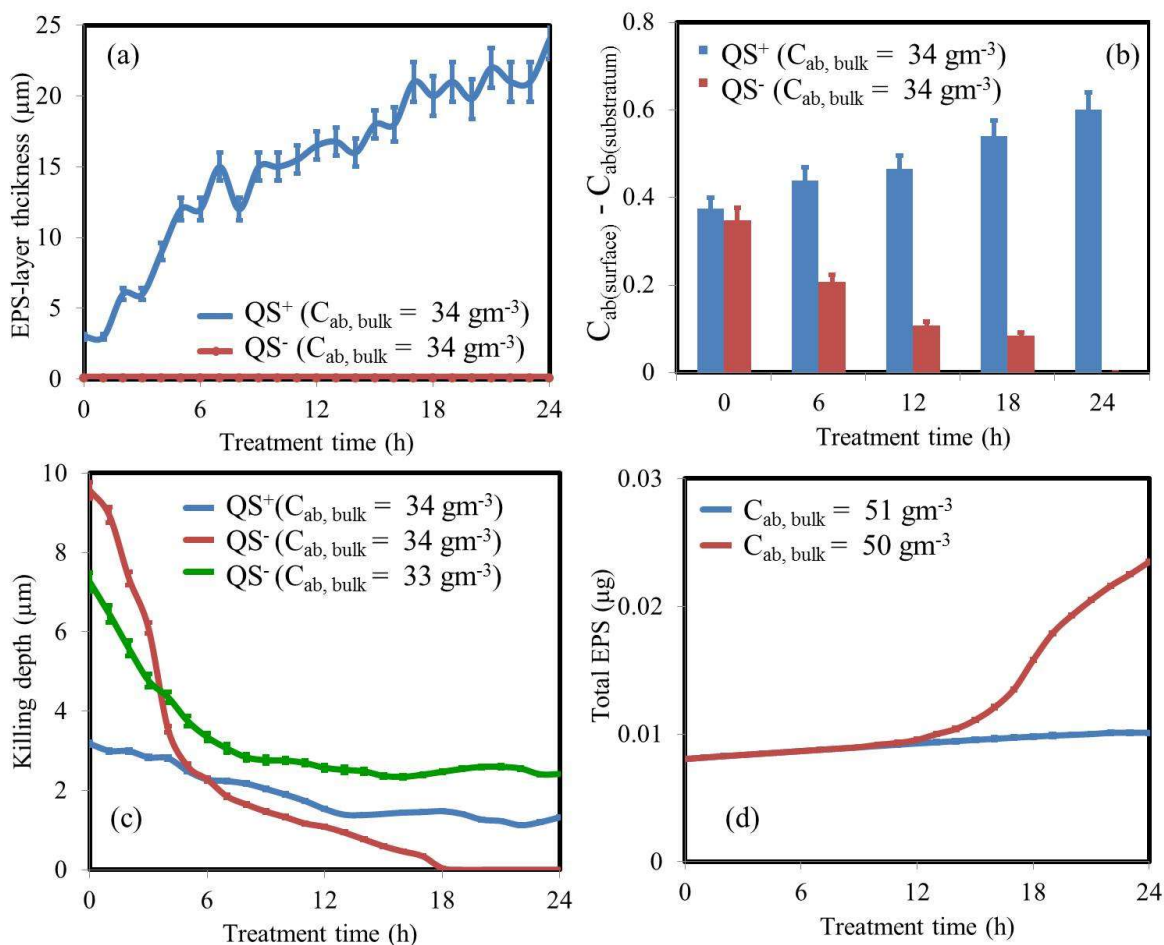
Figure 5.5. Comparison of the response of QS+ and QS- biofilms to antibiotic treatment. Thickness of the cell-devoid layer of EPS at the top of the biofilm plotted as a function of treatment time (a), the difference between the average antibiotic concentrations at the biofilm surface and the substratum for QS+ (blue) and QS- (red) biofilms subjected to $C_{ab,bulk}$ of 34 gm^{-3} (b), the average killing depth for QS+ (blue) and QS- biofilms subjected to $C_{ab,bulk}$ of 34 gm^{-3} (red) and $C_{ab,bulk}$ of 33 gm^{-3} (green) (c), and the total EPS produced for QS+ biofilms subjected to $C_{ab,bulk}$ of 50 gm^{-3} (red) and $C_{ab,bulk}$ of 51 gm^{-3} (blue) (d). Data represent mean ± standard error of mean (SEM) of four replicate simulations.

Next, the responses of the QS (MBEC = 34 gm^{-3}) and QS^{+} (MBEC = 51 gm^{-3}) biofilms subjected to $C_{ab,bulk}$ of 34 gm^{-3} was compared. A cell-devoid layer of EPS is formed at the top of the QS^{+} biofilm, and the thickness of this layer increases as treatment proceeds (Fig. 5.5a). The extent of antibiotic penetration was quantified as the difference between the average antibiotic concentration at the surface of the biofilm and that at the substratum; lower the difference, higher the extent of penetration. Antibiotic penetration in the QS biofilm was significantly lower compared to that in the QS biofilm (Fig. 5.5b), indicating that EPS sequesters antibiotic, thereby lowering the local concentrations in the interior of the biofilm. The largest distance from the surface of the biofilm at which antibiotic-induced cell death occurs was termed the killing depth. In agreement with the observation of fig. 5.5b, the killing depth for the QS biofilms was higher than that for the QS^{+} biofilm. The killing depth decreased monotonically with time for both QS and QS^{+} biofilms as the biofilm thickness reduced. Interestingly, the QS^{+} biofilm subjected to a sub-MBEC treatment ($C_{ab,bulk}$ of 50 gm^{-3}) exhibited enhanced EPS production compared to that when subjected to the MBEC treatment (Fig. 5.5d).
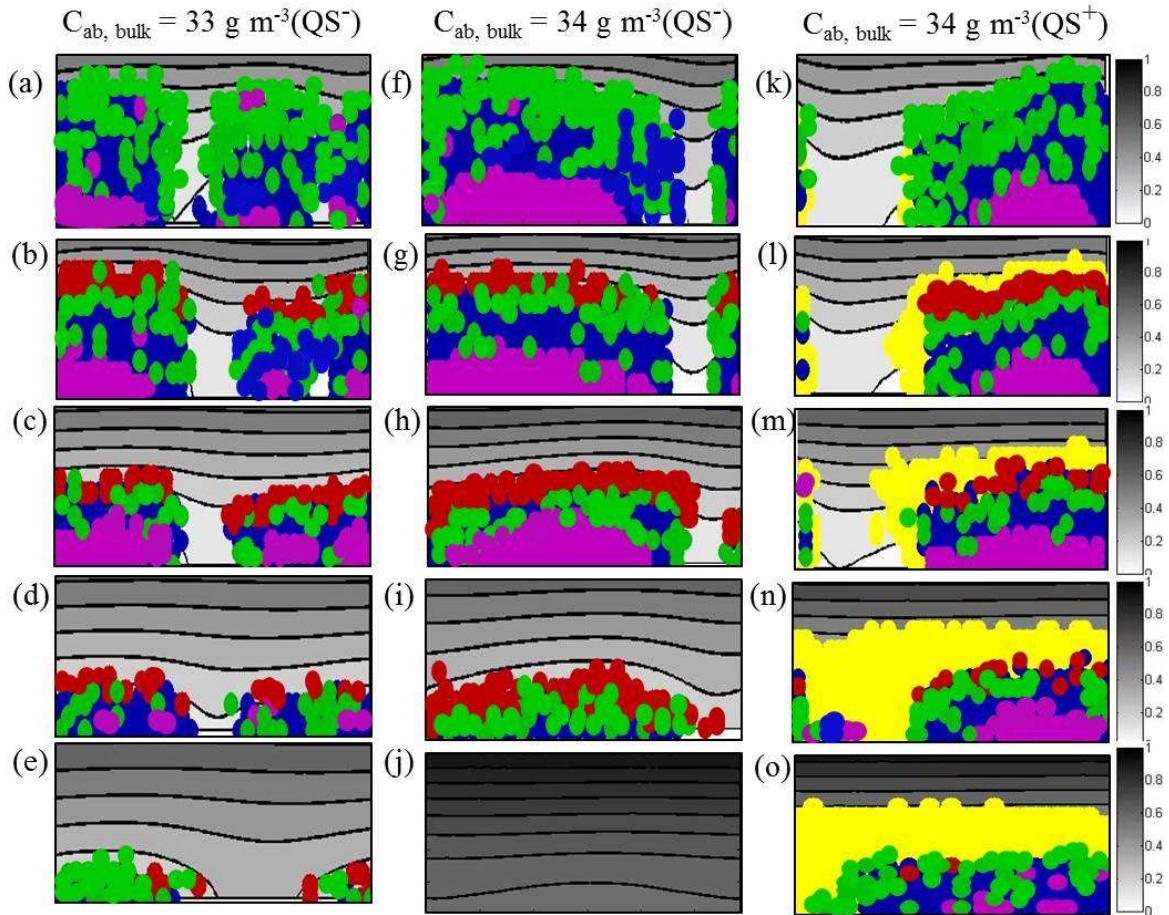
Figure 5.6. QS⁻ Biofilms treated with sub-MBEC (a, b, c, d, e) and MBEC (f, g, h, i, j), and QS⁺ biofilms treated with MBEC (k, l, m, n, o). Visualization of 2D cross-sections showing high growth rate (green), intermediate growth rate cells (cyan), low-growth rate (blue), and locations of cell death (red), of the $C_{N,bulk}$ = 4 gm⁻³ biofilm after 0 h, 1 h, 4 h, 20 h, and 24 h of antibiotic introduction. The yellow color represents EPS in QS⁺ biofilm. The isolines show the antibiotic concentration distribution.

Fig. 5.6 shows representative biofilm cross-sections at various stages of the response, illustrating the formation of surviving cell pockets within antibiotic-treated QS⁻ and QS⁺ biofilms. After the first hour of treatment (panels 5.6a, 5.6e, and 5.6i), dormant cells (pink) were localized in the interior of the biofilm, and were surrounded by layers of cells exhibiting high (green), and intermediate (blue) growth rates. Antibiotic-induced cell death events

(red) occurred at and near the biofilm-bulk liquid interface. For the QS biofilms, thickness reduces as treatment continues, resulting in increased nutrient availability in the bottom layers. This causes the slow-growing (pink) cells to transform into cells with intermediate- (blue) and high- (green) growth rates. This is evident by the diminishing population of slow-growing cells in panels (5.6b), (5.6c), (5.6g), and (5.6h). For the QS biofilm, antibiotic-induced cell death events at the top resulted in the formation of a thin cell-devoid layer of EPS (yellow). This result is in agreement with experimental investigations that indicate that EPS was most abundant at the upper layers of the biofilm [209]. Antibiotic penetration was hindered by an interaction with the matrix of EPS, and results in the protection of bacterial cells in the lower layers. These results are in agreement with previous experimental investigation that suggests that the production of EPS by QS, and the subsequent accumulation in the upper regions of the biofilm, plays a key role in biofilm resistance [25].

5.4 Conclusions

Although bacteria are traditionally investigated as planktonic entities, they predominantly occur as sessile, substratum-associated biofilms. Bacteria associated with the biofilm mode of growth are more resistant to antibiotics, compared to their planktonic counterparts. Several hypotheses have been proposed to explain this resistance including upregulation of virulence factors, formation of persister cells, genetic manipulations, slow penetration of the antibiotic, and the presence of dormant, slow-growing cells. Most of these mechanisms involve antibiotic resistance at the single-cell level, and do not account for the effects of intercellular population dynamics. Physical mechanisms of resistance like retarded penetration of the antibiotic may be a factor in the early stages of treatment, but as treatment proceeds and cells at the top die, antibiotic penetration to the lower layers increases. Hence, retarded penetration of the antibiotic may not be a sufficient explanation as a protecting mechanism in biofilms.

Biofilms comprise of physiologically distinct subpopulations of cells exhibiting varying growth rates, due in part to their adaptation to local environmental conditions. This model is previously characterized this spatial heterogeneity in biofilms [106]. Interestingly,

response of biofilms to an antibiotic challenge is also heterogeneous, with only certain subpopulations becoming resistant while the rest of the biofilm remains sensitive. The main goal was to investigate the influence of the biophysical features of the biofilm mode of growth on antibiotic resistance, when each individual cell itself is not necessarily tolerant to antibiotics. This may help delineate the effect of population dynamics on the antibiotic resistance in biofilms. I also wished to correlate the inherent spatial heterogeneity of biofilms at the cellular level to their heterogeneous response to treatment. Consequently, in this model, each bacterium was modelled as an independent entity, allowing us to monitor structural and chemical heterogeneities in the biofilm and in its response to treatment as a function of time and space.

The minimum antibiotic concentration required to eradicate biofilms is first estimated, followed by estimation of largest antibiotic concentration that the biofilm is able to survive. These conditions are used to further investigate mechanisms of antibiotic resistance in biofilms. Small differences in the bulk antibiotic concentrations were amplified into much larger differences in local antibiotic concentrations to which cells are exposed. Small differences in the bulk antibiotic concentrations were amplified into much larger differences in local antibiotic concentrations to which cells are exposed. When subjected to MBEC and sub-MBEC treatments, the local antibiotic concentration near the substratum for the MBEC-treated biofilm was ~13 times higher compared to that for the sub-MBEC-treated biofilm, although the difference in the bulk antibiotic concentrations was small (1 gm^3). QS$^-$ (non-EPS producing) biofilms, subjected to an antibiotic challenge, responded by increasing the rate of transformation of dormant cells into faster growing, metabolically active cells. In contrast, QS$^+$ biofilms responded by enhancing the rate of EPS production. Overall, insights into these biophysical mechanisms associated with the biofilm mode of growth may pave the way for novel therapeutic strategies to combat the antibiotic resistance of biofilms.

Chapter 6. Future work

6.1 Polymicrobial biofilms

Biofilms can be composed of a bacterial population that develops from a single species or a co-aggregation of multiple bacterial species [1]. By including multiple bacterial species into a single community, the biofilm achieves numerous advantages such as passive resistance [210], metabolic cooperation [211], by-product influence [210], an enlarged gene pool with more efficient DNA sharing[212], induced virulence traits [213], and modulation of host immune response, all of which can promote polymicrobial infection. For instance, when anaerobic bacteria are grown along with aerobic bacteria in a mixed biofilm in oral infections, aerobic bacteria at the surface of dental plaque consume oxygen, thereby providing anaerobic conditions within the deeper layers of the biofilm in which anaerobic bacteria can multiply [214]. Polymicrobial infections are often associated with increased infection severity and poorer patient outcome than mono microbial infections because of complementary resistance to antibiotics [215]. Biofilms of a hospital isolate Bacillus subtilis protect S. aureus from biocide peracetic acid action, thereby contribute to the establishment of chronic nosocomial infections [216].

Alternatively, limited space and nutrients in biofilms can lead to competition between microorganisms resulting in antagonistic interactions, typified by one organism's direct, deleterious impact on another. An example of such antagonistic interaction is the one described between Pseudomonas and Agrobacterium tumefaciens (A. tumefaciens) in which growth rate and motility impacted the fitness of each competitor. P. aeruginosa produces extracellular proteins that is capable of inhibiting the formation of A. tumefaciens biofilms and that this activity is dramatically increased when P. aeruginosa is grown in nutrient limited conditions [217].

These interactions -- cooperative or competitive -- are important factors to elucidate growth dynamics and mechanisms of altered antimicrobial susceptibility of microorganisms growing

within a polymicrobial community. However, the specifics about interactions that occur between microorganisms and how they impact biofilm formation and infection outcomeare not yet fully understood. The species present and the interactions between them critically influence the development and behaviour of the community towards external stresses. Understanding such symbiotic interactions with clinical relevance between microbial species in biofilms will greatly aid in overcoming the limitations of current therapies and in defining potential new targets for treating polymicrobial infections.

6.2 Coculture of S. aureus with P. aeruginosa

To date, biofilm models used to explore the degrees of recalcitrance to killing by antimicrobials that take account of inter-species interactions are limited. The present model used to simulate mono-bacterial biofilm formation requires further refinement to investigate multi-species interactions, such as adding one more bacterial species, and making the code specific to a cystic fibrosis (CF) by incorporating species interactions of two of the most important bacterial opportunistic pathogens of humans,S. aureus and P. aeruginosa involved in the chronic diseases. CF lung infections are chronic and difficult to eradicateP. aeruginosa and S. aureus are two of the most prevalent respiratory pathogens in CF patients and are associated with poor patient outcomes. Both organisms adopt a biofilm mode of growth, which contributes to high tolerance to antibiotic treatment and the recalcitrant nature of these infections. We will determine whether these untreatable infections are due to heightened levels of persister cells, intercellular reservoirs of the pathogens or direct polymicrobial interactions.

6.3 Small colony variants

Hoffman et al. demonstrated that P. aeruginosa protected S. aureus from killing by the antibiotic tobramycin via the development of small colony variants (SCVs) due to exposure to respiratory inhibitor such as P. aeruginosa secreted 2-heptyl-4-hydroxyquinolineN-oxide (HQNO) [218]. SCVs are 10 times smaller than the usualS. aureus colonies [219]. SCVs are characteristically slow growing phenotype and constitute a small fraction ($\sim$0.01%) of the population from which they arise. These phenotypes do not respond to commonly used antibiotics, and they can serve as sources of chronic infection [218]. The intrinsic resistance

of these variants may in turn contribute to the enhanced antibiotic resistance of the biofilms thus formed. The emergence of SCVs during polymicrobial biofilm development represents a new challenge for research. Moreover, the instability of these SCVs wherein they could revert to the parental normal phenotype of rapid growth- thereby causes to a highly dynamic subpopulation serving as a reservoir for recurrent infections, make their experimental investigation difficulty to draw conclusions [220]. Thus formation of SCVs could be incorporated in the model to investigate their role in enhanced antibiotic resistance of biofilms.

6.3.1 Computational methodology

Every S. aureus cell in the domain will be modelled as either wild-type (WT) or as an SCV. In fact, SCVs will be treated as independent cell species since they are phenotypically different from the WT. During colonization, all theS. aureus cells will be WT only. P. aeruginosa, on the other hand, will have only one phenotype i.e. the WT.

Down-regulated P. aeruginosa cells will be assumed to produce and release HQNO molecules at a constant rate of $r_{HQNO,d}$; while up-regulated P. aeruginosa cells will be assumed to produce and release HQNO molecules at a rate$r_{HQNO,u}$will be

$$r_{HQNO,u} = r_{HQNO,d} + Y_{N,HQNO}\left[r_N\left(C_N(\bar{x},t), C_B(\bar{x},t)\right) - mC_B(\bar{x},t)\right] \qquad (6.1)$$

Here, $Y_{N,HQNO}$ is the efficiency at which a part of the nutrient will be used for production of HQNO molecules.

Time evolution of HQNO concentration within the biofilm will be:

$$\frac{\partial C_{HQNO}(\bar{x},t)}{\partial t} = D_{HQNO}\sum_{i=1}^{3}\frac{\partial^2 C_{HQNO}(\bar{x},t)}{\partial x_i{}^2} + r_{HQNO} - \nabla\cdot\left(vC_{HQNO}\right) \qquad (6.2)$$

Here, C_{HQNO} is the local HQNO concentration, $D_{HQNO}$is the diffusivity of HQNO in the biofilm. S. aureus cells will be allowed to transform between the two phenotypic states – WT and SCVs - at rates, depending the local HQNO concentration.

At time t = 0, all the S. aureus cells will be wild-type state only. The phenotypic switching rate from the WT to SCV will be

$$PS^+ = \alpha' \frac{C_{HQNO}(\bar{x},t)}{1+\gamma' C_{HQNO}(\bar{x},t)} \qquad (6.3)$$

while, the transition rate from SCV to WT state will be:

$$PS^- = \beta' \frac{1}{1+\gamma' C_{HQNO}(\bar{x},t)} \qquad (6.4)$$

Where α' and β' are the spontaneous conversion rates for SCVs and WT switching, and γ' is the transition constant.

Within a time interval of Δt, the probabilities of switching from one state to another will be:

$$P_{SCV} = (PS^+)\Delta t$$
$$P_{WT} = (PS^-)\Delta t \qquad (6.5)$$

where P_{SCV} is the probability a cell switching from WT to SCV state, and P_{WT} is the probability of a cell switching from SCV to WT state. During the simulation, a random number will be generated and if the probability of switching is greater than the random number, then the cell switches its phenotypic state.

Another focus of research could be to study the influence of biofilm morphology on antibiotic tolerance. It would involve commencing simulations with pre-determined morphologies-varied shapes, porosities, and diffusion distances etc., followed by subjecting the biofilm to external stresses like antimicrobial treatment. The role of different spatial distributions could also be analysed.

6.4 Experimental methodology

Parallel to modelling polymicrobial biofilms, we seek to perform the experiments that can test obtaining informative predictions from mathematical modelling. In addition, to identify

a mechanism of antibiotic resistance that is dependent on the polymicrobial interactions between P. aeruginosa and S. aureus and "bacterium-derived" matrix – EPS - components.

6.4.1 Biofilm formation

Bacterial strains P. aeruginosa and S. aureus nutrient agar slants will be procured from American Type Culture Collection (ATCC). Overnight grown bacterial cultures will be diluted and used to seed the wells of an 8-chambered cover-glass slide. Biofilms will be allowed to grow for further 24-48 h, replacing media until the conclusion of the experiment. Bacteria cultivate in μ-Slide 8 glass bottom wells help to screen different antimicrobial compounds at a time [221].

6.4.2 Antibiotic treatment

In select experiments biofilms on 8-well glass will be treated with antibiotics -- gentamycin, ciprofloxacin, and tetracycline—for 12 h. The percentage of cells viable after antibiotic treatment will be determined by dividing the number of cells that survived antibiotic treatment by the number of cells in the control and multiplying by 100.

6.4.3 Disruption of biofilm aggregates and Flow cytometric analysis

Biofilms will be removed from glass slide by scraping and rinsing without affecting cell viability. The biofilm suspensions thus obtained will be pooled and sonicated for 10, 30, or 60 min using a sonicator bath for disruption of polymicrobial aggregates. A non-sonicated sample will be included as a control. On these samples, a total cell count will be performed by Flow cytometry (FCM) for every species. FCM presents a fast and precise methodology to count cellular subpopulations in a biofilm. Moreover, it enables detailed investigation of the heterogeneous biofilm population due to its ability to perform multiparametric single-cell analysis [222, 223].

FCM measurements will be performed on a BD FACSAria III flow cytometer. Optical filters will set up such that red fluorescence is measured above 630 nm and green fluorescence is measured at 520 nm, and histograms showing fluorescence intensity against cell number will be generated at different phases of biofilm. For evaluating cells physiological state, 30 μL each bacterial suspension will be transferred to 270 μL of PBS containing 30 mmol/L, 5-

cyano-2,3-ditolyl tetrazolium chloride (CTC). Double staining with SYBR–CTC will be performed by incubating 30 µL of bacterial suspension in 270 µL of PBS containing SYBR and 30 mmol/L CTC. Cells will be incubated 5 min at room temperature prior to fluorescence analysis by FCM [224].

6.4.4 Visualization of biofilms using confocal laser-scanning microscope (CLSM)

For visual observation of the distribution of live and dead bacteria in biofilms, LIVE/DEAD BacLight staining kit will be used. Membrane permeable SYTO9 dye with green fluorescence will be used to stain live bacteria, and membrane impermeable propidium iodide dye with red fluorescence will be used to stain dead bacteria. Biofilms will be incubated with LIVE/DEAD BacLight staining kit in the dark for 30 min at 37°C. PBS will be used to remove non-specific staining. Fluorescence will be observed using a CLSM and the distribution of green live and red dead bacteria will be evaluated [225].

CLSM will capture the biofilm's physical structure through a series of digital images that occupy the same plane, parallel to substratum but vary along the height of the biofilm, often called an "image stack." Advanced and freely accessible program, COMSTAT software will be used to quantify the three-dimensional biofilm images acquired by CLSM. Measurements of the biomass, maximum thickness, mean thickness, roughness, substratum coverage, and surface/volume ratio will be chosen to characterize the biofilm structures developed by both P. aeruginosa or/and S. aureus strains. Using fluorescent microscopy, regions of varying viability can be distinguished with imagery.

6.4.5 Quantification and visualization of EPS

Total polysaccharide content will be determined by the phenol-sulphuric acid method, with protein assessed using the total protein kit [226].

On the other hand, EPS in a biofilm can also be quantified by measuring the total cell volume from a 3-D image of the biofilm using CLSM after staining cells with a florescent dye. The EPS content will be the difference between the volatile solids in the biofilms and the total cell mass, which could be quantified from the measured cell volume [225].

90

Bibliography

1.   Davey, M.E. and A. O'Toole G, Microbial biofilms: from ecology to molecular genetics. Microbiol Mol Biol Rev, 2000. 64(4): p. 847-67.

2.   Donlan, R.M. and J.W. Costerton, Biofilms: survival mechanisms of clinically relevant microorganisms. Clin Microbiol Rev, 2002. 15(2): p. 167-93.

3.   Donlan, R.M., Biofilms: microbial life on surfaces. Emerg Infect Dis, 2002. 8(9): p. 881-90.

4.   Beyth, N., et al., Alternative antimicrobial approach: nano-antimicrobial materials. Evid Based Complement Alternat Med, 2015. 2015: p. 246012.

5.   Ramasamy, M. and J. Lee, Recent Nanotechnology Approaches for Prevention and Treatment of Biofilm-Associated Infections on Medical Devices. Biomed Res Int, 2016. 2016: p. 1851242.

6.   Shunmugaperumal, T., Biofilm Eradication and Prevention: A Pharmaceutical Approach to Medical Device Infections. John Wiley & Sons, Inc. ed. 29 JUN 2010.

7.   Lebeaux, D., J.M. Ghigo, and C. Beloin, Biofilm-related infections: bridging the gap between clinical management and fundamental aspects of recalcitrance toward antibiotics. Microbiol Mol Biol Rev, 2014. 78(3): p. 510-43.

8.   Martens, E. and A.L. Demain, The antibiotic resistance crisis, with a focus on the United States. J Antibiot (Tokyo), 2017. 70(5): p. 520-526.

9.   Laxminarayan, R. and R.R. Chaudhury, Antibiotic Resistance in India: Drivers and Opportunities for Action. PLoS Med, 2016. 13(3): p. e1001974.

10.   Bjarnsholt, T., The role of bacterial biofilms in chronic infections. APMIS Suppl, 2013(136): p. 1-51.

11.   Nickel, J.C. and J.W. Costerton, Bacterial biofilms and catheters: A key to understanding bacterial strategies in catheter-associated urinary tract infection. Can J Infect Dis, 1992. 3(5): p. 261-7.

12.   Cirioni, O., et al., RNAIII-inhibiting peptide significantly reduces bacterial load and enhances the effect of antibiotics in the treatment of central venous catheter-associated Staphylococcus aureus infections. J Infect Dis, 2006. 193(2): p. 180-6.

13.   Olson, M.E., et al., Biofilm bacteria: formation and comparative susceptibility to antibiotics. Can J Vet Res, 2002. 66(2): p. 86-92.

14.   Olsen, I., Biofilm-specific antibiotic tolerance and resistance. Eur J Clin Microbiol Infect Dis, 2015. 34(5): p. 877-86.

15.   Jefferson, K.K., What drives bacteria to produce a biofilm? FEMS Microbiol Lett, 2004. 236(2): p. 163-73.

16.   Costerton, J.W., et al., Microbial biofilms. Annu Rev Microbiol, 1995. 49: p. 711-45.

17. Barraud, N., et al., Involvement of nitric oxide in biofilm dispersal of Pseudomonas aeruginosa. J Bacteriol, 2006. 188(21): p. 7344-53.

18. Stoodley, P., et al., Biofilm material properties as related to shear-induced deformation and detachment phenomena. J Ind Microbiol Biotechnol, 2002. 29(6): p. 361-7.

19. Stoodley, P., et al., Structural deformation of bacterial biofilms caused by short-term fluctuations in fluid shear: an in situ investigation of biofilm rheology. Biotechnol Bioeng, 1999. 65(1): p. 83-92.

20. Tsuneda, S., et al., Extracellular polymeric substances responsible for bacterial adhesion onto solid surface. FEMS Microbiol Lett, 2003. 223(2): p. 287-92.

21. Li, Y.H. and X. Tian, Quorum sensing and bacterial social interactions in biofilms. Sensors (Basel), 2012. 12(3): p. 2519-38.

22. Nadell, C.D., et al., The evolution of quorum sensing in bacterial biofilms. PLoS Biol, 2008. 6(1): p. e14.

23. Koutsoudis, M.D., et al., Quorum-sensing regulation governs bacterial adhesion, biofilm development, and host colonization in Pantoea stewartii subspecies stewartii. Proc Natl Acad Sci U S A, 2006. 103(15): p. 5983-8.

24. Morici, L.A., et al., Pseudomonas aeruginosa AlgR represses the Rhl quorum-sensing system in a biofilm-specific manner. J Bacteriol, 2007. 189(21): p. 7752-64.

25. Davenport, E.K., D.R. Call, and H. Beyenal, Differential protection from tobramycin by extracellular polymeric substances from Acinetobacter baumannii and Staphylococcus aureus biofilms. Antimicrob Agents Chemother, 2014. 58(8): p. 4755-61.

26. Wei, Q. and L.Z. Ma, Biofilm matrix and its regulation in Pseudomonas aeruginosa. Int J Mol Sci, 2013. 14(10): p. 20983-1005.

27. Heffernan, B., C.D. Murphy, and E. Casey, Comparison of planktonic and biofilm cultures of Pseudomonas fluorescens DSM 8341 cells grown on fluoroacetate. Appl Environ Microbiol, 2009. 75(9): p. 2899-907.

28. Ryall, B., G. Eydallin, and T. Ferenci, Culture history and population heterogeneity as determinants of bacterial adaptation: the adaptomics of a single environmental transition. Microbiol Mol Biol Rev, 2012. 76(3): p. 597-625.

29. Pamp, S.J., et al., Tolerance to the antimicrobial peptide colistin in Pseudomonas aeruginosa biofilms is linked to metabolically active cells, and depends on the pmr and mexAB-oprM genes. Mol Microbiol, 2008. 68(1): p. 223-40.

30. Sauer, K., The genomics and proteomics of biofilm formation. Genome Biol, 2003. 4(6): p. 219.

31. Mah, T.F. and G.A. O'Toole, Mechanisms of biofilm resistance to antimicrobial agents. Trends Microbiol, 2001. 9(1): p. 34-9.

32. Stewart, P.S. and M.J. Franklin, Physiological heterogeneity in biofilms. Nat Rev Microbiol, 2008. 6(3): p. 199-210.

33. Walters, M.C., 3rd, et al., Contributions of antibiotic penetration, oxygen limitation, and low metabolic activity to tolerance of Pseudomonas aeruginosa biofilms to ciprofloxacin and tobramycin. Antimicrob Agents Chemother, 2003. 47(1): p. 317-23.

34. Alpkvist, E., et al., Three-dimensional biofilm model with individual cells and continuum EPS matrix. Biotechnol Bioeng, 2006. 94(5): p. 961-79.

35. Chambless, J.D., S.M. Hunt, and P.S. Stewart, A three-dimensional computer model of four hypothetical mechanisms protecting biofilms from antimicrobials. Appl Environ Microbiol, 2006. 72(3): p. 2005-13.

36. Picioreanu, C., J.U. Kreft, and M.C. Van Loosdrecht, Particle-based multidimensional multispecies biofilm model. Appl Environ Microbiol, 2004. 70(5): p. 3024-40.

37. Kreft, J.U. and J.W. Wimpenny, Effect of EPS on biofilm structure and function as revealed by an individual-based model of biofilm growth. Water Sci Technol, 2001. 43(6): p. 135-41.

38. Alpkvist, E. and I. Klapper, A multidimensional multispecies continuum model for heterogeneous biofilm development. Bull Math Biol, 2007. 69(2): p. 765-89.

39. Duddu, R., D.L. Chopp, and B. Moran, A two-dimensional continuum model of biofilm growth incorporating fluid flow and shear stress based detachment. Biotechnol Bioeng, 2009. 103(1): p. 92-104.

40. Kreft, J.U., et al., Individual-based modelling of biofilms. Microbiology, 2001. 147(Pt 11): p. 2897-912.

41. Ardre, M., et al., An individual-based model for biofilm formation at liquid surfaces. Phys Biol, 2015. 12(6): p. 066015.

42. Wanner, O. and W. Gujer, A multispecies biofilm model. Biotechnol Bioeng, 1986. 28(3): p. 314-28.

43. Klapper, I. and J. Dockery, Finger Formation in Biofilm Layers. SIAM Journal on Applied Mathematics, 2002. 62(3): p. 853-869.

44. Karimi, A., et al., Interplay of physical mechanisms and biofilm processes: review of microfluidic methods. Lab Chip, 2015. 15(1): p. 23-42.

45. Edgerton, A.M.a.M., Real-Time Approach to Flow Cell Imaging of Candida albicans Biofilm Development. J. Fungi, 2017. 3(1).

46. Wang, L., et al., Bacterial growth, detachment and cell size control on polyethylene terephthalate surfaces. Sci Rep, 2015. 5: p. 15159.

47. Sauer, K., et al., Pseudomonas aeruginosa displays multiple phenotypes during development as a biofilm. J Bacteriol, 2002. 184(4): p. 1140-54.

48. Limoli, D.H., C.J. Jones, and D.J. Wozniak, Bacterial Extracellular Polysaccharides in Biofilm Formation and Function. Microbiol Spectr, 2015. 3(3).

49. Renner, L.D. and D.B. Weibel, Physicochemical regulation of biofilm formation. MRS Bull, 2011. 36(5): p. 347-355.

50. Kirov, S.M., et al., Biofilm differentiation and dispersal in mucoid Pseudomonas aeruginosa isolates from patients with cystic fibrosis. Microbiology, 2007. 153(Pt 10): p. 3264-74.

51. Rochex, A. and J.M. Lebeault, Effects of nutrients on biofilm formation and detachment of a Pseudomonas putida strain isolated from a paper machine. Water Res, 2007. 41(13): p. 2885-92.

52. Sauer, K., et al., Characterization of nutrient-induced dispersion in Pseudomonas aeruginosa PAO1 biofilm. J Bacteriol, 2004. 186(21): p. 7312-26.

53. Stoodley, P., et al., Influence of hydrodynamics and nutrients on biofilm structure. J Appl Microbiol, 1998. 85 Suppl 1: p. 19S-28S.

54. Stoodley, P., et al., Growth and detachment of cell clusters from mature mixed-species biofilms. Appl Environ Microbiol, 2001. 67(12): p. 5608-13.

55. Sawyer, L.K., and S. W. Hermanowicz, Detachment of biofilm bacteria due to variations in nutrient supply Water Sci. Technol., 1998. 37: p. 211-214.

56. Rice, S.A., et al., Biofilm formation and sloughing in Serratia marcescens are controlled by quorum sensing and nutrient cues. J Bacteriol, 2005. 187(10): p. 3477-85.

57. Hunt, S.M., et al., Hypothesis for the role of nutrient starvation in biofilm detachment. Appl Environ Microbiol, 2004. 70(12): p. 7418-25.

58. Fagerlind, M.G., et al., Dynamic modelling of cell death during biofilm development. J Theor Biol, 2012. 295: p. 23-36.

59. James, G.A., et al., Digital image analysis of growth and starvation responses of a surface-colonizing Acinetobacter sp. J Bacteriol, 1995. 177(4): p. 907-15.

60. Werner, E., et al., Stratified growth in Pseudomonas aeruginosa biofilms. Appl Environ Microbiol, 2004. 70(10): p. 6188-96.

61. Melaugh, G., et al., Shaping the Growth Behaviour of Biofilms Initiated from Bacterial Aggregates. PLoS One, 2016. 11(3): p. e0149683.

62. Williamson, K.S., et al., Heterogeneity in Pseudomonas aeruginosa biofilms includes expression of ribosome hibernation factors in the antibiotic-tolerant subpopulation and hypoxia-induced stress response in the metabolically active population. J Bacteriol, 2012. 194(8): p. 2062-73.

63. Fux, C.A., S. Wilson, and P. Stoodley, Detachment characteristics and oxacillin resistance of Staphyloccocus aureus biofilm emboli in an in vitro catheter infection model. J Bacteriol, 2004. 186(14): p. 4486-91.

64. Alvarez-Ortega, C., et al., Genetic determinants involved in the susceptibility of Pseudomonas aeruginosa to beta-lactam antibiotics. Antimicrob Agents Chemother, 2010. 54(10): p. 4159-67.

65. Atkinson, S. and P. Williams, Quorum sensing and social networking in the microbial world. J R Soc Interface, 2009. 6(40): p. 959-78.

66. Quinones, B., G. Dulla, and S.E. Lindow, Quorum sensing regulates exopolysaccharide production, motility, and virulence in Pseudomonas syringae. Mol Plant Microbe Interact, 2005. 18(7): p. 682-93.

67. Sakuragi, Y. and R. Kolter, Quorum-sensing regulation of the biofilm matrix genes (pel) of Pseudomonas aeruginosa. J Bacteriol, 2007. 189(14): p. 5383-6.

68. Novick, R.P. and E. Geisinger, Quorum sensing in staphylococci. Annu Rev Genet, 2008. 42: p. 541-64.

69. de Kievit, T.R. and B.H. Iglewski, Bacterial quorum sensing in pathogenic relationships. Infect Immun, 2000. 68(9): p. 4839-49.

70. Ng, W.L. and B.L. Bassler, Bacterial quorum-sensing network architectures. Annu Rev Genet, 2009. 43: p. 197-222.

71. Queck, S.Y., et al., RNAIII-independent target gene control by the agr quorum-sensing system: insight into the evolution of virulence regulation in Staphylococcus aureus. Mol Cell, 2008. 32(1): p. 150-8.

72. von Bodman, S.B., D.R. Majerczak, and D.L. Coplin, A negative regulator mediates quorum-sensing control of exopolysaccharide production in Pantoea stewartii subsp. stewartii. Proc Natl Acad Sci U S A, 1998. 95(13): p. 7687-92.

73. Flemming, H.C., T.R. Neu, and D.J. Wozniak, The EPS matrix: the "house of biofilm cells". J Bacteriol, 2007. 189(22): p. 7945-7.

74. Shih, P.C. and C.T. Huang, Effects of quorum-sensing deficiency on Pseudomonas aeruginosa biofilm formation and antibiotic resistance. J Antimicrob Chemother, 2002. 49(2): p. 309-14.

75. Gristina, A.G., et al., Comparative in vitro antibiotic resistance of surface-colonizing coagulase-negative staphylococci. Antimicrob Agents Chemother, 1989. 33(6): p. 813-6.

76. Vu, B., et al., Bacterial extracellular polysaccharides involved in biofilm formation. Molecules, 2009. 14(7): p. 2535-54.

77.   Xue, Z., et al., Pseudomonas aeruginosa inactivation mechanism is affected by capsular extracellular polymeric substances reactivity with chlorine and monochloramine. FEMS Microbiol Ecol, 2013. 83(1): p. 101-11.

78.   Tseng, B.S., et al., The extracellular matrix protects Pseudomonas aeruginosa biofilms by limiting the penetration of tobramycin. Environ Microbiol, 2013. 15(10): p. 2865-78.

79.   Brackman, G., et al., The Quorum Sensing Inhibitor Hamamelitannin Increases Antibiotic Susceptibility of Staphylococcus aureus Biofilms by Affecting Peptidoglycan Biosynthesis and eDNA Release. Sci Rep, 2016. 6: p. 20321.

80.   Singh, S., et al., Understanding the Mechanism of Bacterial Biofilms Resistance to Antimicrobial Agents. Open Microbiol J, 2017. 11: p. 53-62.

81.   Lewis, K., Riddle of biofilm resistance. Antimicrob Agents Chemother, 2001. 45(4): p. 999-1007.

82.   Beaudoin, T., et al., The biofilm-specific antibiotic resistance gene ndvB is important for expression of ethanol oxidation genes in Pseudomonas aeruginosa biofilms. J Bacteriol, 2012. 194(12): p. 3128-36.

83.   Zhang, L. and T.F. Mah, Involvement of a novel efflux system in biofilm-specific resistance to antibiotics. J Bacteriol, 2008. 190(13): p. 4447-52.

84.   Poole, K., Bacterial stress responses as determinants of antimicrobial resistance. J Antimicrob Chemother, 2012. 67(9): p. 2069-89.

85.   Zhang, L., et al., Identification of genes involved in Pseudomonas aeruginosa biofilm-specific resistance to antibiotics. PLoS One, 2013. 8(4): p. e61625.

86.   Soto, S.M., Role of efflux pumps in the antibiotic resistance of bacteria embedded in a biofilm. Virulence, 2013. 4(3): p. 223-9.

87.   Kinniment, S.L. and J.W. Wimpenny, Measurements of the distribution of adenylate concentrations and adenylate energy charge across Pseudomonas aeruginosa biofilms. Appl Environ Microbiol, 1992. 58(5): p. 1629-35.

88.   Huang, C.T., et al., Spatial patterns of alkaline phosphatase expression within bacterial colonies and biofilms in response to phosphate starvation. Appl Environ Microbiol, 1998. 64(4): p. 1526-31.

89.   Haagensen, J.A., et al., Differentiation and distribution of colistin- and sodium dodecyl sulfate-tolerant cells in Pseudomonas aeruginosa biofilms. J Bacteriol, 2007. 189(1): p. 28-37.

90.   Kim, J., et al., Tolerance of dormant and active cells in Pseudomonas aeruginosa PA01 biofilm to antimicrobial agents. J Antimicrob Chemother, 2009. 63(1): p. 129-35.

91.   Brooun, A., S. Liu, and K. Lewis, A dose-response study of antibiotic resistance in Pseudomonas aeruginosa biofilms. Antimicrob Agents Chemother, 2000. 44(3): p. 640-6.

92.   Ceri, H., et al., The Calgary Biofilm Device: new technology for rapid determination of antibiotic susceptibilities of bacterial biofilms. J Clin Microbiol, 1999. 37(6): p. 1771-6.

93.   Qi, L., et al., Relationship between Antibiotic Resistance, Biofilm Formation, and Biofilm-Specific Resistance in Acinetobacter baumannii. Front Microbiol, 2016. 7: p. 483.

94.   Aka, S.T. and S.H. Haji, Sub-MIC of antibiotics induced biofilm formation of Pseudomonas aeruginosa in the presence of chlorhexidine. Braz J Microbiol, 2015. 46(1): p. 149-54.

95.   Yang, Y.B., et al., Sub-MICs of Azithromycin Decrease Biofilm Formation of Streptococcus suis and Increase Capsular Polysaccharide Content of S. suis. Front Microbiol, 2016. 7: p. 1659.

96.   Linares, J.F., et al., Antibiotics as intermicrobial signaling agents instead of weapons. Proc Natl Acad Sci U S A, 2006. 103(51): p. 19484-9.

97.   Subrt, N., L.R. Mesak, and J. Davies, Modulation of virulence gene expression by cell wall active antibiotics in Staphylococcus aureus. J Antimicrob Chemother, 2011. 66(5): p. 979-84.

98.   Haddadin, R.N., et al., The effect of subminimal inhibitory concentrations of antibiotics on virulence factors expressed by Staphylococcus aureus biofilms. J Appl Microbiol, 2010. 108(4): p. 1281-91.

99.   Frank, K.L., et al., In vitro effects of antimicrobial agents on planktonic and biofilm forms of Staphylococcus lugdunensis clinical isolates. Antimicrob Agents Chemother, 2007. 51(3): p. 888-95.

100.   Bagge, N., et al., Pseudomonas aeruginosa biofilms exposed to imipenem exhibit changes in global gene expression and beta-lactamase and alginate production. Antimicrob Agents Chemother, 2004. 48(4): p. 1175-87.

101.   Shen, Y., et al., Experimental and Theoretical Investigation of Multispecies Oral Biofilm Resistance to Chlorhexidine Treatment. Sci Rep, 2016. 6: p. 27537.

102.   Williamson, K. and P.L. McCarty, A model of substrate utilization by bacterial films. J Water Pollut Control Fed, 1976. 48(1): p. 9-24.

103.   Lamotta, E.J., Internal diffusion and reaction in biological films. Environ Sci Technol, 1976. 10(8): p. 765-9.

104.   Beerman, H., et al., DNA ploidy of primary breast cancer and local recurrence after breast-conserving therapy. Br J Cancer, 1991. 64(1): p. 139-43.

105.   Zhang, X., et al., Simulation of Bacillus subtilis biofilm growth on agar plate by diffusion-reaction based continuum model. Phys Biol, 2016. 13(4): p. 046002.

106.   Machineni, L., et al., Influence of Nutrient Availability and Quorum Sensing on the Formation of Metabolically Inactive Microcolonies Within Structurally Heterogeneous

Bacterial Biofilms: An Individual-Based 3D Cellular Automata Model. Bull Math Biol, 2017. 79(3): p. 594-618.

107. Frederick, M.R., et al., A mathematical model of quorum sensing regulated EPS production in biofilm communities. Theor Biol Med Model, 2011. 8: p. 8.

108. Emerenini, B.O., et al., A Mathematical Model of Quorum Sensing Induced Biofilm Detachment. PLoS One, 2015. 10(7): p. e0132385.

109. Kreft, J.U., G. Booth, and J.W. Wimpenny, BacSim, a simulator for individual-based modelling of bacterial colony growth. Microbiology, 1998. 144 (Pt 12): p. 3275-87.

110. Jayathilake, P.G., et al., A mechanistic Individual-based Model of microbial communities. PLoS One, 2017. 12(8): p. e0181965.

111. Cheng Li, a.Y.Z.a.C.Y., Individual based modeling of Pseudomonas aeruginosa biofilm with three detachment mechanisms. RSC Advances, 2015

112. Anguige, K., J.R. King, and J.P. Ward, A multi-phase mathematical model of quorum sensing in a maturing Pseudomonas aeruginosa biofilm. Math Biosci, 2006. 203(2): p. 240-76.

113. Dodds, M.G., K.J. Grobe, and P.S. Stewart, Modeling biofilm antimicrobial resistance. Biotechnol Bioeng, 2000. 68(4): p. 456-65.

114. Szomolay, B., et al., Adaptive responses to antimicrobial agents in biofilms. Environ Microbiol, 2005. 7(8): p. 1186-91.

115. Cogan, N.G., R. Cortez, and L. Fauci, Modeling physiological resistance in bacterial biofilms. Bull Math Biol, 2005. 67(4): p. 831-53.

116. Cogan, N.G., B. Szomolay, and M. Dindos, Effect of periodic disinfection on persisters in a one-dimensional biofilm model. Bull Math Biol, 2013. 75(1): p. 94-123.

117. Roberts, M.E. and P.S. Stewart, Modeling antibiotic tolerance in biofilms by accounting for nutrient limitation. Antimicrob Agents Chemother, 2004. 48(1): p. 48-52.

118. Roberts, M.E. and P.S. Stewart, Modelling protection from antimicrobial agents in biofilms through the formation of persister cells. Microbiology, 2005. 151(Pt 1): p. 75-80.

119. Claudi, B., et al., Phenotypic variation of Salmonella in host tissues delays eradication by antimicrobial chemotherapy. Cell, 2014. 158(4): p. 722-33.

120. Wanner O, E.H., Morgenroth E, Noguera D, Picioreanu C, Rittmann BE, Van Loosdrecht MCM, Mathematical Modeling of Biofilms 2006: IWA Scientific and Technical Report No.18, IWA Publishing.

121. Chang, I., et al., A three-dimensional, stochastic simulation of biofilm growth and transport-related factors that affect structure. Microbiology, 2003. 149(Pt 10): p. 2859-71.

122. Picioreanu, C., M.C. Van Loosdrecht, and J.J. Heijnen,Effect of diffusive and convective substrate transport on biofilm structure formation: a two-dimensional modeling study. Biotechnol Bioeng, 2000.69(5): p. 504-15.

123. Eberl H, M.E., Noguera D, Picioreanu C, Rittmann B, van Loosdrecht M, Wanner O Mathematical modeling of biofilms.IWA Publishing, 2006.

124. Castro, S.L., et al.,Induction of attachment-independent biofilm formation and repression of Hfq expression by low-fluid-shear culture of Staphylococcus aureus.Appl Environ Microbiol, 2011. 77(18): p. 6368-78.

125. Guo, P., A.M. Weinstein, and S. Weinbaum,A hydrodynamic mechanosensory hypothesis for brush border microvilli. Am J Physiol Renal Physiol, 2000.279(4): p. F698-712.

126. Falsetta, M.L., et al., Symbiotic relationship between Streptococcus mutans and Candida albicans synergizes virulence of plaque biofilms in vivo.Infect Immun, 2014. 82(5): p. 1968-81.

127. Postgate, J.R. and J.R. Hunter,The survival of starved bacteria. J Gen Microbiol, 1962. 29: p. 233-63.

128. Picioreanu, C., M.C. van Loosdrecht, and J.J. Heijnen,Mathematical modeling of biofilm structure with a hybrid differential-discrete cellular automaton approach.Biotechnol Bioeng, 1998. 58(1): p. 101-16.

129. Picioreanu, C., M.C. van Loosdrecht, and J.J. Heijnen, A new combined differential-discrete cellular automaton approach for biofilm modeling: application for growth in gel beads. Biotechnol Bioeng, 1998.57(6): p. 718-31.

130. Wang, G. and W.M. Post, A theoretical reassessment of microbial maintenance and implications for microbial ecology modeling.FEMS Microbiol Ecol, 2012.81(3): p. 610-7.

131. Nystrom, T., Not quite dead enough: on bacterial life, culturability, senescence, and death. Arch Microbiol, 2001. 176(3): p. 159-64.

132. Nystrom, T., Conditional senescence in bacteria: death of the immortals.Mol Microbiol, 2003. 48(1): p. 17-23.

133. Chambless, J.D. and P.S. Stewart, A three-dimensional computer model analysis of three hypothetical biofilm detachment mechanisms.Biotechnol Bioeng, 2007. 97(6): p. 1573-84.

134. Picioreanu, C., M.C. van Loosdrecht, and J.J. Heijnen,Two-dimensional model of biofilm detachment caused by internal stress from liquid flow.Biotechnol Bioeng, 2001. 72(2): p. 205-18.

135. Stewart, P.S., A model of biofilm detachment. Biotechnol Bioeng, 1993.41(1): p. 111-7.

136. Pizarro, G.E., et al., Two-dimensional cellular automaton model for mixed-culture biofilm. Water Sci Technol, 2004. 49(11-12): p. 193-8.

137.   Fozard, J.A., et al., Inhibition of quorum sensing in a computational biofilm simulation. Biosystems, 2012. 109(2): p. 105-14.

138.   Leisner, M., et al., Kinetics of genetic switching into the state of bacterial competence. Biophys J, 2009. 96(3): p. 1178-88.

139.   Davis, D., Eisen, Ginsberg,   , Bacterial Physiology: Microbiology. Vol. Second Edition, Maryland:. 1973. : 96-97.

140.   Koerber, A.J., et al., A mathematical model of partial-thickness burn-wound infection by Pseudomonas aeruginosa: quorum sensing and the build-up to invasion.Bull Math Biol, 2002. 64(2): p. 239-59.

141.   Moskowitz, S.M., et al., Clinically feasible biofilm susceptibility assay for isolates of Pseudomonas aeruginosa from patients with cystic fibrosis. J Clin Microbiol, 2004. 42(5): p. 1915-22.

142.   Hall-Stoodley, L., J.W. Costerton, and P. Stoodley, Bacterial biofilms: from the natural environment to infectious diseases.Nat Rev Microbiol, 2004. 2(2): p. 95-108.

143.   Ma, R., et al., Modeling of diffusion transport through oral biofilms with the inverse problem method. Int J Oral Sci, 2010. 2(4): p. 190-7.

144.   Stoodley, P., D. Debeer, and Z. Lewandowski, Liquid flow in biofilm systems. Appl Environ Microbiol, 1994. 60(8): p. 2711-6.

145.   Hunter, R.C. and T.J. Beveridge, High-resolution visualization of Pseudomonas aeruginosa PAO1 biofilms by freeze-substitution transmission electron microscopy. J Bacteriol, 2005. 187(22): p. 7619-30.

146.   Jefferson, K.K., D.A. Goldmann, and G.B. Pier, Use of confocal microscopy to analyze the rate of vancomycin penetration through Staphylococcus aureus biofilms. Antimicrob Agents Chemother, 2005. 49(6): p. 2467-73.

147.   Lawrence, J.R., et al., Optical sectioning of microbial biofilms. J Bacteriol, 1991. 173(20): p. 6558-67.

148.   Yang, X., et al., Quantifying biofilm structure using image analysis. J Microbiol Methods, 2000. 39(2): p. 109-19.

149.   Costerton, J.W., et al., Bacterial biofilms in nature and disease. Annu Rev Microbiol, 1987. 41: p. 435-64.

150.   Stoodley, P., et al., Biofilms as complex differentiated communities. Annu Rev Microbiol, 2002. 56: p. 187-209.

151.   Bassler, B.L., et al., Intercellular signalling in Vibrio harveyi: sequence and function of genes regulating expression of luminescence.Mol Microbiol, 1993. 9(4): p. 773-86.

152. Matz, C., et al., Microcolonies, quorum sensing and cytotoxicity determine the survival of Pseudomonas aeruginosa biofilms exposed to protozoan grazing.Environ Microbiol, 2004. 6(3): p. 218-26.

153. McDougald, D., et al., Should we stay or should we go: mechanisms and ecological consequences for biofilm dispersal.Nat Rev Microbiol, 2012. 10(1): p. 39-50.

154. Potera, C., Forging a link between biofilms and disease. Science, 1999. 283(5409): p. 1837, 1839.

155. Deretic, V., et al., Conversion of Pseudomonas aeruginosa to mucoidy in cystic fibrosis: environmental stress and regulation of bacterial virulence by alternative sigma factors.J Bacteriol, 1994. 176(10): p. 2773-80.

156. Rayner, M.G., et al., Evidence of bacterial metabolic activity in culture-negative otitis media with effusion. JAMA, 1998. 279(4): p. 296-9.

157. Blaser, J., et al.,In vivo verification of in vitro model of antibiotic treatment of device-related infection. Antimicrob Agents Chemother, 1995.39(5): p. 1134-9.

158. Darouiche, R.O., et al.,Vancomycin penetration into biofilm covering infected prostheses and effect on bacteria. J Infect Dis, 1994. 170(3): p. 720-3.

159. Stickler, D.J., et al.,Biofilms on indwelling urethral catheters produce quorum-sensing signal molecules in situ and in vitro. Appl Environ Microbiol, 1998.64(9): p. 3486-90.

160. Ward, K.H., et al., Mechanism of persistent infection associated with peritoneal implants.J Med Microbiol, 1992. 36(6): p. 406-13.

161. Gefen, O. and N.Q. Balaban,The importance of being persistent: heterogeneity of bacterial populations under antibiotic stress.FEMS Microbiol Rev, 2009. 33(4): p. 704-17.

162. Gefen, O., et al., Single-cell protein induction dynamics reveals a period of vulnerability to antibiotics in persister bacteria.Proc Natl Acad Sci U S A, 2008. 105(16): p. 6145-9.

163. Keren, I., et al., Specialized persister cells and the mechanism of multidrug tolerance in Escherichia coli. J Bacteriol, 2004. 186(24): p. 8172-80.

164. Keren, I., et al., Persister cells and tolerance to antimicrobials.FEMS Microbiol Lett, 2004. 230(1): p. 13-8.

165. Kussell, E., et al., Bacterial persistence: a model of survival in changing environments. Genetics, 2005. 169(4): p. 1807-14.

166. Mulcahy, L.R., et al.,Emergence of Pseudomonas aeruginosa strains producing high levels of persister cells in patients with cystic fibrosis.J Bacteriol, 2010. 192(23): p. 6191-9.

167. Stewart, P.S. and M.J. Franklin, Physiological heterogeneity in biofilms. Nat Rev Micro, 2008. 6(3): p. 199-210.

168.   Pu, Y., et al., Enhanced Efflux Activity Facilitates Drug Tolerance in Dormant Bacterial Cells. Mol Cell, 2016. 62(2): p. 284-94.

169.   De Beer, D., R. Srinivasan, and P.S. Stewart,Direct measurement of chlorine penetration into biofilms during disinfection. Appl Environ Microbiol, 1994.60(12): p. 4339-44.

170.   Grobe, K.J., J. Zahller, and P.S. Stewart, Role of dose concentration in biocide efficacy against Pseudomonas aeruginosa biofilms. J Ind Microbiol Biotechnol, 2002.29(1): p. 10-5.

171.   Rutherford, S.T. and B.L. Bassler, Bacterial quorum sensing: its role in virulence and possibilities for its control. Cold Spring Harb Perspect Med, 2012. 2(11).

172.   Fuqua, C. and E.P. Greenberg, Listening in on bacteria: acyl-homoserine lactone signalling. Nat Rev Mol Cell Biol, 2002.3(9): p. 685-95.

173.   Davies, D.G., et al., The involvement of cell-to-cell signals in the development of a bacterial biofilm. Science, 1998. 280(5361): p. 295-8.

174.   Tan, C.H., et al., The role of quorum sensing signalling in EPS production and the assembly of a sludge community into aerobic granules.ISME J, 2014. 8(6): p. 1186-97.

175.   Boyd, A. and A.M. Chakrabarty, Role of alginate lyase in cell detachment of Pseudomonas aeruginosa. Appl Environ Microbiol, 1994. 60(7): p. 2355-9.

176.   Janissen, R., et al.,Spatiotemporal distribution of different extracellular polymeric substances and filamentation mediate Xylella fastidiosa adhesion and biofilm formation.Sci Rep, 2015. 5: p. 9856.

177.   Ma, L., et al., Assembly and development of the Pseudomonas aeruginosa biofilm matrix. PLoS Pathog, 2009. 5(3): p. e1000354.

178.   Lewis, K., Persister cells, dormancy and infectious disease. Nat Rev Microbiol, 2007. 5(1): p. 48-56.

179.   Jayaraman, A. and T.K. Wood, Bacterial quorum sensing: signals, circuits, and implications for biofilms and disease. Annu Rev Biomed Eng, 2008. 10: p. 145-67.

180.   Langebrake, J.B., et al., Traveling waves in response to a diffusing quorum sensing signal in spatially-extended bacterial colonies. J Theor Biol, 2014. 363: p. 53-61.

181.   Anguige, K., J.R. King, and J.P. Ward, Modelling antibiotic- and anti-quorum sensing treatment of a spatially-structured Pseudomonas aeruginosa population.J Math Biol, 2005. 51(5): p. 557-94.

182.   Bester, E., et al., Planktonic-cell yield of a pseudomonad biofilm. Appl Environ Microbiol, 2005. 71(12): p. 7792-8.

183.   Kroukamp, O., R.G. Dumitrache, and G.M. Wolfaardt,Pronounced effect of the nature of the inoculum on biofilm development in flow systems. Appl Environ Microbiol, 2010. 76(18): p. 6025-31.

184. Flemming, H.C., et al., Biofilms: an emergent form of bacterial life. Nat Rev Microbiol, 2016. 14(9): p. 563-75.

185. Leid, J.G., Bacterial Biofilms Resist Key Host Defenses. Microbe 2009. 4(Number 2,): p. 66-70.

186. Hathroubi, S., et al., Biofilms: Microbial Shelters Against Antibiotics. Microb Drug Resist, 2017. 23(2): p. 147-156.

187. Hall, C.W. and T.F. Mah, Molecular mechanisms of biofilm-based antibiotic resistance and tolerance in pathogenic bacteria. FEMS Microbiol Rev, 2017. 41(3): p. 276-301.

188. Gupta, K., et al., Antimicrobial tolerance of Pseudomonas aeruginosa biofilms is activated during an early developmental stage and requires the two-component hybrid SagS. J Bacteriol, 2013. 195(21): p. 4975-87.

189. He, X. and J. Ahn, Differential gene expression in planktonic and biofilm cells of multiple antibiotic-resistant Salmonella Typhimurium and Staphylococcus aureus. FEMS Microbiol Lett, 2011. 325(2): p. 180-8.

190. Wood, T.K., S.J. Knabel, and B.W. Kwan, Bacterial persister cell formation and dormancy. Appl Environ Microbiol, 2013. 79(23): p. 7116-21.

191. Lewis, K., Multidrug tolerance of biofilms and persister cells. Curr Top Microbiol Immunol, 2008. 322: p. 107-31.

192. LaFleur, M.D., C.A. Kumamoto, and K. Lewis, Candida albicans biofilms produce antifungal-tolerant persister cells. Antimicrob Agents Chemother, 2006. 50(11): p. 3839-46.

193. Sultana, S.T., D.R. Call, and H. Beyenal, Eradication of Pseudomonas aeruginosa biofilms and persister cells using an electrochemical scaffold and enhanced antibiotic susceptibility npj Biofilms and Microbiomes, 2016. 2(1): p. 2.

194. Gilbert, P., et al., The physiology and collective recalcitrance of microbial biofilm communities. Adv Microb Physiol, 2002. 46: p. 202-56.

195. Kostakioti, M., M. Hadjifrangiskou, and S.J. Hultgren, Bacterial biofilms: development, dispersal, and therapeutic strategies in the dawn of the postantibiotic era. Cold Spring Harb Perspect Med, 2013. 3(4): p. a010306.

196. Stewart, P.S. and J.W. Costerton, Antibiotic resistance of bacteria in biofilms. Lancet, 2001. 358(9276): p. 135-8.

197. de la Fuente-Nunez, C., et al., Bacterial biofilm development as a multicellular adaptation: antibiotic resistance and new therapeutic strategies. Curr Opin Microbiol, 2013. 16(5): p. 580-9.

198. Yang, L., et al., In situ growth rates and biofilm development of Pseudomonas aeruginosa populations in chronic lung infections. J Bacteriol, 2008. 190(8): p. 2767-76.

199. Kolpen, M., et al., Increased bactericidal activity of colistin on Pseudomonas aeruginosa biofilms in anaerobic conditions. Pathog Dis, 2016. 74(1): p. ftv086.

200. Borriello, G., et al., Oxygen limitation contributes to antibiotic tolerance of Pseudomonas aeruginosa in biofilms. Antimicrob Agents Chemother, 2004. 48(7): p. 2659-64.

201. Mulcahy, L.R., V.M. Isabella, and K. Lewis, Pseudomonas aeruginosa biofilms in disease. Microb Ecol, 2014. 68(1): p. 1-12.

202. Hoffman, L.R., et al., Aminoglycoside antibiotics induce bacterial biofilm formation. Nature, 2005. 436(7054): p. 1171-5.

203. Kiran, S., et al., Enzymatic quorum quenching increases antibiotic susceptibility of multidrug resistant Pseudomonas aeruginosa. Iran J Microbiol, 2011. 3(1): p. 1-12.

204. Kaplan, J.B., Antibiotic-induced biofilm formation. Int J Artif Organs, 2011. 34(9): p. 737-51.

205. Sailer, F.C., B.M. Meberg, and K.D. Young, beta-Lactam induction of colanic acid gene expression in Escherichia coli. FEMS Microbiol Lett, 2003. 226(2): p. 245-9.

206. Schaule, G., H.C. Flemming, and H.F. Ridgway, Use of 5-cyano-2,3-ditolyl tetrazolium chloride for quantifying planktonic and sessile respiring bacteria in drinking water. Appl Environ Microbiol, 1993. 59(11): p. 3850-7.

207. Manuel, C.M., O.C. Nunes, and L.F. Melo, Dynamics of drinking water biofilm in flow/non-flow conditions. Water Res, 2007. 41(3): p. 551-62.

208. Cerca, N., et al., Effects of growth in the presence of subinhibitory concentrations of dicloxacillin on Staphylococcus epidermidis and Staphylococcus haemolyticus biofilms. Appl Environ Microbiol, 2005. 71(12): p. 8677-82.

209. Roldan, M.H.-M.a.M., Characterization of Photosynthetic Biofilms from Roman Catacombs via 3D Imaging and Subcellular Identification of Pigments. COALITION, 2007(15).

210. Elias, S. and E. Banin, Multi-species biofilms: living with friendly neighbors. FEMS Microbiol Rev, 2012. 36(5): p. 990-1004.

211. Fischbach, M.A. and J.L. Sonnenburg, Eating for two: how metabolism establishes interspecies interactions in the gut. Cell Host Microbe, 2011. 10(4): p. 336-47.

212. Madsen, J.S., et al., The interconnection between biofilm formation and horizontal gene transfer. FEMS Immunol Med Microbiol, 2012. 65(2): p. 183-95.

213. Peters, B.M., et al., Polymicrobial interactions: impact on pathogenesis and human disease. Clin Microbiol Rev, 2012. 25(1): p. 193-213.

214. Marsh, P.D., Dental plaque as a biofilm and a microbial community - implications for health and disease. BMC Oral Health, 2006. 6 Suppl 1: p. S14.

215. Liu, S., et al., Polymicrobial and Monomicrobial Infections after Spinal Surgery: A Retrospective Study to Determine which Infection is more Severe. Asian Spine J, 2017. 11(3): p. 427-436.

216. Bridier, A., et al., Biofilms of a Bacillus subtilis hospital isolate protect Staphylococcus aureus from biocide action. PLoS One, 2012. 7(9): p. e44506.

217. Hibbing, M.E. and C. Fuqua, Inhibition and dispersal of Agrobacterium tumefaciens biofilms by a small diffusible Pseudomonas aeruginosa exoproduct(s). Arch Microbiol, 2012. 194(6): p. 391-403.

218. Hoffman, L.R., et al., Selection for Staphylococcus aureus small-colony variants due to growth in the presence of Pseudomonas aeruginosa. Proc Natl Acad Sci U S A, 2006. 103(52): p. 19890-5.

219. Kahl, B.C., et al., Thymidine-dependent Staphylococcus aureus small-colony variants are associated with extensive alterations in regulator and virulence gene expression profiles. Infect Immun, 2005. 73(7): p. 4119-26.

220. Maduka-Ezeh, A.N., et al., Antimicrobial susceptibility and biofilm formation of Staphylococcus epidermidis small colony variants associated with prosthetic joint infection. Diagn Microbiol Infect Dis, 2012. 74(3): p. 224-9.

221. Aung, T.T., et al., Biofilms of Pathogenic Nontuberculous Mycobacteria Targeted by New Therapeutic Approaches. Antimicrob Agents Chemother, 2015. 60(1): p. 24-35.

222. Ambriz-Avina, V., J.A. Contreras-Garduno, and M. Pedraza-Reyes, Applications of flow cytometry to characterize bacterial physiological responses. Biomed Res Int, 2014. 2014: p. 461941.

223. Kerstens, M., et al., A flow cytometric approach to quantify biofilms. Folia Microbiol (Praha), 2015. 60(4): p. 335-42.

224. Cerca, F., et al., SYBR green as a fluorescent probe to evaluate the biofilm physiological state of Staphylococcus epidermidis, using flow cytometry. Can J Microbiol, 2011. 57(10): p. 850-6.

225. Harrison, J.J., et al., The use of microscopy and three-dimensional visualization to evaluate the structure of microbial biofilms cultivated in the Calgary Biofilm Device. Biol Proced Online, 2006. 8: p. 194-215.

226. Stewart, T.J., et al., Characterization of extracellular polymeric substances (EPS) from periphyton using liquid chromatography-organic carbon detection-organic nitrogen detection (LC-OCD-OND). Environ Sci Pollut Res Int, 2013. 20(5): p. 3214-23.